

AD-A272 606



NAVAL POSTGRADUATE SCHOOL
Monterey, California

2



S **DTIC**
ELECTE
NOV 16 1993
A

THESIS

**NORMAL MODES OF VIBRATION
OF THE PHALANX GUN**

by

John C. Peterschmidt

June 1993

Thesis Advisors:

William B. Colson
Joshua H. Gordis

Approved for public release; distribution is unlimited

93-27748



REPORT DOCUMENTATION PAGE

Form Approved
OMB No 0704-0188

Public reporting burden for this collection of information is estimated to average 1 hour per response, including the time for reviewing instructions, searching existing data sources, gathering and maintaining the data needed, and completing and reviewing the collection of information. Send comments regarding this burden estimate or any other aspect of this collection of information, including suggestions for reducing this burden, to Washington Headquarters Services, Directorate for Information Operations and Reports, 1215 Jefferson Davis Highway, Suite 1204, Arlington, VA 22202-4302, and to the Office of Management and Budget, Paperwork Reduction Project (0704-0188), Washington, DC 20503.

1. AGENCY USE ONLY (Leave blank)		2. REPORT DATE June 1993		3. REPORT TYPE AND DATES COVERED Master's Thesis	
4. TITLE AND SUBTITLE NORMAL MODES OF VIBRATION OF THE PHALANX GUN				5. FUNDING NUMBERS	
6. AUTHOR(S) John C. Peterschmidt					
7. PERFORMING ORGANIZATION NAME(S) AND ADDRESS(ES) Naval Postgraduate School Monterey, CA 93943-5000				8. PERFORMING ORGANIZATION REPORT NUMBER	
9. SPONSORING / MONITORING AGENCY NAME(S) AND ADDRESS(ES) Naval Postgraduate School Monterey, CA 93943-5000				10. SPONSORING / MONITORING AGENCY REPORT NUMBER	
11. SUPPLEMENTARY NOTES The views expressed in this thesis are those of the author and do not reflect the official policy of the Department of Defense or the U. S. Government.					
12a. DISTRIBUTION / AVAILABILITY STATEMENT Approved for public release; distribution unlimited				12b. DISTRIBUTION CODE	
13. ABSTRACT (Maximum 200 words) In order to investigate the physics behind the dispersion and test future design changes, a detailed finite element model of the PHALANX gun was developed. This is the first finite element model of the gun ever. The normal modes of a single barrel have been matched favorably with those of a real barrel. This model has been used to calculate the normal modes of vibration of the whole gun in order to predict the motion of the complex system. Barrel tip displacement, which plays a critical role in the dispersion pattern, was determined after applying the periodic firing excitation force and damping. Its motion corresponds well to the 2 mradian dispersion. In addition, its first mode of vibration at 14 Hz appears to be significant in the analysis of the dispersion data. This analysis has focused attention on certain components of the gun, such as the double angular contact bearing, which may be a leading cause of the dispersion pattern. Finally, this gun model can also support design changes such as the additon of barrel restraints or the proposed new barrels and their effect on dispersion predicted prior to any actual hardware tests or procurement orders.					
14. SUBJECT TERMS PHALANX CIWS, PHALANX round dispersion, finite element code, modal analysis, dynamic response, frequency response functions				15. NUMBER OF PAGES 186	
				16. PRICE CODE	
17. SECURITY CLASSIFICATION OF REPORT UNCLASSIFIED	18. SECURITY CLASSIFICATION OF THIS PAGE UNCLASSIFIED	19. SECURITY CLASSIFICATION OF ABSTRACT UNCLASSIFIED	20. LIMITATION OF ABSTRACT UL		

Approved for public release: distribution is unlimited.

NORMAL MODES OF VIBRATION OF THE PHALANX GUN

by

John C. Peterschmidt

Lieutenant, United States Navy

B. S., Marquette University, 1987

Submitted in partial fulfillment of the
requirements for the degree of

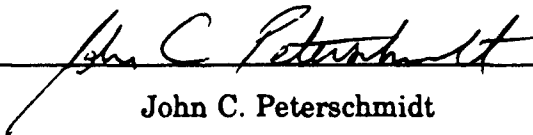
MASTER OF SCIENCE IN PHYSICS

from the

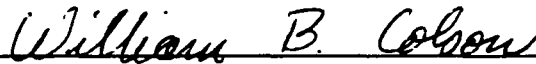
NAVAL POSTGRADUATE SCHOOL

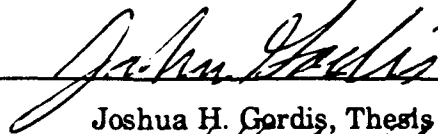
June 1993

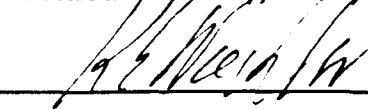
Author:


John C. Peterschmidt

Approved by:


William B. Colson, Thesis Advisor


Joshua H. Gordis, Thesis Advisor


Karlheinz E. Woehler, Chairman,
Department of Physics

ABSTRACT

The PHALANX Close-In-Weapons System provides the last layer of defense against an incoming anti-ship missile. Current dispersion data shows that the rotating six-barrel system firing at 75 shots/second gives variable dispersion greater than 2 mradian. This results in a 4 m spread at its maximum 2000 m range. Computer simulations have shown that a fast missile can penetrate to within a couple hundred yards of the ship, where even if it was destroyed, the resulting ballistic debris would hit the ship in a shotgun blast pattern.

In order to investigate the physics behind the dispersion and test future design changes, a detailed finite element model of the PHALANX gun was developed. This is the first finite element model of the gun ever. The normal modes of a single barrel have been matched favorably with those of a real barrel. This model has been used to calculate the normal modes of vibration of the whole gun in order to predict the motion of the complex system. Barrel tip displacement, which plays a critical role in the dispersion pattern, was determined after applying the periodic firing excitation force and damping. Its motion corresponds well to the 2 mradian dispersion. In addition, its first mode of vibration at 14 Hz appears to be significant in the analysis of the dispersion data. This analysis has focused attention on certain components of the gun, such as the double angular contact bearing, which may be a leading cause of the dispersion pattern. Finally, this gun model can also support design changes such as the addition of barrel restraints or the proposed new barrels and their effect on dispersion predicted prior to any actual hardware tests or procurement orders.

DTIC QUALITY INSPECTED 5

Accession For	
NTIS - G4&I	<input checked="" type="checkbox"/>
DTIC - TAB	<input type="checkbox"/>
Unannounced	<input type="checkbox"/>
Justification	
By	
Distribution/	
Availability Codes	
Dist	Avail. and/or Special
A-1	

Table of Contents

I. INTRODUCTION	1
II. MOTIVATION FOR STUDYING THE PHALANX GUN	5
A. DESCRIPTION OF THE PHALANX SYSTEM	5
B. PHALANX ROUND DISPERSION	10
C. THE BALLISTIC DEBRIS PROBLEM	15
III. FINITE ELEMENT THEORY	22
A. THE DECISION TO USE FINITE ELEMENT MODELING	22
B. THE DISCRETIZATION OF A SIMPLE ROD	25
C. MATRIX FORM OF EQUILIBRIUM EQUATIONS	30
D. FREE VIBRATION IN A STRUCTURE OF ELEMENTS	34
IV. MODEL DESCRIPTION	41
A. TYPES OF FINITE ELEMENTS USED IN THE MODEL	41
1. Brick Elements	42
2. Thin Shell Elements	44
3. Beam Elements	45
4. Spring Elements	46
5. Rigid Elements	47
B. CONSTRUCTION OF THE PHALANX GUN	49
1. Gun Barrels	50
2. Muzzle Clamp	50

3. Mid-Barrel Clamp	51
4. Stub Rotor	52
5. Rotor	52
6. Double Row Contact Bearing	54
7. Needle Bearing	57
8. Gun Body	60
9. Recoil Adapters	61
10. Ball Joint	63
C. BOUNDARY CONDITIONS	65
D. COMPARISON BETWEEN THE REAL AND MODELED GUN	68
V. MODES OF VIBRATION	71
A. MODES OF VIBRATION OF THE GUN BARRELS	71
B. MODES OF VIBRATION OF THE COMPLETE GUN MODEL	75
1. First Flexible Mode	78
2. Second Flexible Mode	80
3. Third Flexible Mode	83
4. Fourth Flexible Mode	84
5. Fifth Flexible Mode	85
6. Sixth Flexible Mode	86
C. MODAL TRUNCATION	86
VI. DRIVING AND DAMPING OF THE PHALANX GUN	88
A. DYNAMIC ANALYSIS OF THE GUN MODEL	88
B. DAMPING IN THE PHALANX GUN	90

C.	DRIVING THE PHALANX GUN	96
D.	RESPONSE OF THE GUN MODEL	104
E.	FREQUENCY RESPONSE FUNCTIONS	107
F.	OTHER FACTORS AFFECTING DISPERSION	111
VII.	SUGGESTIONS FOR FUTURE WORK	115
A.	REFINING THE GUN MODEL	115
1.	Muzzle and Mid-Barrel Clamps	116
2.	Gun Body Housing	117
3.	Rotor	119
4.	Stub Rotor	120
5.	Recoil Adapters	120
B.	VALIDATION OF THE MODEL THROUGH TESTING	121
C.	ADDITIONAL MODELING	122
1.	Modifying the Existing Firing Force	122
2.	Adding Additional Forces	123
3.	Additional Modeling	123
VIII.	CONCLUSIONS	126
APPENDIX A.	GUN BARREL NORMAL MODES	129
APPENDIX B.	GUN MODEL MODE SHAPES	134
LIST OF REFERENCES	173
INITIAL DISTRIBUTION LIST	176

ACKNOWLEDGEMENT

The author is grateful for the unbounded guidance and support provided by Dr. W. B. Colson and Dr. J. H. Gordis. The author would also like to thank Mike Hatch for his volunteerism and enthusiasm in making this project all that much better. Also, the author would like to thank his partner, LT Don MacNeil, who provided the drive in helping finish this work in such a short time. In addition, the author especially would like to thank his parents, Bill and Sue, who have given the author more than he could ever have asked for. Thanks also goes to the author's lifelong friends, Jon and Pam Benson, Bill Knowles and Joe Murphy for all their encouragement. Finally, the author wishes to give a special thanks to Pattie McCluskey who inspired the author during the final mile.

I. INTRODUCTION

The PHALANX Close-In-Weapon-System (CIWS) is considered to be a ship's last layer of defense against incoming missiles. The PHALANX CIWS is shown in Figure 1-1. Nearly every ship of the current 465 ship U. S. fleet has at least one of these gun mounts. For some ships, it is the only means of missile defense. Although it has been in the fleet for over a decade, it has never been tested in combat, so its effectiveness has largely been measured by either missile range tests or computer simulations. Within the past five years, there has been documented concern that this defensive weapon system may not be that effective, especially in defeating sophisticated missiles that are currently available to Third World countries. The problem of its effectiveness is attributed almost entirely to that of the gun itself and not its fire control system [Ref. 1]. At the maximum range of the PHALANX gun, the incoming missile or patrol boat presents a small cross-section. The angular dispersion of bullets leaving the gun can diminish the gun's ability to hit targets, especially as the target's size decreases, becomes more maneuverable, or increases its velocity.

As part of a class project, supervised by Professor W. B. Colson, the problems associated with the gun were illustrated in some of the best case scenarios. Specifically, a computer simulation was used to study a PHALANX engagement of an incoming anti-ship missile. The results of this class project, discussed in Chapter II, provided the motivation for this thesis.

The purpose of this study has been to use a sophisticated computer code to create a finite element model of the PHALANX gun in order to better understand its complex dynamic behavior. The Naval Postgraduate School has access to one of the most advanced finite element codes available in private industry today, called I-DEAS (Integrated Design Engineering Analysis) which is developed and

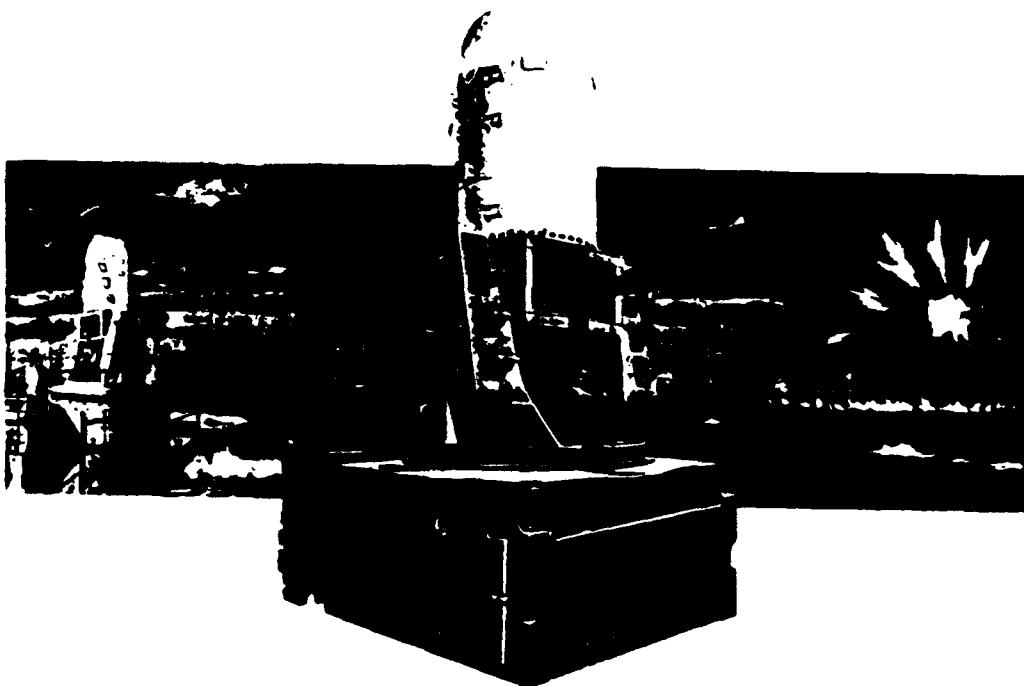


Figure 1-1. The PHALANX Close-In Weapon System [Ref. 2].

supported by SDRC (Structural Dynamics Research Corporation). The finite element model was used to predict barrel tip displacement through such causes as barrel oscillations and the coupling of the barrels to the gun mount through its bearings. In addition, the finite element model provides an important tool for the evaluation of future design changes of the PHALANX gun system. Chapter III discusses the benefits of using this type of computer code and the theory behind its development.

Chapter IV then discusses how raw data from blueprints and technical discussions with engineers familiar with the PHALANX CIWS was molded into a model of the gun. Field trips to Hughes Missile Systems Company, Pomona,

California, and the USS ARKANSAS provided further modeling information. Valuable finite element modeling experience by Mike Hatch, an expert on rotating computer disk systems and Professor J. H. Gordis, a former SDRC mechanical vibration theorist, greatly enhanced the effectiveness of the model.

In Chapter V, the normal modes of vibration are calculated for the PHALANX gun. Solving for the normal modes is an important and insightful step into understanding the dynamic response of any structure. Determining which normal modes of a structure are excited after applying particular excitation forces and setting boundary conditions ultimately determines how that structure will behave. In analogy, any color of light can be made up of the three primary colors, red, blue, and yellow. The response of any system can be defined in terms of its normal modes. The dynamic response package of I-DEAS uses modal degrees of freedom instead of physical degrees of freedom, in order to greatly reduce the dynamic response solving time.

Chapter VI discusses how these normal modes are used in a dynamic response analysis. Damping is defined for the gun system and the primary driving force of the gun while firing is applied. The resulting motion of the barrel tip, which gives a good indication of the dispersion pattern, is then displayed for each of the three translational directions. More importantly, the frequency response functions are also calculated and are used to reveal which normal modes are being excited and to what extent. Such an analysis may ultimately lead to tuning a problem mode so that its excitation is limited, and the resulting barrel tip motion is correspondingly reduced.

Recommendations for follow-on modifications of the model are listed in Chapter VII. Although the current model has been correlated in a number of ways with the real gun, it is important to refine the model further so as to enhance its accuracy while reducing its total number of degrees of freedom. By reducing the model's degrees of freedom, the computer solve time is shortened which can lead to

a smoother animation picture, thus providing better insight into its dynamic behavior. Also, if the proposed muzzle restraint and isogrid is added, it will be important to keep the model's complexity within a manageable budget.

Although the primary purpose of this study was to build and demonstrate the practical value of a finite element model of the gun, some preliminary analysis of it was performed and the results are discussed in Chapter VIII. Of key interest is the first flexible mode of vibration at 14 Hz and the double angular contact bearing and the effects they may have on the dispersion pattern.

The purpose of this study has been multi-faceted. While this computer model will be important in predicting the observed dispersion pattern, it can also serve as a program manager's tool in helping make future design decisions. Components can be swapped out with new ones, and their effect on the dynamic behavior of the gun can be predicted long before any hardware tests are actually performed. In summary, a tool of the 1990's is being used to improve 1950's technology.

II. MOTIVATION FOR STUDYING THE PHALANX GUN

A. DESCRIPTION OF THE PHALANX SYSTEM

The PHALANX Close-In Weapon System (CIWS) is a ship-based, stand alone gun mount designed to disable an incoming missile or, in a recent application, engaging fast patrol boats. It has been actively deployed for over a decade in virtually every ship of the U. S. fleet, and has had to undergo continual review and various modifications to match the ever "fluid" world threat. In that past decade, the missile it was initially designed to destroy has become faster, smaller, smarter and more maneuverable. Furthermore, the U. S. fleet has also made a transition from operating in the open, "blue water," sea to the coastal, "brown water," environment. With this change in operating areas, small speed boats, which were considered an insignificant challenge in blue water, now have exposed a weakness in surface combatants. Rather than building a new weapon system to deal with this threat, the U. S. Navy has decided to adapt the PHALANX CIWS into an anti-patrol boat mode. These two growing threats, with their decreasing radar cross-section, and increasing ability to pop-up with little notice, requires the PHALANX to move beyond its original design envelope. The primary area of concern with the PHALANX gun is to tighten its dispersion pattern to put more rounds on target, sooner and hence destroy the target at a greater range from the ship. This is the focus of this study.

Before discussing the nature of the problem, it is important to have an overall understanding of the gun system. Figure 2-1 shows a component breakdown of the PHALANX weapon system. Starting at the top, the dome structure contains an air search radar which provides the initial threat detection. It has a maximum effective range for detection greater than 4500 m (5000 yds). It provides 360

degrees, horizon to azimuth search coverage. Once a target has been identified by the search radar and the computer determines that it meets the criteria of a threat to the ship, the gun mount slews to the target bearing and transfers tracking of it to the fire control radar. This radar is mounted below the search radar, on the side of the cylindrical structure, and is physically boresighted to the gun boresight. It is a high resolution radar whose purpose is to track the target as well as the outgoing rounds. The fire control computer sends the necessary servo information to keep this tracking radar, and hence the gun, locked on target [Ref. 2].

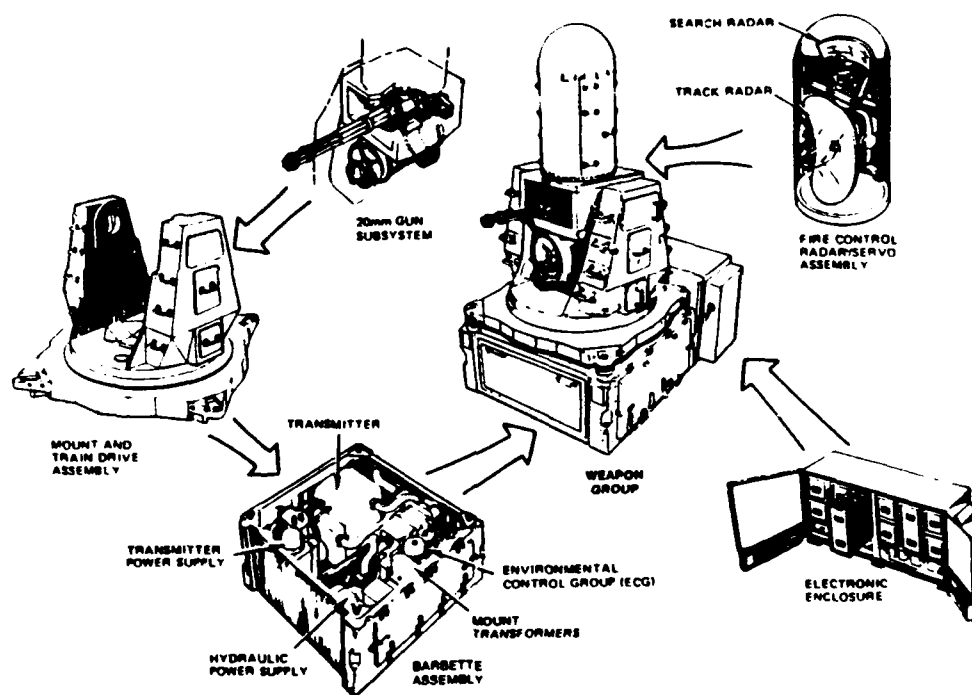


Figure 2-1. Subsystems of the PHALANX Close-in Weapon System [Ref. 2].

Below this radar is the heart of the weapon system. It is the six-barrel M61A1 gatling machine gun as shown in Figure 2-2. It fires 20 mm (0.79 in)

tungsten (formerly depleted uranium) penetrators at a velocity of 1100 m/s (3600 ft/sec). An example of a projectile is shown in Figure 2-3. The penetrators are designed to mostly maintain their shape as they hit and pass through the target. In this way, the penetrators can transfer their high momentum to the target in a concentrated manner, rather than fragment and perhaps partially reflect off the target. In experimental studies conducted at the Naval Surface Warfare Center in Dahlgren, Virginia, it takes on average six hits to destroy an incoming missile. Tests are currently being conducted against patrol boats, but no data is available yet.

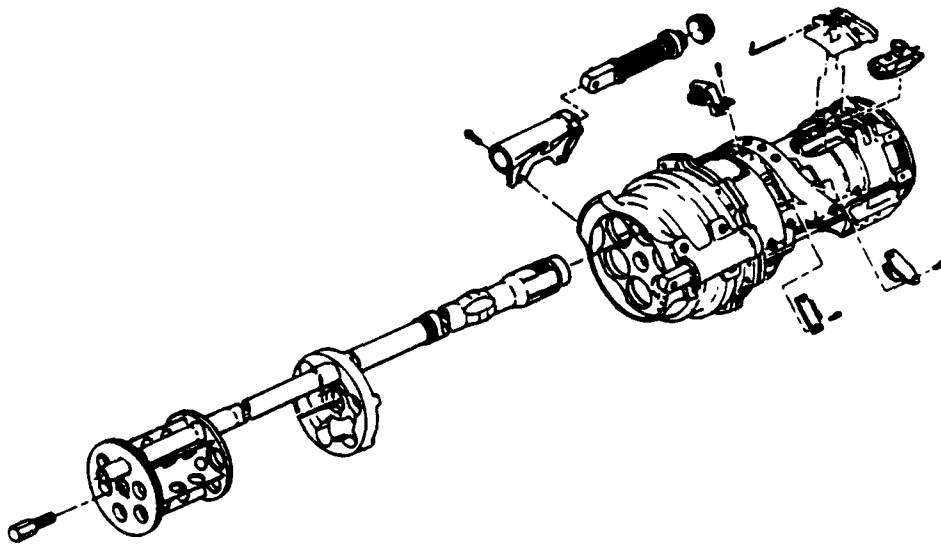


Figure 2-2. M61A1 PHALANX gatling machine gun [Ref 3.].

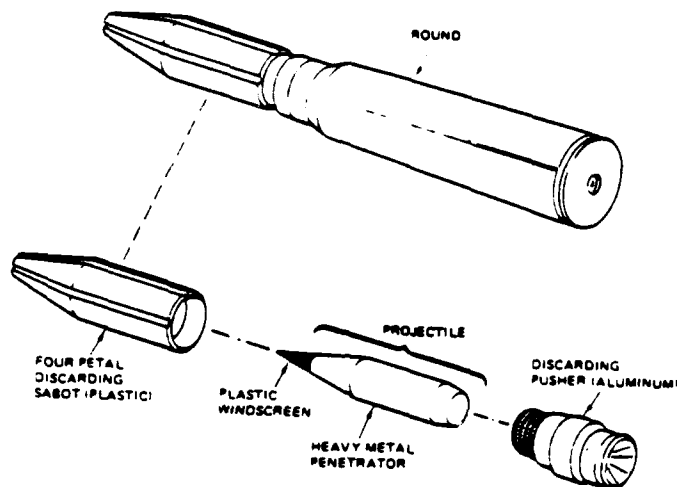


Figure 2-3. Mk 149 PHALANX round [Ref. 2].

The gun has a selectable firing rate of either 3000 shots per minute or 4500 shots per minute. A typical missile engagement can last from three to five seconds so that the higher firing rate is used more often. This means that somewhere between 225 and 375 bullets are fired at the missile. For engagements longer than five seconds, the barrels begin to deteriorate significantly due to the high barrel temperature. Therefore, this type of firing burst is strongly discouraged. The ammunition magazine is suspended below the gun and has been upgraded to hold 1500 rounds allowing for roughly three engagements. Only one barrel fires at a time near the top of the barrel group while the spent casing extraction and breech loading occurs during the rest of the rotation cycle.

The effective range of the gun is about 2000 m (2187 yds). However, the gun, after calculating the target speed, begins firing when the target is about 5 seconds from the firing cutoff point at 100 m (328 ft) from the ship. If the target is moving fast, the gun will fire so that the rounds will begin intercepting the target at 2000 m. If the target is moving slow, the gun will wait until the target is 5 seconds from the ship even though this range could be much less than the maximum 2000 m range. The firing algorithm will be different for the anti-patrol boat surface mode.

Beneath the gun is a cubical structure which houses the computer, radar electronics, and associated cooling systems. This is the brain of the system. It determines the threat, time to impact, where to point the gun, when to start firing, how to move the gun based on observing both the target and outgoing rounds, and when to cease the engagement. It is a closed-loop spotting system in that the computer receives feedback on how close the rounds are coming to the target and calculates the necessary gun movements to ensure intercept. Figure 2-4 illustrates the concept of close-loop spotting. The fire control computer calculates aim error by measuring the projectile miss angle at the target and subsequently corrects the gun's aimpoint. When the fire control computer determines that the target is destroyed, that is, when the target's speed or radar cross-section drops below a certain threshold, then the firing stops and the gun slews back to its horizontal position and resumes the search mode. For ships with two or more mounts, they are able to talk to each other in order to prevent engaging the same target. [Ref. 2]

PHALANX defines an air target as something heading towards the ship, or something that could be heading towards the ship after a 9 G turn. This precludes the possibility that the gun will shoot down the ship's own outbound missiles. The speed of the target has to be above a certain limit, so that friendly helicopters, and such, are not accidentally engaged. The PHALANX gun is designed to protect the ship on which it is mounted, so it will not attempt to defend other ships.

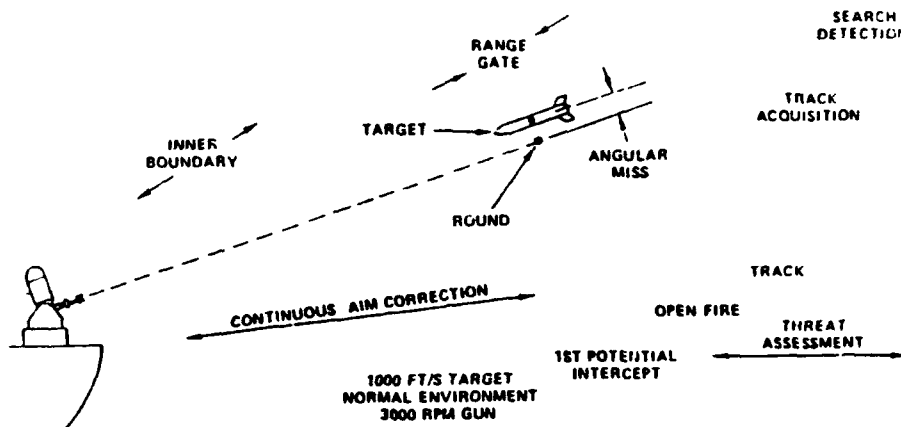


Figure 2-4. Geometry of PHALANX missile engagement [Ref. 4].

B. PHALANX ROUND DISPERSION

Based on dispersion data provided during a data gathering trip to Hughes Missile Systems Division, Pomona, California, it was learned that the PHALANX weapon system *knows* where the target is, but has had a hard time hitting it effectively as evidenced by the dispersion pattern shown in Figure 2-5. Here, one can see the six individual barrel dispersion patterns, which are generally good individually. However, the target is the object at the center of this particular dispersion pattern where virtually no rounds have fallen. The fire control system is doing its job by keeping the target at the center of the gun's dispersion pattern. It appears that much of the dispersion can be associated with the six barrel-gun

system. To elaborate on dispersion, Figure 2-6 shows the geometry used to define dispersion. The probability of a penetrator passing through a circle of radius r and standard deviation σ is given by the distribution,

$$p(r) = \frac{e^{-\frac{r^2}{2\sigma^2}}}{2\pi\sigma^2} \quad (2.1)$$

It is assumed that all the penetrators pass through a circle of infinite radius, so that,

$$\int_0^{2\pi} \int_0^\infty r p(r) dr d\theta = 1 \quad (2.2)$$

The probability that a penetrator will pass within a circle of radius one σ , $P_{<\sigma}$, can be determined by integrating equation (2.1) in polar coordinates from $r=0$ to $r=\sigma$,

$$\begin{aligned} P_{<\sigma} &= \int_0^\sigma \int_0^{2\pi} p(r) r dr d\theta \\ &= \int_0^\sigma \frac{e^{-r^2}}{2\sigma^2} r dr 2\pi \end{aligned} \quad (2.3)$$

Simplifying and solving the equation yields,

$$\begin{aligned} P_{<\sigma} &= \int_0^{1/2} e^{-z} dz \\ &= \left[-e^{-z} \right]_0^{1/2} \\ &= -e^{-1/2} + 1 = 0.39 \end{aligned}$$

Therefore, 39 percent of the penetrators fall within one σ while 61 percent fall outside. In the dispersion example of Figure 2-6, 39 percent of the penetrators of a PHALANX gun will pass within a circle of one $\sigma = 1.2$ milliradians. Part of the dispersion (~1 milliradian) can be attributed to spin induced yaw after the bullet leaves the barrel. But, a significant part of the dispersion is directly attributed to

barrel tip motion. The observed 2.4 milliradians of dispersion corresponds to 3.6 mm of barrel tip displacement of a 1.52 m (59.8 in) long barrel.

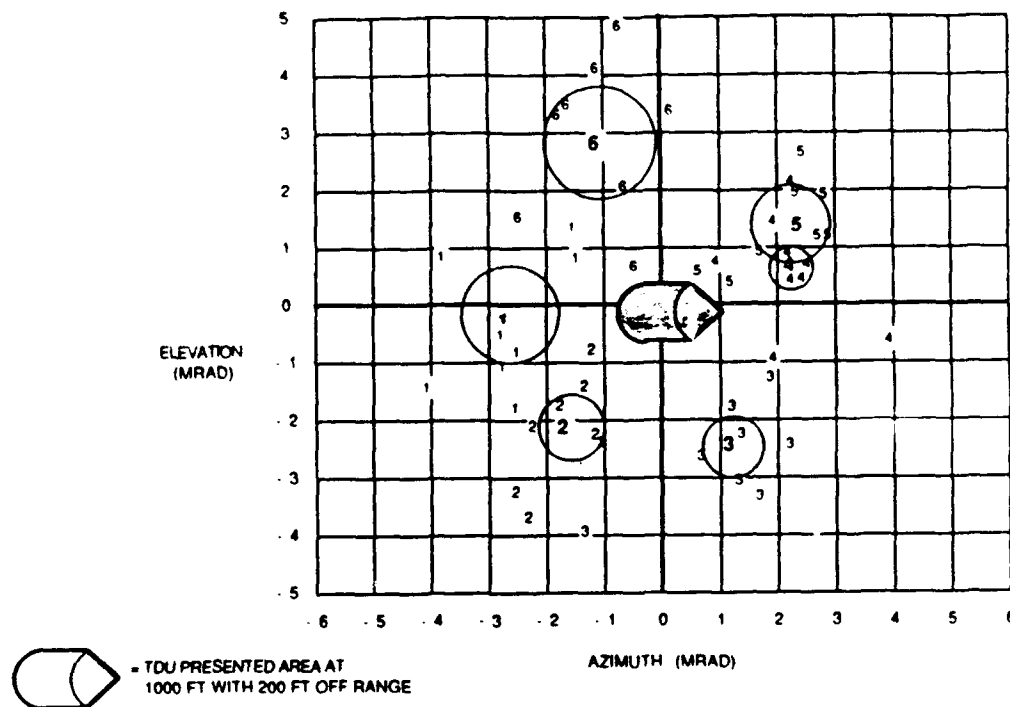


Figure 2-5. Experimental dispersion pattern of the PHALANX gun. Note that the target drone is at the center while the individual barrel dispersion patterns fall all around it [Ref. 3].

Other dispersion patterns shown in Figure 2-7 show a less pronounced doughnut-shaped pattern than in Figure 2-5, but it is still generally visible, with the target remaining unscathed in the center. The dispersion patterns were measured using an Oehler and battenboard system at a test facility in China Lake as shown in Figure 2-8. An Oehler system consists of a set of four microphones which will listen for the acoustic shock wave of the passing supersonic projectile. The arrival time of each microphone is compared with the other microphones and a

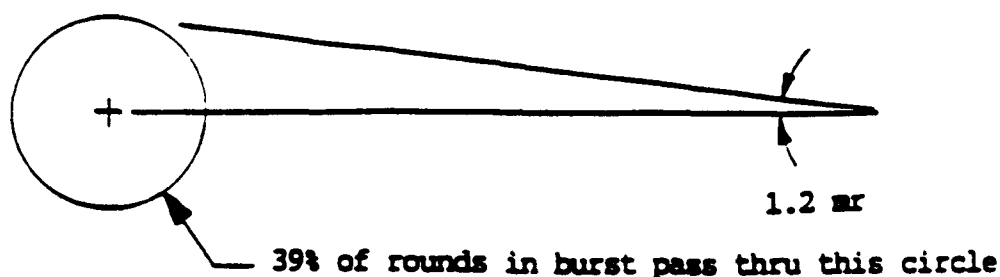


Figure 2-6. Illustration of radial dispersion as defined for the PHALANX gun [Ref. 3].

bullet position is calculated. The battenboard follows the Oehler system and is used to record the round pattern and to distinguish between the pusher plugs, which drive the round through the barrel (see Figure 2-3), and the rounds themselves. This observation set-up was designed to test the gun dispersion and not that of the ammunition.

The PHALANX dispersion pattern measurements also show that the six-barrel system gives a dispersion pattern greater than that of a single barrel fired separately. Thus, the structural dynamics of the six-barrel system appears to warrant an in-depth analysis. According to the Hughes data, the PHALANX gun system has a typical dispersion range of 1.2 to 1.5 milliradians and a maximum of

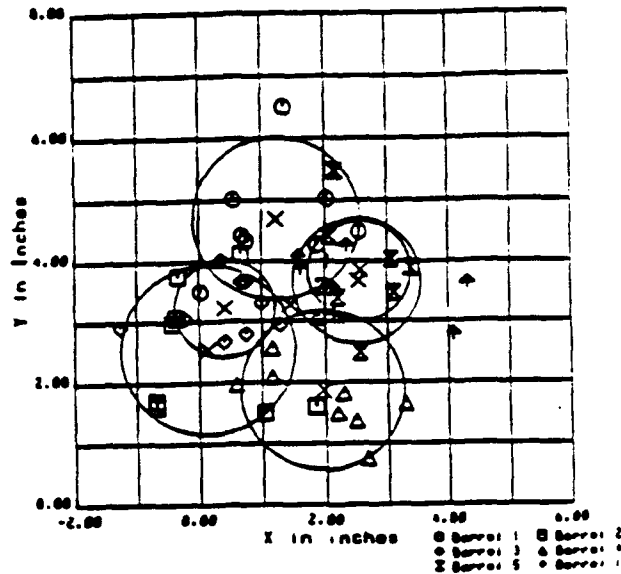


Figure 2-7. A less pronounced circular PHALANX dispersion pattern [Ref 3].

1.6 milliradians. The U. S. Navy would like to achieve an average dispersion of less than 1.2 milliradians. In order to achieve this goal, the dynamics of the gun system will have to be better understood before any type of fix can be fully implemented. This is the premise behind this study. What effect the observed dispersion has on target destruction is the subject of the next section and was the motivation for undertaking this project.

Dispersion Test Set-Up

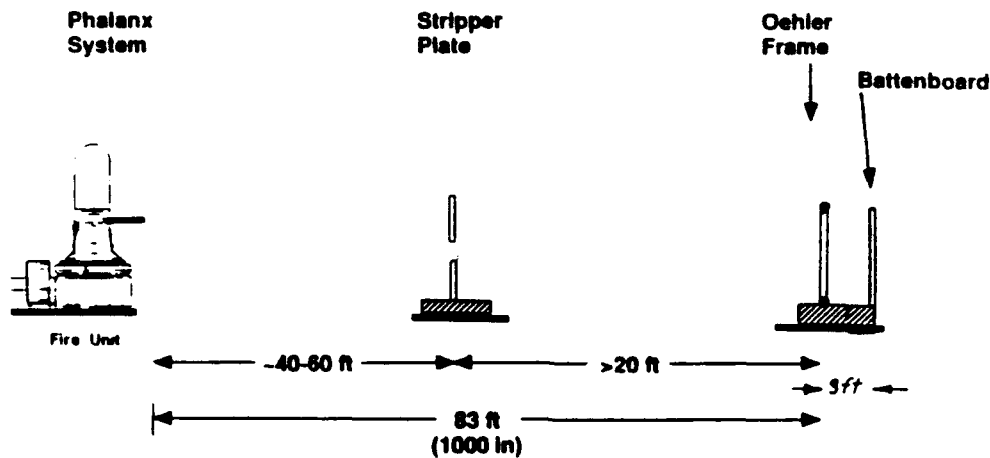


Figure 2-8. Experimental set-up for observing the PHALANX dispersion patterns [Ref. 3].

C. THE BALLISTIC DEBRIS PROBLEM

Although the maximum effective range of the PHALANX gun is 2000 m, field and computer simulations have shown that the destruction of an incoming missile does not occur, if at all, until after the missile is within 1000 m (3281 ft) of the ship. On the surface this does not appear to be a problem. As part of a class computer simulation project, the resulting debris from the destroyed missile continues on a ballistic trajectory toward the ship at roughly the speed of the missile. The fragment sizes, which can be on the order of a few to a hundred pounds, coupled with their high velocity, which is typically from 1000 m/s to 1500 m/s, would cause a great deal of damage to an unarmored superstructure which

usually houses sensitive electronics, antennas and not to mention sailors. Metallic particles at 1000 m/s would easily punch holes through several bulkheads before being stopped. Although the PHALANX gun "worked" in destroying the missile, the ship would still suffer tremendous damage. A solution to this problem would be to obviously destroy the missile at a greater distance from the ship. In order to achieve this goal the dispersion pattern would have to be tightened so more hits occurred at near the beginning of the PHALANX engagement rather than at the end.

To clarify these points further, a computer simulation is used to describe fragment trajectories. In this model, a missile is assumed to be destroyed after one or several of the PHALANX rounds detonates the warhead of the missile. The range at which this detonation occurs is varied so that the number of fragments that hit the ship can be determined. The fragment size, shape and mass is approximated by distributing the fragment terminal velocities by the exponential distribution,

$$p(v_t) = \frac{e^{-\frac{v_t}{\sigma_t}}}{\sigma_t} \quad , \quad (2.4)$$

where v_t is a fragment terminal velocity, and σ_t is the characteristic terminal velocity which is derived from typical fragment attributes. The terminal velocity is calculated by the expression

$$v_t = \sqrt{\frac{2mg}{C\rho A}} \quad , \quad (2.5)$$

where m is the mass of the fragment, g is the acceleration of gravity, C is the coefficient of air drag, ρ is the density of air and A is the debris fragment surface area. Additional velocity components caused by the force of the explosion are assigned to the fragments along each of the three coordinate axes. These velocities are determined from a Gaussian distribution with a standard deviation of σ_v in

each direction. The value of $\sigma_v = 10$ m/s was provided by the Naval Surface Warfare Center, Dahlgren. When the values of the variables described above are entered into the simulation program, the results appear like that of Figure 2-9. This figure shows a typical best case scenario where the missile blew up at the maximum PHALANX range of 2000 m. It is divided up into a side view, top view, and an end view showing how the missile disintegrates as viewed from the ship. The missile is destroyed at the left most edge in the top and side views. The "ship" is represented as the right hand edge of these views. The black dots are the missile debris fragments and the black lines represent their trajectories. The "ocean" is at the bottom edge of each view. It is easy to record ship hits as those that reach the right hand edge. In this particular case, the missile was traveling at a fast speed of $v_m = 1000$ m/s (3281 ft/s) and a height of 10 m above the water when it exploded. NF stands for the number of fragments. Here 6 missile fragments hit the ship with a velocity of around 100 m/s (328 ft/s).

In Figure 2-10, the missile has the same characteristics, but now does not explode until it is intercepted by the last PHALANX bullet at a range $R = 500$ m (1641 ft) from the ship. The resulting debris hits the ship in a "shotgun blast" pattern where 18 of the 20 fragments reach the ship. This latter case is the more likely of the two scenarios for a nonmaneuvering, medium speed missile [Ref. 5].

If the missile was more sophisticated in that it "jinked," or performed random maneuvers, or if it had a higher speed, then the intercept range is even more reduced. Therefore, it is readily apparent that significant debris from an effectively engaged missile is going to hit the defending ship in virtually every case. Such debris would certainly not destroy the ship, but might seriously impair her ability to fight.

In other simulations, performed by Professor W. B. Colson, at the Naval Postgraduate School, the effectiveness of the gun in destroying an incoming missile is tested. In this simulation, the round dispersion is assumed to have a Gaussian

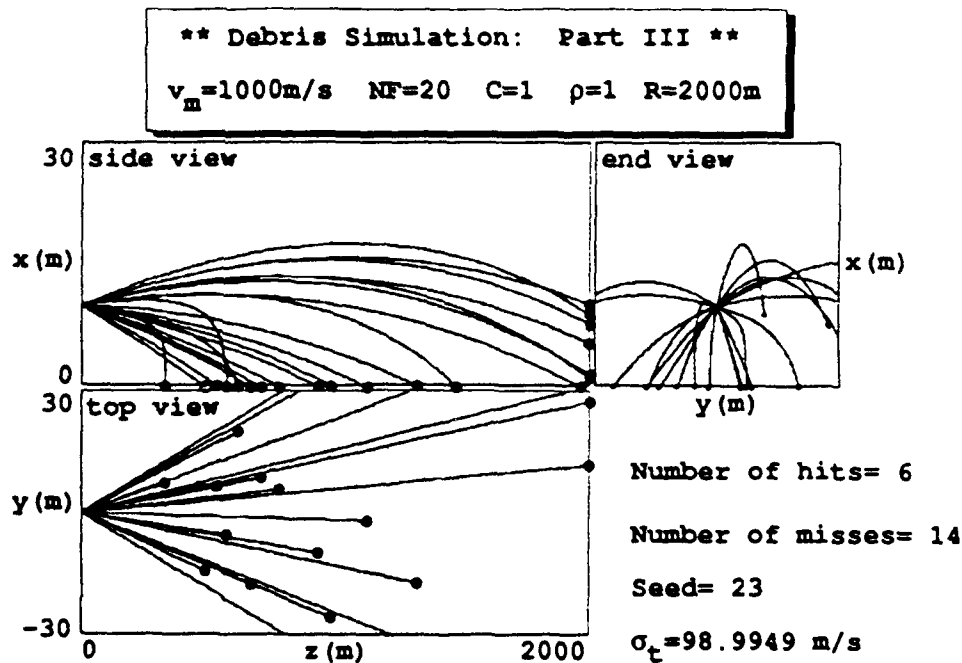


Figure 2-9. Trajectories of fragments of a missile destroyed by a PHALANX gun at a range $R = 2000 \text{ m}$. Notice 6 of the 20 missile fragments hit the ship which is at the right hand edge of each view.

distribution with a standard deviation using a typical PHALANX dispersion value of $\delta\theta = 2$ milliradians. Figure 2-11 shows the results of a PHALANX engagement with an incoming missile which has a speed of $v_m = 600 \text{ m/s}$ (1969 ft/s) and a physical cross-section of 0.20 m (7.9 in). In this scenario, the missile speed is not unusual, but it does begin a terminal 5 G maneuver at a range of roughly 2000 m (6562 ft). The PHALANX gun destroys the missile at a range of roughly 200 m (656 ft) after it was only hit three times. The number of hits required to destroy the missile is chosen randomly and is better than the usual six. The effect of the

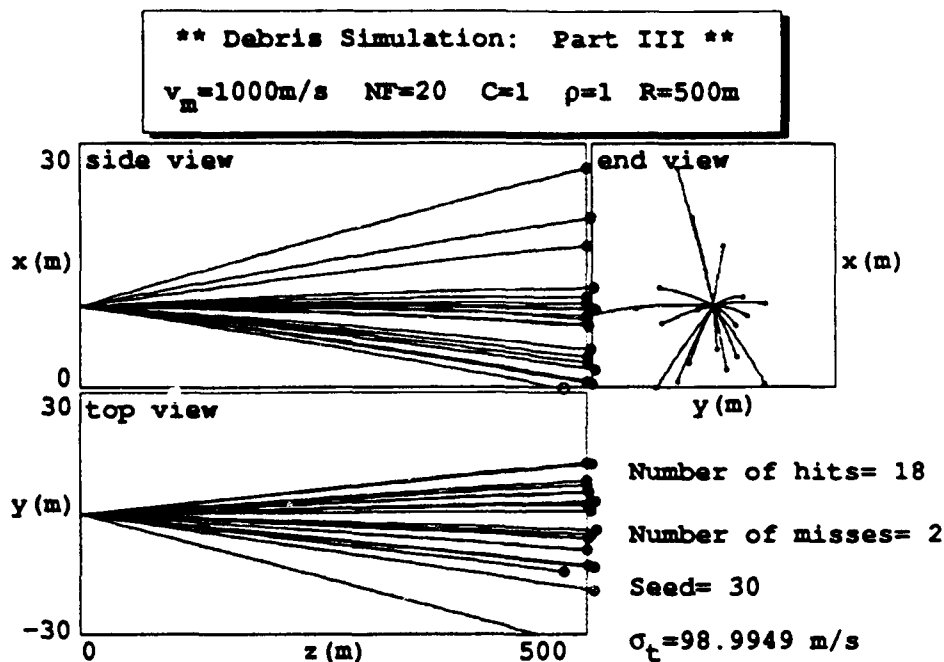


Figure 2-10. An incoming missile is destroyed by the PHALANX gun at a range of 500m. Most of its debris hits the ship.

maneuver was to allow the missile to penetrate to within 200 m of the ship when it exploded and sends almost all of its debris at the ship.

Another engagement is shown in Figure 2-12 where the missile does not have a terminal maneuver, but has a higher speed of 800 m/s (2625 ft/s). In this case, the missile is also destroyed, but like before, it is not destroyed far enough away from the ship so all of its debris strikes the ship. [Ref. 5]

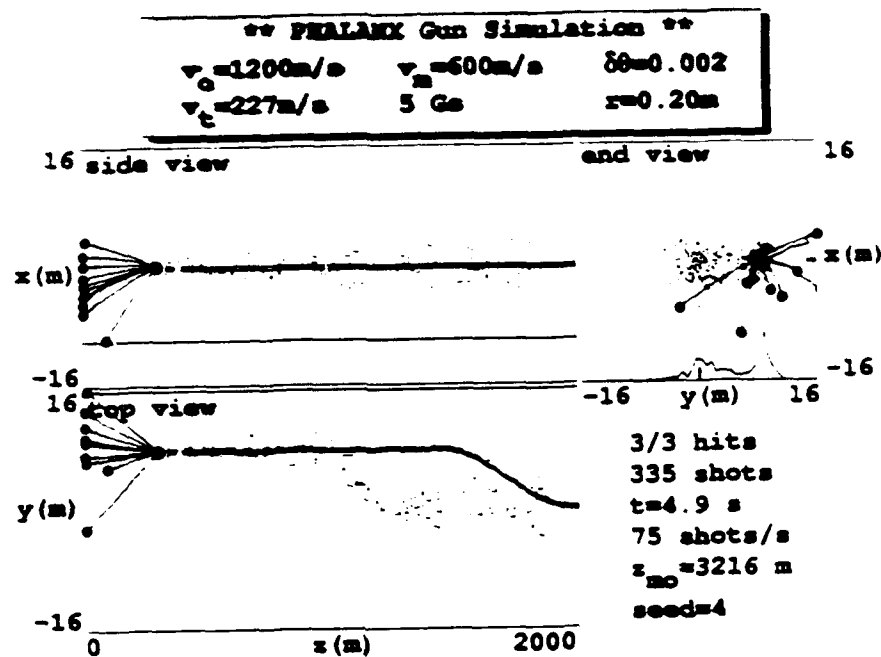


Figure 2-11. A terminal missile maneuver defeats the PHALANX gun [Ref. 5].

These studies provided the motivation for trying to improve the dispersion of the PHALANX gun. In order to make such improvements, the gun dynamics have to be first understood. This study attempts to provide a solid foundation upon which to study the gun. In an era of reduced defense spending, but not necessarily one of reduced potential for hostilities, the PHALANX gun is going to remain a ship's last layer of defense into the next century.

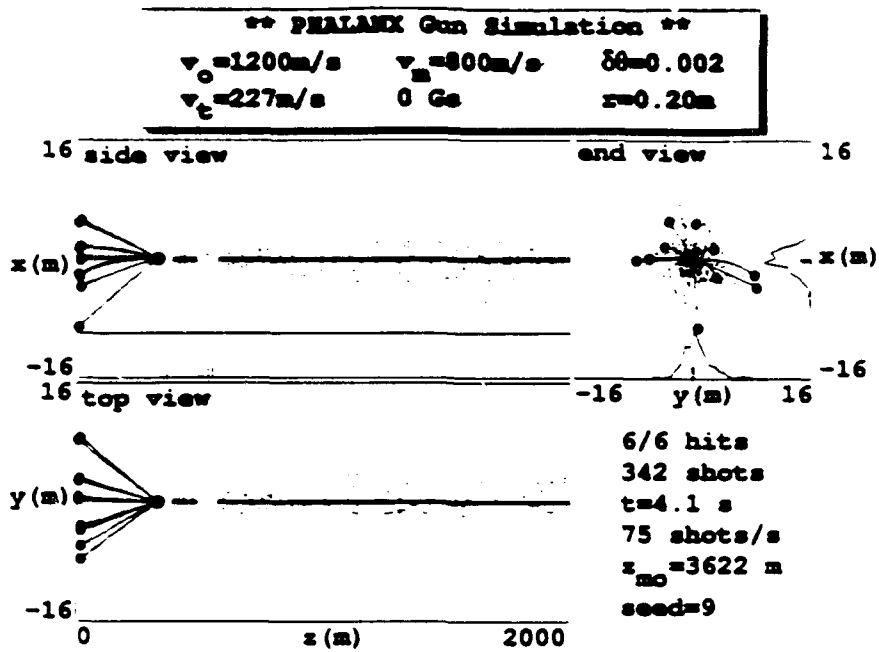


Figure 2-12. A high speed, nonmaneuvering missile defeats the PHALANX gun [Ref. 5].

III. FINITE ELEMENT THEORY

A. THE DECISION TO USE FINITE ELEMENT MODELING

In order to investigate the mechanical dynamics behind the dispersion of the PHALANX six-barrel system and to study the various design factors which influence projectile trajectory and accuracy, it was decided that a finite element computer model would be the best method for gaining insight into this complex system. Many aspects of the gun dynamics would have been difficult if not impossible to understand by studying the gun itself during its operation due to its high rate of fire and extremely high barrel temperatures as well as with problems of on-sight availability. Even high speed film does not provide as much benefit or nearly the flexibility as a computer model. A finite element analysis can provide a thorough model of the gun where various driving forces can be applied and the gun's response, such as barrel tip motion, calculated. This also allows individual components to be studied in detail to understand their affect on the overall dispersion pattern. Furthermore, this finite element computer model is adaptable enough to support redesigning the PHALANX barrels and perhaps the thrust bearing, as well as further modifications, such as a change in projectile size or the addition of a gun barrel restraint. Finally, a computer code provides an economical solution by leapfrogging past design changes made possible by computer simulation instead of expensive hardware tests.

The finite element computer code called I-DEAS (Integrated Design Engineering Analysis) developed by SDRC (Structural Dynamics Research Corporation) was chosen to model the PHALANX gun due to its existing on-site license with the Naval Postgraduate School and its "completeness." That is, it precluded the need for other software packages allowing for a much smoother

transition between model construction and testing. I-DEAS is made up of the following set of modules: Solid Modeling, Drafting, Finite Element Modeling and Analysis, System Dynamics, Test Data Analysis, and Manufacturing. This study uses a two-step approach. The first step uses the Finite Element Modeling and Analysis Module to develop a finite element model of the gun. This module allows normal modes, stresses, and static deflections to be calculated after the structure's material properties and loads are defined. In the second step, the completed finite element model is transferred to the System Dynamics Analysis module where an in-depth forced response analysis is then performed.

The primary purpose behind the finite element modeling of the PHALANX gun is to better understand some of the causes behind the apparent dispersion pattern. Specifically, barrel tip displacement plays a critical role in the dispersion. One of the best ways to predict the motion of a system while being excited is to first solve for its *normal modes*. Normal modes of vibration have the useful property of being able to describe *any* complex motion (due to arbitrary initial conditions) as a superposition of normal mode amplitudes. So what are normal modes of vibration? Briefly, every structure, with its inherent mass and stiffness, has its own distinctive set of normal modes. A structure vibrating at one of its natural frequencies does so with a characteristic pattern of amplitude distribution called a normal mode of vibration. A more mathematical explanation will be provided as the theory behind finite elements unfolds in this chapter. After modeling a structure as a series of finite elements and connecting points, or nodes, the computer code solves for these normal modes of vibration. Then, this model with its normal modes is transferred to the Systems Dynamics Analysis module where excitation forces and damping can be applied. The response, such as barrel tip displacement, can then be calculated. A fourier transform of the time response, which performs a transient integration, estimates which normal modes are excited and their relative degrees of excitation. This same information can be revealed

using a frequency response function which is the method presented in Chapter VI. This latter method has the added benefit of not requiring a fourier transform. The resulting dispersion could then be modified, for example, by *tuning* these normal modes to different frequencies.

The finite element method provides a discrete representation of a dynamical system [Ref. 6]. It involves the systematic solution of partial differential equations allowing the structural analysis of the complex systems to be easily performed by digital computers. Developed in the late 1950's, it has been made more accessible with the advent of powerful desktop computers. It is especially useful for structures that contain a large number of degrees of freedom, where a variety of materials are used or where discontinuities such as thickness variations, holes, or curved beams are present [Ref. 7]. These types of structures make exact solutions virtually impossible.

The finite element method breaks down a structure into simple, discrete pieces such as beams, plates, or bricks, each of which is responsible for carrying some portion of the load applied to the structure. The equations describing the motion or elasticity of these discrete elements can be solved individually with boundary conditions matched at their nodal points to get the overall dynamic response of the structure. The calculated solution is not exact, but, with good modeling practice the error can be reduced to tolerable levels. Moreover, there is no other way to solve the problem. For displacement based finite element modeling, the error decreases monotonically. The finite elements and nodes are assembled to correspond as close as possible to the geometry of the actual structure being modeled. More elements are assembled in areas where the greatest stress gradient or curvature is expected or where the greatest accuracy of solution is needed. This often leads to a trade-off between computational speed and computer storage on the one hand and the necessary accuracy on the other.

B. THE DISCRETIZATION OF A SIMPLE ROD

As an illustration of the finite element method, consider a single rod element of length L as shown in Figure 3.1 below. It has a node at each end point whose coordinates in the element's local coordinate system (x,y) are $x = 0$ for node 1 and $x = L$ for node 2. This element is situated in a global coordinate system (x,z) which would be used to describe a structure of elements.

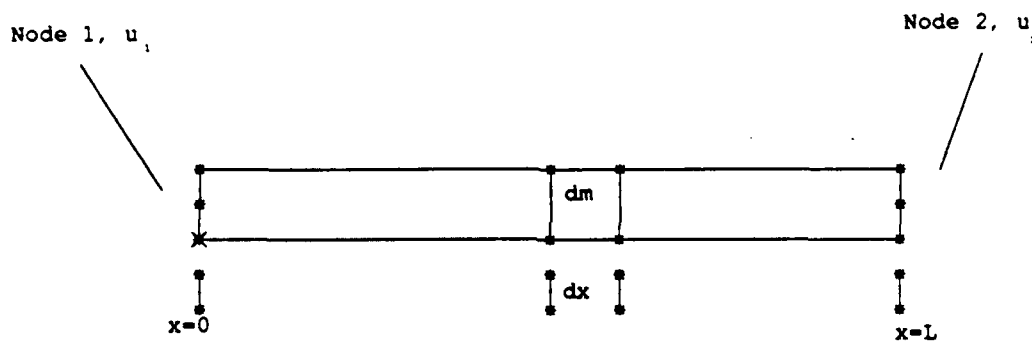


Figure 3-1. A single rod element.

To structurally represent the rod's continuous distribution of mass, it will be broken down into an infinite number of discretized mass units dm . These mass units are then idealized by tracking their positions to the coordinates at the end of

the rod, specifically its nodes. Finally, an axial force is applied to the element along the rod's local x - axis which will cause an axial deformation.

In order to investigate the forces and displacements of this rod element it will be beneficial to use a displacement field variable ($u = u(x,t)$) to describe the positions of the nodes at any instant in time. This is important since it is at these node points that the rod element is coupled to the rest of the structure. Any load information transmitted from the rest of the structure is applied to the rod element at its nodes. Therefore, the response anywhere along the rod can be described in terms of the response at the element's endpoints, that is, its nodal degrees of freedom, which are finite. This is a finite discretization of an infinite element system. An exact solution of the displacement field is difficult considering that the force and moment distribution as well as the boundary conditions at the ends of the rod are not known. However, an approximation can be made by considering a finite number of degrees of freedom for the displacement fields of each element [Ref. 7]. The coordinates for nodes 1 and 2 at any instant in time are respectively,

$$u_1 = u(0,t) \quad (3.1)$$

and

$$u_2 = u(L,t) \quad (3.2)$$

Since the load is an axial force, only displacements along the local x - axis are considered, so the rod deformation can be described by these two displacement degrees of freedom, u_1 and u_2 .

The displacement field is a linear motion in x since there are two axial degrees of freedom [Ref. 7]. It is written as

$$u(x,t) = c_1 + c_2 x \quad (3.3)$$

where c_1 and c_2 are unknown constants. Substituting equation (3.3) into equations (3.1) and (3.2) yields

$$u_1 = c_1 \quad (3.4)$$

$$u_2 = c_1 + c_2 L \quad , \quad (3.5)$$

which forms a system of simultaneous equations

$$\begin{bmatrix} 1 & 0 \\ 1 & L \end{bmatrix} \begin{bmatrix} c_1 \\ c_2 \end{bmatrix} = \begin{bmatrix} u_1 \\ u_2 \end{bmatrix} \quad , \quad (3.6)$$

where

$$\begin{bmatrix} 1 & 0 \\ 1 & L \end{bmatrix}^{-1} = \frac{1}{L} \begin{bmatrix} L & 0 \\ -1 & 1 \end{bmatrix} \quad . \quad (3.7)$$

Solving for the c_i coefficients gives

$$c_1 = u_1 \quad (3.8)$$

and

$$c_2 = \frac{(-u_1 + u_2)}{L} \quad . \quad (3.9)$$

Substituting equations (3.8) and (3.9) into equation (3.3)

$$\begin{aligned} u(x,t) &= u_1 - \frac{u_1 x}{L} + \frac{u_2 x}{L} \\ &= \left[1 - \frac{x}{L} \right] u_1 + \left[\frac{x}{L} \right] u_2 \\ &= \alpha_1(x) u_1(t) + \alpha_2(x) u_2(t) \quad , \end{aligned} \quad (3.10)$$

where

$$\alpha_1(x) = 1 - \frac{x}{L} \quad , \quad (3.11)$$

and

$$\alpha_2(x) = \frac{x}{L} \quad , \quad (3.12)$$

or in matrix notation

$$u(x,t) = \left\{ \alpha \right\} \begin{bmatrix} u_1 \\ u_2 \end{bmatrix} , \quad (3.13)$$

where

$$\left\{ \alpha \right\} = \left\{ \alpha_1(x) \quad \alpha_2(x) \right\} . \quad (3.14)$$

The response anywhere along the rod can now be described in terms of the nodal coordinates and the *interpolation* functions or *shape functions* $\alpha_i(x)$. These functions interpolate the element displacement between the nodes according to the boundary conditions and movement of the nodes. They also form a basis set where any motion of the rod can be described as a linear combination of these shape functions.

The boundary conditions defined earlier (see Figure 3-1) for the element impose the following requirements on the shape functions, α_i :

$$\alpha_1(0) = 1 \quad \alpha_2(0) = 0 \quad (3.15)$$

$$\alpha_1(L) = 0 \quad \alpha_2(L) = 1 \quad , \quad (3.16)$$

where each shape function represents the element shape when a unit displacement is applied. Looking at Figure 3-2, it is apparent that the shape functions can now be written explicitly as

$$\alpha_1(x) = 1 - \frac{x}{L}$$

$$\alpha_2(x) = \frac{x}{L} .$$

The shape functions do not give an exact solution of the displacement field between the nodes, but as the number of elements are increased along the length of the rod a better solution is obtained. Referring to Figure 3-3, an exact solution of the displacement field can be written as

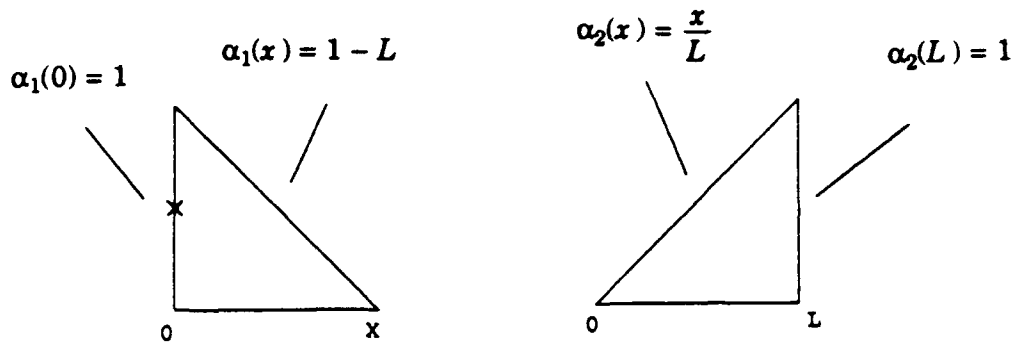


Figure 3-2. Shape functions α_i .

$$\begin{bmatrix} x' \\ y' \end{bmatrix} = x' \begin{bmatrix} 1 \\ 0 \end{bmatrix} + y' \begin{bmatrix} 0 \\ 1 \end{bmatrix} \quad , \quad (3.17)$$

where x' and y' are the coordinates of a point P along the length of the rod and the quantities $\begin{bmatrix} 1 \\ 0 \end{bmatrix}$ and $\begin{bmatrix} 0 \\ 1 \end{bmatrix}$ are the basis vectors. Therefore, any point along the length of the continuous rod can be described in terms of the basis vectors. However, it is the quantities x' and y' which are unknown and must be determined according to the motion of its endpoints. This is a linear assumption that is only valid if the transverse displacement is small, that is, $x/L \ll 1$.

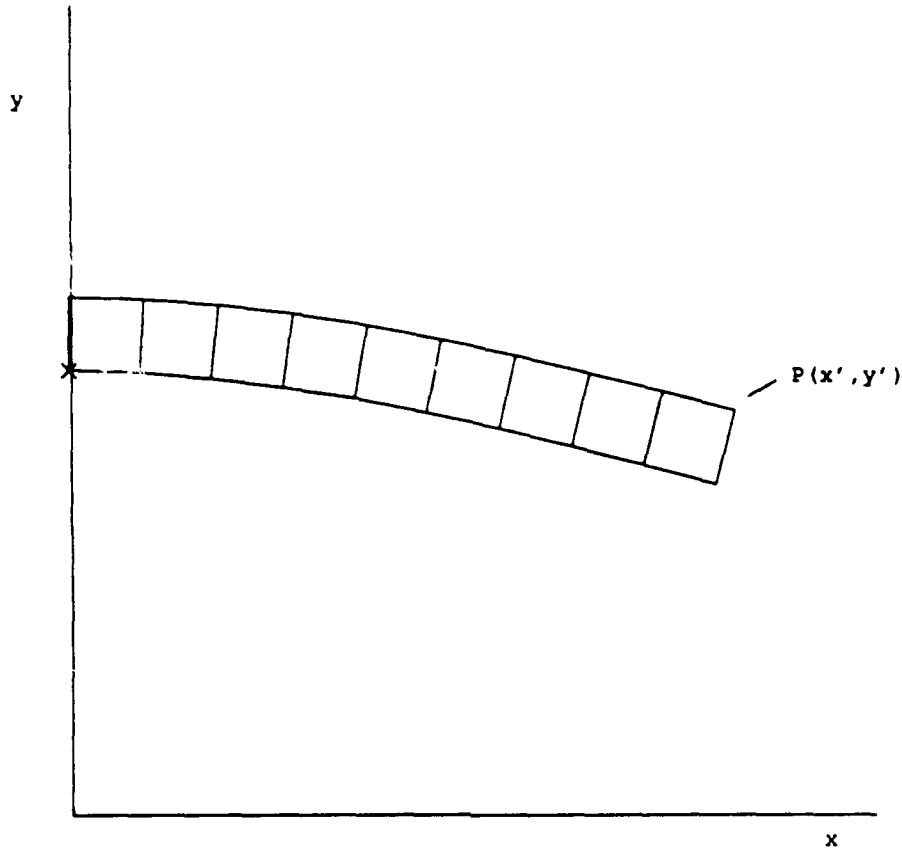


Figure 3-3. Diagram of a point P along a deformed rod.

C. MATRIX FORM OF EQUILIBRIUM EQUATIONS

Since each normal mode of vibration is made up of the periodic exchange of kinetic and potential energies within the structure, it is necessary to determine the kinetic and potential energies for each element [Ref. 8]. Specifically, the mass and stiffness matrices of the element can be deduced after applying Lagrange's equation to the internal kinetic and potential energies. In the case of the rod, its kinetic energy T and strain energy U are respectively

$$T = \frac{\gamma}{2} \int_0^L [\dot{u}(x, t)]^2 dx \quad (3.18)$$

$$U = \frac{EA}{2} \int_0^L \left[\frac{du(x, t)}{dx} \right]^2 dx \quad , \quad (3.19)$$

where γ is the density per unit length and E is Young's modulus of elasticity and it is assumed that the rod is uniform with a constant cross-sectional area A . The strain energy occurs due to any axial elongation of the rod where $du(x,t)/dx$ is its corresponding strain rate of change.

Differentiating equation (3.10) with respect to time yields

$$\dot{u} = \alpha_1(x)\dot{u}_1(t) + \alpha_2(x)\dot{u}_2(t) \quad (3.20)$$

and with respect to x gives

$$\frac{du}{dx} = \alpha'_1(x)u_1(t) + \alpha'_2(x)u_2(t) \quad (3.21)$$

Now substituting these expressions back into equations (3.18) and (3.19) defines the rod's internal kinetic and potential energies respectively as

$$T = \frac{\gamma}{2} \int_0^L [\alpha_1(x)\dot{u}_1 + \alpha_2(x)\dot{u}_2]^2 dx \quad (3.22)$$

$$U = \frac{EA}{2} \int_0^L [\alpha'_1(x)u_1 + \alpha'_2(x)u_2]^2 dx \quad (3.23)$$

The equations of motion can be derived from T and U by applying Lagrange's equation. It is defined as

$$\frac{d}{dt} \left(\frac{\partial L}{\partial \dot{q}_i} \right) - \frac{\partial L}{\partial q_i} = 0 \quad , \quad (i = 1, 2, 3, \dots, n) \quad (3.24)$$

where L is the Lagrangian of the system. For conservative systems, where the sum of potential and kinetic energies remains constant, and mechanisms of energy loss such as internal friction are ignored, the Lagrangian is the difference between kinetic and potential energies:

$$L = T - U \quad (3.25)$$

It is important to note that damping as a form of energy loss can be added into the equations of motion later (see Chapter VI). The generalized coordinates q_i ($i=1, 2, 3, \dots, n$) describe the configuration of the system, with n degrees of freedom

and hence n equations [Ref. 9]. In the case of the rod element, the generalized coordinates are

$$q_1 = u_1 \quad q_2 = u_2 \quad ,$$

so that

$$\begin{bmatrix} q \end{bmatrix} = \begin{bmatrix} u_1 \\ u_2 \end{bmatrix} \quad . \quad (3.26)$$

Now applying Lagrange's equation

$$\frac{\partial T}{\partial \dot{u}_1} = \gamma \int_0^L [\alpha_1(x) \dot{u}_1 + \alpha_2(x) \dot{u}_2] \alpha_1(x) dx \quad (3.27)$$

$$\frac{\partial U}{\partial u_1} = EA \int_0^L [\alpha'_1(x) u_1 + \alpha'_2(x) u_2] \alpha'_1(x) dx \quad . \quad (3.28)$$

Therefore, the element mass matrix coefficients can be written as

$$m_{ij} = \gamma \int_0^L \alpha_i(x) \alpha_j(x) dx \quad , \quad (3.29)$$

and the stiffness coefficients matrix as

$$k_{ij} = EA \int_0^L \alpha'_i(x) \alpha'_j(x) dx \quad . \quad (3.30)$$

So the equations of motion can be written in the familiar Newtonian mechanical forms

$$\begin{bmatrix} F_1 \\ F_2 \end{bmatrix} = \begin{bmatrix} k_{11} & k_{12} \\ k_{21} & k_{22} \end{bmatrix} \begin{bmatrix} u_1 \\ u_2 \end{bmatrix} \quad , \quad (3.31)$$

$$\begin{bmatrix} F_1 \\ F_2 \end{bmatrix} = \begin{bmatrix} m_{11} & m_{12} \\ m_{21} & m_{22} \end{bmatrix} \begin{bmatrix} \ddot{u}_1 \\ \ddot{u}_2 \end{bmatrix} \quad . \quad (3.32)$$

It is important to note that equations (3.29) and (3.30) have the general quadratic form with n variables q_i of the type

$$\sum_{i=1}^n a_{ij} q_i q_j \quad , \quad (3.33)$$

where the a_{ij} (i.e. γ and EA) are coefficients independent of q_i [Ref. 9]. This form is diagonal if it contains terms with squares of q_i namely $a_{11}q_1^2$, $a_{22}q_2^2$, etc., but no cross terms like $a_{12}q_1q_2$ [Ref. 9].

However, if there are cross terms in either the mass or stiffness matrices, then there are a set of n *coupled* differential equations which describe the motion of the system. In the physical sense, this means that the motion of one node influences the motion of the other through these coupling terms. They are linearly independent. So the problem now is to simultaneously diagonalize the mass and stiffness matrices if they are not already diagonalized. It is possible to excite a normal mode of one node without exciting any other modes. The set of vectors that diagonalize the modal matrix are called "normal modes." This diagonalization is achieved by performing a linear transformation involving the orthogonal modal matrix ϕ , whose columns are the eigenvectors of the matrix K with respect to M of the eigenproblem

$$(K - \omega^2 M)\phi = 0 \quad . \quad (3.34)$$

Once the matrices are diagonalized, and hence uncoupled, then the n equations of motion are easily solved for less than n , rather than solving for n coupled (simultaneous) differential equations, and more importantly, each uncoupled differential equation is one of the normal modes. This process is called a transition to normal coordinates. It is important to note that the physical nature of the problem has not been changed, rather, the normal coordinates merely capture the physical configuration of the system so as to greatly simplify the mathematical description of the system.

D. FREE VIBRATION IN A STRUCTURE OF ELEMENTS

Now that the equations of motion of a single rod element are understood, a whole structure can now be composed of elements like these. The equation of motion for an assembly of element matrices is

$$[M] \ddot{\underline{x}} + [K] \underline{x} = 0 \quad , \quad (3.35)$$

where $[M]$ and $[K]$ are square matrices and the quantities with a single underline imply a column matrix. As an example, if the original continuous rod is represented by eight connected elements instead of one, as shown in Figure 3-4, each one with its own 2×2 stiffness matrix, K_i , then the equation of motion would appear as

$$[F] = \begin{bmatrix} [K_1] & . & . & . \\ . & [K_2] & . & . \\ . & . & . & . \\ . & . & . & [K_8] \end{bmatrix} \begin{bmatrix} u_1 \\ u_2 \\ . \\ u_8 \end{bmatrix} \quad , \quad (3.36)$$

where each element stiffness matrix, K_i , has an overlapping stiffness with adjacent elements at their common degrees of freedom.

The general method for solving the free vibration problem, that is, finding the eigensolution of (3.35) is to use a solution of the form

$$\underline{x}(t) = C \underline{\phi} e^{i\omega t} \quad (3.37)$$

where $\underline{x}(t)$ is the column matrix

$$\underline{x}(t) = \begin{bmatrix} x_1(t) \\ x_2(t) \end{bmatrix} \quad (3.38)$$

describing the position of the element end points or nodes. The solution consists of a vector spatial part,

$$\underline{\phi} = \begin{bmatrix} \phi_1 \\ \phi_2 \end{bmatrix} \quad , \quad (3.39)$$

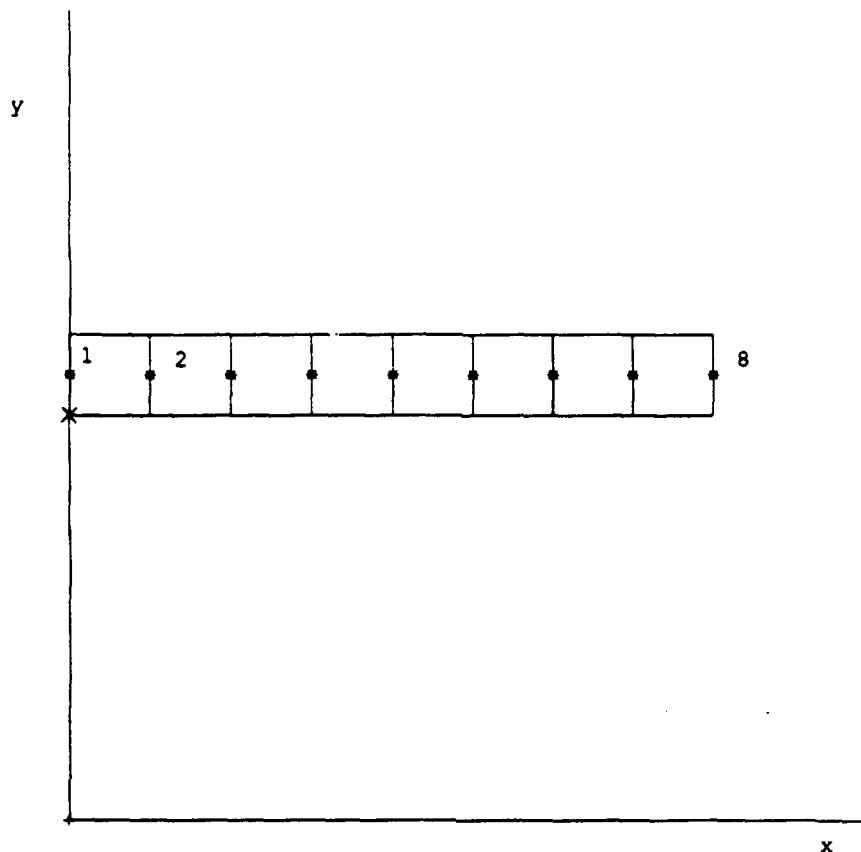


Figure 3-4. Continuous rod divided into 8 elements.

scalar temporal part, $e^{i\omega t}$ and a complex constant C . This form of solution was used since the mass and stiffness associated with each element is similar to a mass/spring system which executes simple harmonic motion.

Taking the necessary derivatives of the solution and substituting back into the equation of motion yields the homogeneous equation

$$(-\omega^2[M]\underline{\phi} + [K]\underline{\phi})Ce^{i\omega t} = 0 \quad (3.40)$$

If $C = 0$ then there would be no motion, so that possible solutions to this equation have to come from

$$([K] - \omega^2[M])\underline{\phi} = 0 \quad (3.41)$$

which is an eigenvalue problem. Part of the process in finding solutions to eigenvalue problems is to take its determinant

$$\det([K] - \omega^2[M]) = 0 \quad , \quad (3.42)$$

which is called the "characteristic equation." This is the necessary and sufficient condition for these n homogeneous equations in n unknowns to possess a non-trivial solution. The values of ω^2 which render $([K] - \omega^2[M])^{-1}$ singular are called eigenvalues. For two degrees of freedom, there will be two roots of this equation, ω_1 and ω_2 . The nodes can vibrate in simple harmonic motion with only these two frequencies. To determine the actual motion of the system, ω_1 and ω_2 are substituted back into equation (3.37) to find $x_1(t)$ and $x_2(t)$ for each frequency. Since the equation of motion is homogeneous, the coefficients C_1 and C_2 are undetermined which means the system can vibrate with an arbitrary amplitude for either characteristic frequency. The relation between C_1 and C_2 is essentially a phase relation. [Ref. 9]

The next step is to apply this method to the whole system of elements with n degrees of freedom. Starting with the eigenproblem defined earlier

$$([K] - \omega^2[M])\phi = 0 \quad , \quad (3.41)$$

except now $[K]$ and $[M]$ are made up of a whole series of two by two matrices, one for each element. For systems with many degrees of freedom and especially with cross terms appearing in the mass and stiffness matrices, the n coupled differential equations describing the motion now become difficult to solve. However, a relatively easy method to solve such a complex system is to simultaneously diagonalize the matrices $[M]$ and $[K]$. Then, it is trivial to find the eigenvalues and eigenvectors. In this case, the diagonal elements are now the eigenvalues and the eigenvectors are then the columns of the matrix used to diagonalize $[M]$ and $[K]$.

The method used to render $[M]$ and $[K]$ diagonal is a transformation to normal coordinates. The problem is to find an orthogonal matrix Φ which simultaneously diagonalizes $[M]$ and $[K]$. If $[\Phi]$ is orthogonal then for unity modal mass normalization

$$[\Phi]^T [M] [\Phi] = [I] \quad , \quad (3.43)$$

or

$$[\Phi]^T [M] = [\Phi]^{-1} \quad .$$

Recall that the identity matrix can be defined as

$$\Phi^{-1} \Phi = \Phi^T \Phi = I \quad , \quad (3.44)$$

where

$$I = \begin{bmatrix} 1 & 0 & . & . \\ 0 & 1 & 0 & . \\ . & 0 & 1 & 0 \\ . & . & 0 & 1 \end{bmatrix} \quad . \quad (3.45)$$

The process of simultaneously diagonalizing the $[M]$ and $[K]$ matrices can begin by rearranging the eigenproblem equation (3.35) as

$$[K] \underline{\Phi} = \omega^2 [M] \underline{\Phi} \quad . \quad (3.46)$$

Corresponding to the i th and j th normal modes are the vector equations

$$[K] \underline{\Phi}^i = \omega_i^2 [M] \underline{\Phi}^i \quad , \quad (3.47)$$

and

$$[K] \underline{\Phi}^j = \omega_j^2 [M] \underline{\Phi}^j \quad . \quad (3.48)$$

Using the identity matrix to make them scalar equations, equation (3.47) is multiplied by $\underline{\Phi}^{jT}$, where the transpose changes the $n \times 1$ column matrix into a $1 \times n$ row matrix, and equation (3.48) is multiplied by $\underline{\Phi}^{iT}$ so that

$$\underline{\Phi}^{jT} [K] \underline{\Phi}^i = \omega_i^2 \underline{\Phi}^{jT} [M] \underline{\Phi}^i \quad , \quad (3.49)$$

and

$$\underline{\phi}^{iT} [K] \underline{\phi}^j = \omega_j^2 \underline{\phi}^{iT} [M] \underline{\phi}^j \quad . \quad (3.50)$$

Since $[K]$ and $[M]$ are real, symmetric matrices $[K] = [K]^T$ and $[M] = [M]^T$. Making use of this property, the transpose of equation (3.50) yields

$$\underline{\phi}^{jT} [K] \underline{\phi}^i = \omega_j^2 \underline{\phi}^{jT} [M] \underline{\phi}^i \quad , \quad (3.51)$$

which when subtracted from equation (3.49) gives the scalar equation

$$0 = (\omega_i^2 - \omega_j^2) \underline{\phi}^{jT} [M] \underline{\phi}^i \quad . \quad (3.52)$$

If $\omega_i \neq \omega_j$, there are two different normal modes, then

$$\begin{Bmatrix} \phi_1^1 & \phi_2^1 \end{Bmatrix} \begin{bmatrix} M_{11} & M_{21} \\ M_{21} & M_{22} \end{bmatrix} \begin{Bmatrix} \phi_1^2 \\ \phi_2^2 \end{Bmatrix} = 0 \quad . \quad (3.53)$$

One of the key characteristics of normal modes is that every normal mode is orthogonal to every other mode. Specifically,

$$\underline{\phi}^{jT} [M] \underline{\phi}^i = \begin{cases} 0 & i \neq j \\ M_i & i = j \end{cases} \quad . \quad (3.54)$$

The mass matrix $[M]$ is now diagonalized into a new *modal* mass matrix M_i . This matrix M_i is a measure of how much mass is participating in the i th normal mode. Similarly for the non-diagonal stiffness matrix $[K]$

$$\underline{\phi}^{jT} [K] \underline{\phi}^i = \begin{cases} 0 & i \neq j \\ K_i & i = j \end{cases} \quad . \quad (3.55)$$

Therefore, diagonalization is achieved by a linear transformation using the orthogonal modal matrix Φ , now defined as

$$[\Phi] = \begin{Bmatrix} [\phi^i] & [\phi^j] \end{Bmatrix} \quad (3.56)$$

which represents the spatial and temporal parts of the mode shape. It is composed

of the eigenvectors ϕ^i and ϕ^j . The eigenvalues form a *spectral matrix*

$$\begin{bmatrix} \omega_i^2 & 0 \\ 0 & \omega_j^2 \end{bmatrix}$$

Returning to the equation of motion

$$[M]\ddot{\underline{x}} + [K]\underline{x} = 0 \quad , \quad (3.35)$$

and introducing the orthogonal modal matrix as part of the solution

$$\underline{x} = [\Phi]\underline{q} \quad , \quad (3.57)$$

which when substituted back into equation (3.35) yields

$$[M][\Phi]\ddot{\underline{q}} + [K][\Phi]\underline{q} = 0 \quad . \quad (3.58)$$

To perform a linear transformation, this equation is multiplied by $[\Phi]^T$ so that

$$[\Phi]^T[M][\Phi]\ddot{\underline{q}} + [\Phi]^T[K][\Phi]\underline{q} = 0 \quad . \quad (3.59)$$

which diagonalizes $[M]$ and $[K]$, to create a new normalized relation

$$\begin{bmatrix} M_{11} & 0 & . & . \\ 0 & M_{22} & 0 & . \\ . & 0 & . & 0 \\ . & . & 0 & M_{ij} \end{bmatrix} \begin{bmatrix} \ddot{q}_1 \\ \ddot{q}_2 \\ . \\ \ddot{q}_j \end{bmatrix} + \begin{bmatrix} K_{11} & 0 & . & . \\ 0 & K_{22} & 0 & . \\ . & 0 & . & 0 \\ . & . & 0 & K_{ij} \end{bmatrix} \begin{bmatrix} q_1 \\ q_2 \\ . \\ q_j \end{bmatrix} = 0 \quad . \quad (3.60)$$

Now the n coupled differential equations are uncoupled. Every i th normal mode now has its own i th row which can be lifted out, such as

$$M_i \ddot{q}_i + K_i q_i = 0 \quad (3.61)$$

which is like the familiar harmonic oscillator mass/spring system where

$$\ddot{q}_i + \frac{K_i}{M_i} q_i = 0 \quad ,$$

or

$$\ddot{q}_i + \omega_i^2 q_i = 0 \quad .$$

Any arbitrary motion of the system can thus be written as a linear combination of the eigenvectors

$$\begin{bmatrix} x_1 \\ x_2 \end{bmatrix} = q_1 \begin{bmatrix} \phi_1 \end{bmatrix} + q_2 \begin{bmatrix} \phi_2 \end{bmatrix} \quad , \quad (3.62)$$

where $q_1 = A \cos \omega_1 t$ and $q_2 = A \cos \omega_2 t$. Here A is an amplitude coefficient based on the perturbing force. Hence, the finite element computer code solves for the normal modes of a structure by finding a modal matrix Φ which will diagonalize $[M]$ and $[K]$.

Therefore a normal mode is made up of a particular eigenvalue (frequency) and a particular eigenvector (mode shape), which is orthogonal to every other normal mode. A normal mode describes how much mass and stiffness is involved in the structure as it vibrates. That is, the coordinate q_i is a measure of how much the mode shape Φ_i is present. The value of finding the normal modes of a structure is that any complex motion can be represented as a linear combination of normal modes. For such an intricate system as the PHALANX gun, where there are many components contributing to its dynamic response, to find its normal modes suddenly makes it a far easier system to understand. That is, if the normal modes of the gun are obtained, which then forms a modal component model, when excitation forces are applied, the resulting displacements are the result of exciting certain normal modes. An analogy to this is that any color can be made up of various amounts of the primary colors red, blue and yellow. So in order to obtain a set of accurate normal modes the finite element model must be as close a representation of the real gun as possible which is the topic of the next chapter.

IV. MODEL DESCRIPTION

A. TYPES OF FINITE ELEMENTS USED IN THE MODEL

At the outset of this project, the gun barrels alone were thought to be a primary source of dispersion. In fact, previous to this project, the Navy had already let a contract for a new barrel design. So, the initial proposal for research by the Naval Postgraduate School called for a finite element model of the six-barrel system. However, in consultation with Mike Hatch, a private-industry finite element expert, it was agreed that in order to truly represent the complex dynamics of the gun, it would be important to model not just the barrels, but the whole gun assembly through to its grounding points to the gun mount. This holistic approach, while greatly expanding the scope of the work, would not only offer a much better assessment of the gun system, but would greatly expand its applications as well. The school would also be the first organization to model the complete gun assembly, thus offering a complete model in one package. The benefits of such a model are many. Once the model was assembled and the dynamic response validated against the current dispersion pattern, new components could be "swapped out" in the model and their effect on dispersion would provide a valuable assessment. Not only could individual components such as the barrels be tested, but combinations of components could be tested together. This model therefore, would go a long way toward understanding the dynamics of the gun as well as providing a valuable tool for finding ways to tighten the dispersion pattern.

Once blueprints of the model were received, the next big decision involved the appropriate selection of finite elements to represent each component. In all there are ten different parts of the gun, counting duplications such as the barrels, as just

one component. The finite element modeling experience of Professor Gordis and Mike Hatch was helpful in deciding which areas of the gun system should be modeled with great detail and areas where time-consuming attention could be safely passed over. Table 4-1 lists the components and the corresponding element choices. Before discussing the properties of the elements that were used in the model, it is important to give an overall view on element selection. Each element comes with a price. Some, such as bricks, are more *expensive* to use than others since they require more nodal points to define them, in this case eight. Others, such as beam elements, as discussed in the previous chapter, require only two nodes. In order to shorten the computational time and make the resulting modal shape animation as smooth as possible, it is important to choose as many less expensive elements as possible. At the same time, to accurately represent the real gun, the expensive elements are sometimes the best choice. Hence, it is a balance that often goes through several iterations before a final choice is made. As can be seen in Table 4-1, the gun is comprised of five categories of elements, with many different variations within each category, such as changes in dimensions, material properties, etc. The following subsections describe the general properties of each category of element used in the model.

1. Brick Elements

As mentioned before, the solid brick elements are the most complex elements to use in that they require eight nodes to define. A single brick element is shown in Figure 4-1. A brick element is one of the most versatile elements to use since it allows modeling of any structure with any geometry [Ref. 10]. The general geometry of the brick is that its width is roughly comparable to its length. It is a three-dimensional solid whose nodes are allowed to translate along each axis, but not rotate. Therefore, it has only three degrees of freedom. It is best used to represent solid, invariant structures without many intricate details or

curvature, such as engine blocks or in our case the breech. Furthermore, more bricks are required to reflect bending and shear than do thin shells or beam elements. A structure represented with bricks often looks the most realistic. However, it comes with the price of reduced accuracy, especially if not enough bricks are used, and in any case, it is usually the most inefficient element to use [Ref. 11].

TABLE 4-1. ELEMENT SELECTION

Elementary Model	
Component	Element Types
Muzzle Clamps	Bricks, Thin Shells, Rigid Elements
Mid-Barrel Clamps	Bricks, Rigid Elements
Barrels	Beams with tubular cross-section
Stub Rotor	Bricks, Thin Shells
Rotor	Bricks
Needle Bearing	Bricks, Springs
Casing	Thin Shells
Thrust Bearing	Bricks, Springs
Recoil Adapters	Bricks, Rigid Elements, Springs
Ball Joint	Rigid Elements, Springs

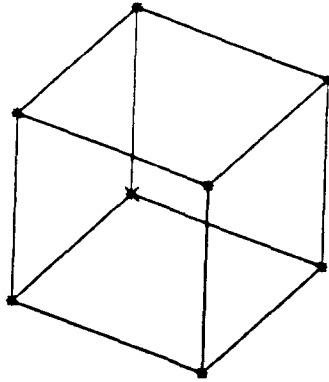


Figure 4-1. A solid linear brick element.

2. Thin Shell Elements

A thin shell or plate element is a two-dimensional solid whose thickness is small compared to its length or in-plane dimensions. A thin shell element is shown in Figure 4-2. It is a much more efficient element to use than a solid brick since it only requires four nodes to define its shape. Its thickness is defined when the element is created, but it does not show up in the display. The best applications for it are in modeling situations where a wall or membrane has a nearly constant thickness or its thickness varies linearly from one edge to another. The element's nodes are allowed to not only translate, but rotate as well, thus giving it six degrees of freedom. These additional degrees of freedom allow fewer thin shell elements to be used than brick elements in obtaining the same accuracy for bending and shear motion. One disadvantage in using thin shell elements is

that they are not able to model stresses that vary through its thickness as can brick elements [Ref. 11].

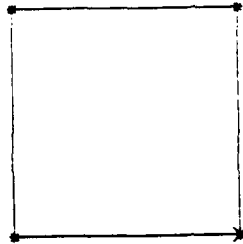


Figure 4-2. A thin shell element.

3. Beam Elements

Beam elements are the simplest elements in that they only require two nodes to define them. The cross section of the beam is defined when the beam is created and can have as detailed and complex a shape as the user desires. Figure 4-3 shows a beam element as it appears in the display of the finite element model and its cross section which only appears when referencing the beam's properties. This cross section is invariant along the element's length. To represent a beam of varying cross-section, several elements are required. For example, the gun barrels are represented using beam elements, where the barrels' varying thickness is reflected in the varying cross-section of 12 elements. The nodes are allowed the

full six degrees of freedom which is useful in displaying bending and deflection. Again referring to the modeled gun barrels, the beam elements provide a smooth animation picture which gives better insight into the dynamics of the gun. A possible problem with using beam elements is that they do not show stress through their cross section and the cross sections can be easily oriented the wrong way [Ref. 11]. However, in most cases, there is more interest in the maximum, outer fiber stress than that of the inner stress.

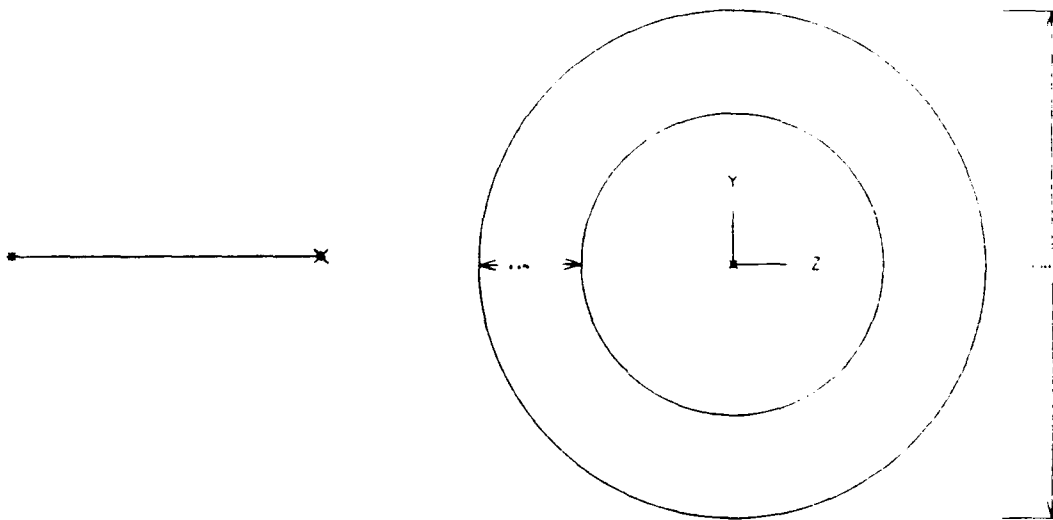


Figure 4-3. (a) A beam element. (b) A representative beam element's cross section.

4. Spring Elements

Spring elements can be defined with two nodes (node-to-node) or in terms of one node (node-to-ground). They can also be either a translational spring operating along a defined axis, or a rotational spring which represents the bending moment or torque that is required to rotate one node relative to another or to

ground [Ref. 12]. Figure 4-4 shows a node-to-node and a node-to-ground spring. The stiffness is defined along each axis or uniaxially for a translational spring or about an axis for a rotating spring. Three rotational degrees of freedom are assigned to each node. In the PHALANX gun model they were used to represent the stiffness of the ball bearings and the recoil shock absorbers.



Figure 4-4. (a) A node-to-node spring element. (b) A node-to-ground spring element.

5. Rigid Elements

Rigid elements are massless, infinitely stiff bars used to connect components together. That is, the rigid element implies that the motion of the nodes on the element are to be related to each other as if they were connected together by an infinitely rigid bar [Ref. 12]. Two nodes that are connected together with a rigid element move together according to a linear algebraic expression called a constraint relation. An example of such a relation is given

below.

$$x_1 - 0.5x_2 = 0 \quad . \quad (4.1)$$

In this example, the first term describes the distance node 1 moves in the x direction and the second term that of node 2 in the x direction. The right hand side of the equation, which is a constant term, must be zero when solving for the normal modes of vibration. This equation can be written in matrix notation as

$$\begin{bmatrix} x_1 \\ x_2 \end{bmatrix} = \begin{bmatrix} 0.5 \\ 1 \end{bmatrix} \begin{bmatrix} x_2 \end{bmatrix} \quad . \quad (4.2)$$

Representing the coefficient matrix with T , this relation can then be written as

$$x_{original} = Tx_c \quad , \quad (4.3)$$

where the nodal position is defined in terms of a coefficient matrix and the constrained node matrix x_c . Substituting this equation into the equation of motion

$$F = KTx_c \quad , \quad (4.4)$$

and multiplying by the transpose of the coefficient matrix T yields

$$T_c^T F = T_c^T KTx_c \quad , \quad (4.5)$$

which reduces to the constrained equation of motion,

$$F_c = K_c x_c \quad . \quad (4.6)$$

This is an example of how constraint equations transform an unconstrained stiffness matrix K to a constrained stiffness matrix K_c . A rigid element can be used to connect from two to thirty-two nodes together. Figure 4-5 shows a rigid element connecting five nodes together. Each node at the element's end points are allowed all translations and rotations that are allowed for that node. For example, if the rigid element is connected to a node of a brick element, then it is only allowed to translate. In the PHALANX gun model, rigid elements were used to connect the barrels to the clamps and stub rotor and the recoil adapter springs to

the gun body. "End release codes" can also be defined allowing the simulation of hinges or ball-and-socket joints [Ref. 12].

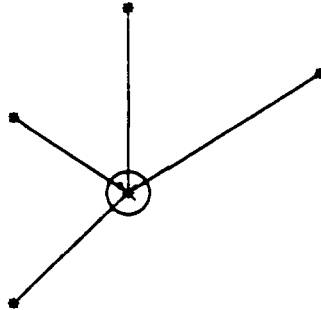


Figure 4-5. A rigid element connecting five nodes together.

A further classification within each element category is the element order. That is, the number of nodes per element can be increased to increase the order of the equations used to interpolate the strain between them. There are two nodes required for each edge in a linear element, three for a parabolic and four nodes for a cubic [Ref. 11]. All the elements used in this model have linear order.

B. CONSTRUCTION OF THE PHALANX GUN MODEL

A breakdown of the components used in the construction of the PHALANX gun model is shown in Figure 4-6. This is a hidden line image which shows the geometry of the elements on the side of the gun parts facing the viewer. Figure 4-7 is a shaded image of the completely assembled gun. Here, the individual elements

cannot be seen, but the effect of lighting and solid colors gives a realistic picture of the gun it represents. Both figures provide a brief overview of how the gun is assembled. The six barrels each slide through the stub rotor and are screwed into the rotor a distance of approximately 7.6 cm (3 inches). The stub rotor itself is bolted to the rotor and serves to support the barrels near their base. The six-barrels are connected together with a mid-barrel clamp and a forward muzzle clamp. This whole assembly is now attached to the gun body through a rear needle bearing and a double-roller contact bearing. The assembled gun body is coupled to the rest of the CIWS mount at three locations. Two recoil adapters are positioned on either side of the gun body where they connect the gun body to the mount via a pivot joint. The third grounding point is a ball joint at the rear of the gun body. All of these components will be explained in further detail in the following subsections.

1. Gun Barrels

The six rifled barrels are approximately 150 cm (59 inches) long with an inner diameter of 2 cm (0.787 inches) and weigh about 8.2 kg (18 lb). The barrels are secured to the breech with interrupted locking lugs that mate after the barrels are screwed in past three threads [Ref. 13]. As mentioned before, the six barrels are represented using beam elements. Each barrel is made up of 39 elements with 12 different cross-sections. Figure 4-8 shows a single barrel with its elements separated.

2. Muzzle Clamp

The muzzle clamp restricts barrel movement near the barrel tips. It consists of two plates held together with a steel web meshing. The clamp also restrains individual barrel movement during firing and a self-locking nut is used to secure the clamp to all the barrels [Ref. 13]. The plates are represented using

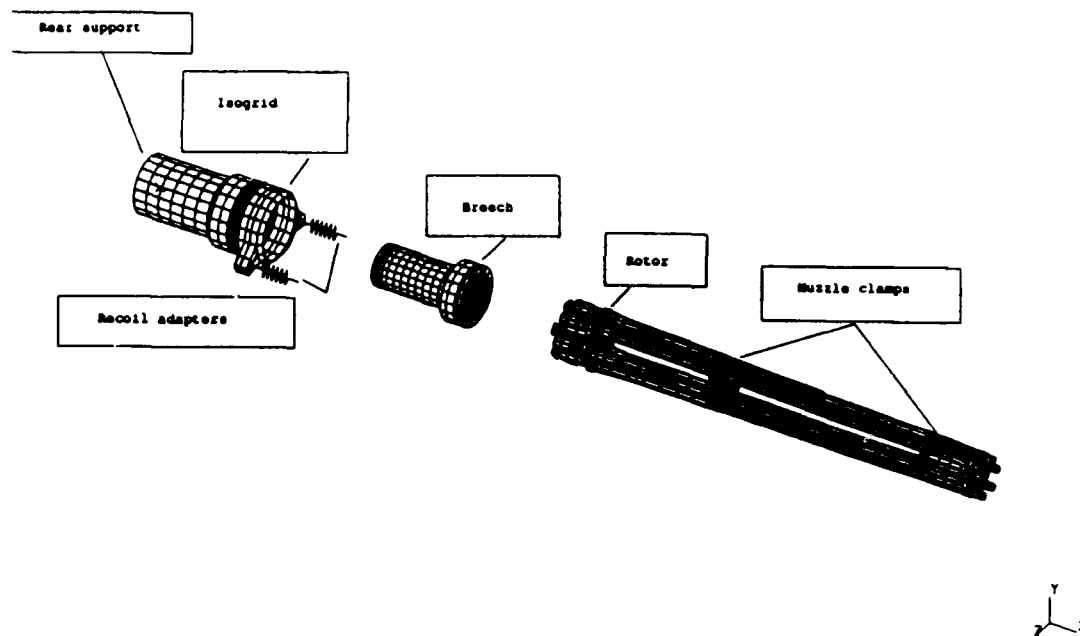


Figure 4-6. A hidden line image of the disassembled components of the PHALANX gun.

brick elements while the web meshing is modeled with thin shells as can be seen in Figure 4-9.

3. Mid-Barrel Clamp

The mid-barrel clamp is positioned roughly near the center of the barrel group. It physically locks the barrels to the clamp with tabs that fit into cutouts in each barrel. It prevents the barrels from becoming unscrewed in the rotor during firing. The mid-barrel clamp, as shown in Figure 4-10, is represented entirely with bricks.

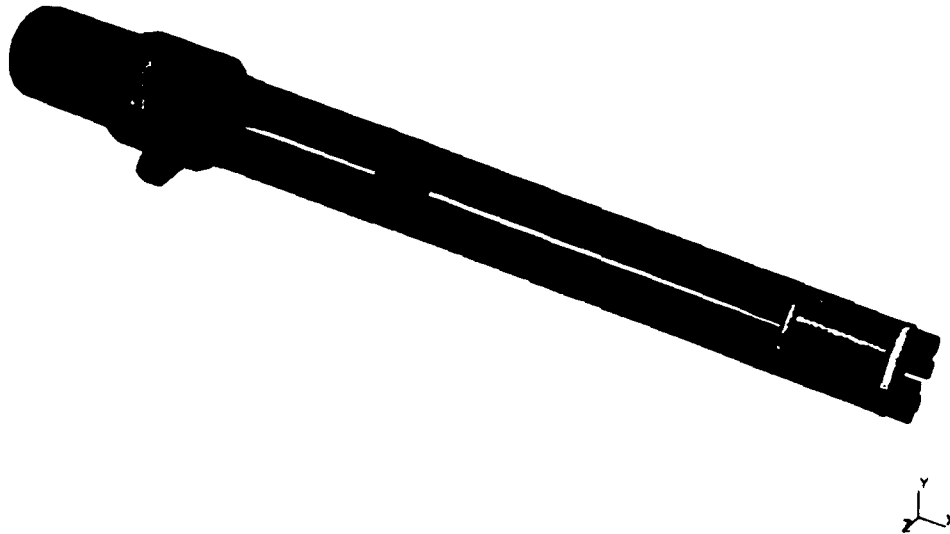


Figure 4-7. A shaded image of the PHALANX gun.

4. Stub Rotor

The stub rotor which is bolted to the rotor supports the base end of the six barrels. It permits alignment of the barrels so that the locking lugs can be engaged [Ref. 13]. Like the muzzle clamp it consists of two plates separated by a metal meshing. Figure 4-11 shows the modeling of it with bricks and thin shells.

5. Rotor

The rotor is the most massive component in the gun body. It is hydraulically rotated at a speed of 750 rpm (12.5 Hz) in the counterclockwise

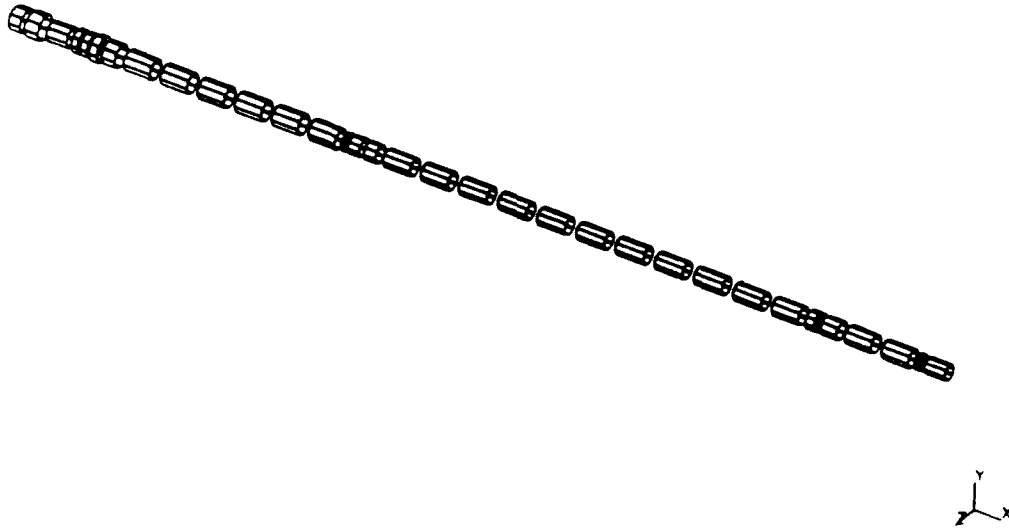


Figure 4-8. A single barrel with with 39 beam elements.

direction when viewed from the rear [Ref. 13]. The gun assembly, which is shown in Figure 4-12, is bolted onto the front of it. The rotor is shown in Figure 4-13 and is made entirely of bricks. The rotor is coupled to the gun body through the rear needle bearing and the forward double roller contact bearing.

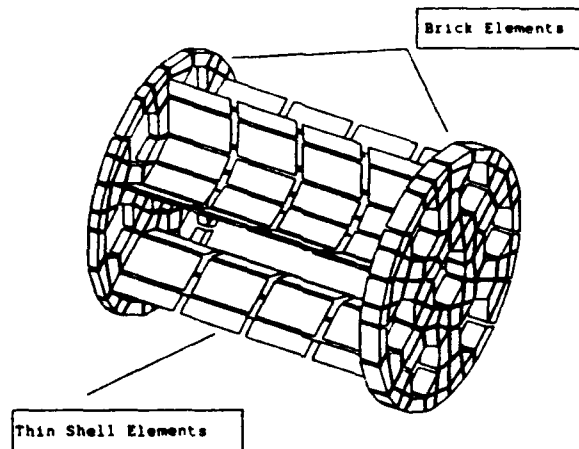


Figure 4-9. The muzzle clamp represented with brick and thin shell elements.

6. Double Row Contact Bearing

The double row angular contact bearing, often referred to in this text as a thrust bearing, consists of two rows of ball bearings for a total of 76 balls. The inner race attaches to the rotor while its outer race attaches to the gun body. Its purpose is to align the rotor/gun assembly and transfer the firing load to the rest of the gun body. It provides both radial and axial support. Figure 4-14 shows the races represented by bricks. The ball bearings are modeled using springs with the loaded contact angle being represented by an angle determined through an accepted computer program from Mike Hatch.

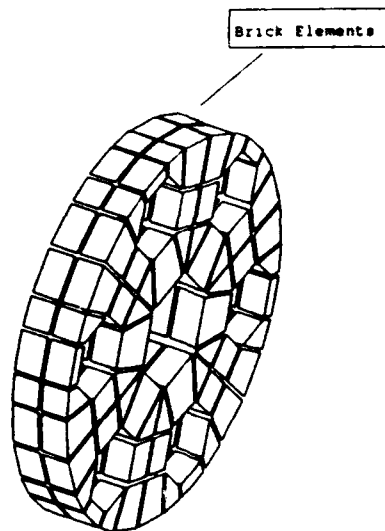


Figure 4-10. The mid-barrel clamp represented with bricks.

After the decision was made to model the whole gun subsystem, careful attention was given to the blueprints of the gun body. It then became readily apparent that the two bearings were playing a critical role in the dynamics of the gun. They provide the only means of support to the rotating and firing six-barrel gun assembly. Therefore, the intricate details of the bearings, especially the double row bearing, were modeled as can be seen from a cutaway view showing the cross section of the double row bearing in Figure 4-15. It is also noteworthy that this bearing is mounted to the rotor through a narrow lip which was also accurately modeled and is pointed out in that figure. The entire firing and rotating forces are transmitted through this lip which seems to be subjecting it to a severe stress.

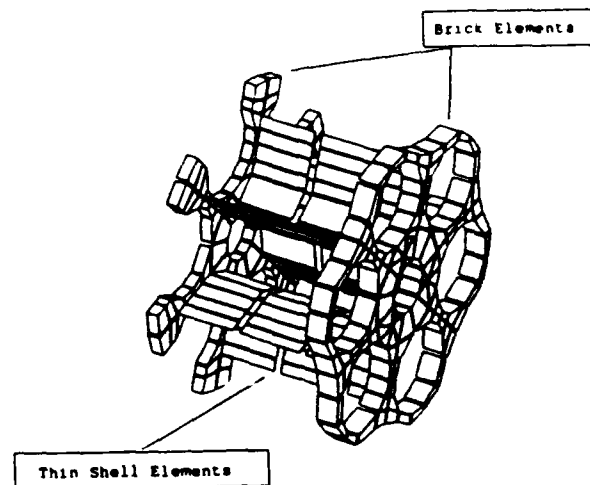


Figure 4-11. The stub rotor represented with bricks and thin shells.

Obtaining the axial, radial and torsional stiffness values for the double row contact bearing was difficult since the manufacturer, Kaydon Bearing in Muskegon, Michigan did not have records for this bearing in this application. However, after supplying Kurt Sheridan of Kaydon with the reaction force information, determined from the finite element model, he was able to provide approximate figures of the bearing stiffness and contact angle. With this information Mike Hatch was then able to provide spring stiffness values and an angle with which to mount the springs in relation to the inner and outer races. There are a total of 36 springs, one for each of the 18 elements used to define its circumference then multiplied by two to represent the double row of bearings.

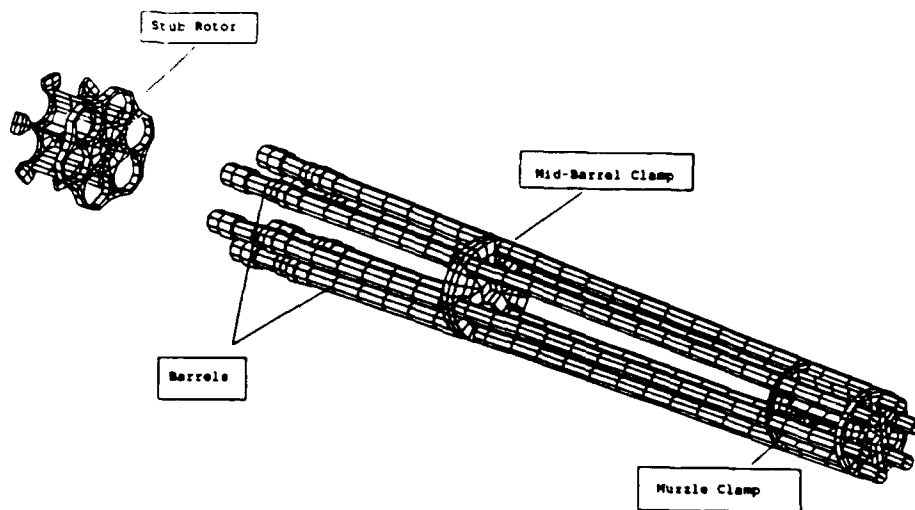


Figure 4-12. The gun barrels with clamps and stub rotor.

7. Needle Bearing

The needle bearing provides the rear support for the rotor. It serves only as a radial support and not as a thrust absorber. The inner race of the bearing is attached to the rear wall of the gun body while the outer race is attached to the rotor. Figure 4-16 is a translucent picture showing the inner assembly of the gun body. In this figure it is possible to see both the needle bearing and the double row bearing and their relation to the rotor and gun body. Similar to the double row bearing, the bearing stiffness is represented with 18 springs. In order to correctly represent the actual bearing stiffness, $K_{bearing}$, an effective spring stiffness, K_{eff} , must be calculated. No matter which way the rotor moves on the real gun, it

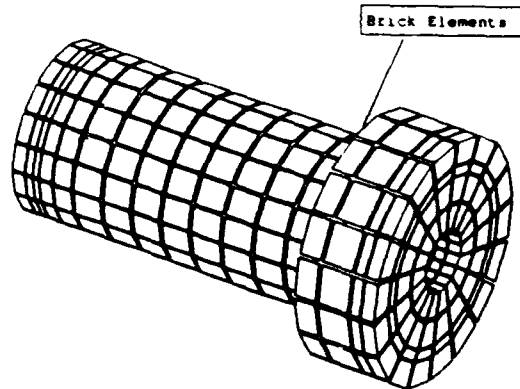


Figure 4-13. The rotor represented with bricks.

experiences a constant bearing stiffness, whereas in the modeled gun which has only 18 springs, the angle between them must be taken into account. Figure 4-17 demonstrates the geometry needed to make this calculation. Consider a force applied in any one direction to the model bearing. The equation of motion would be

$$F = K_{tot}X \quad (4.7)$$

Here, K_{tot} is the total spring stiffness value that would take into account all 18 springs. However, $K_{tot} \neq K_{bearing}$ since as it stands now, the modeled bearing will present a larger spring stiffness than the actual bearing. To correct for this

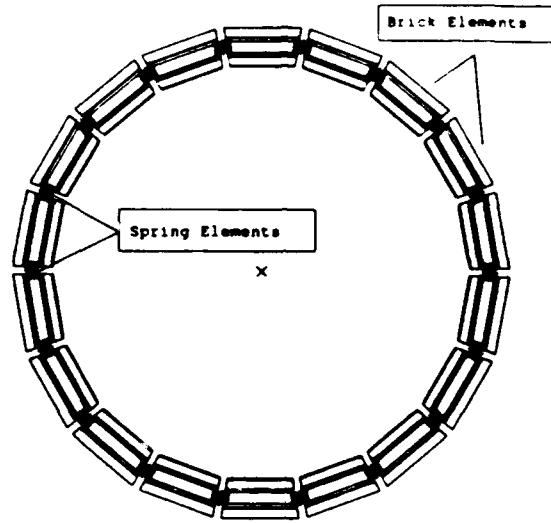


Figure 4-14. The double row contact bearing.

problem, the 20° angle between the springs must be described by the relation

$$K_{tot} = \sum_{i=0}^{i=18} K_{eff} \cos \alpha_i = K_{bearing} \quad (4.8)$$

Solving for K_{eff} gives

$$K_{eff} \sum_{i=0}^{i=18} \cos \alpha_i = K_{bearing} \quad (4.9)$$

where

$$K_{bearing} = K_{eff} (2 \cos 0^\circ + 4 \cos 20^\circ + 4 \cos 40^\circ + \dots) \quad (4.10)$$

Rearranging terms gives,

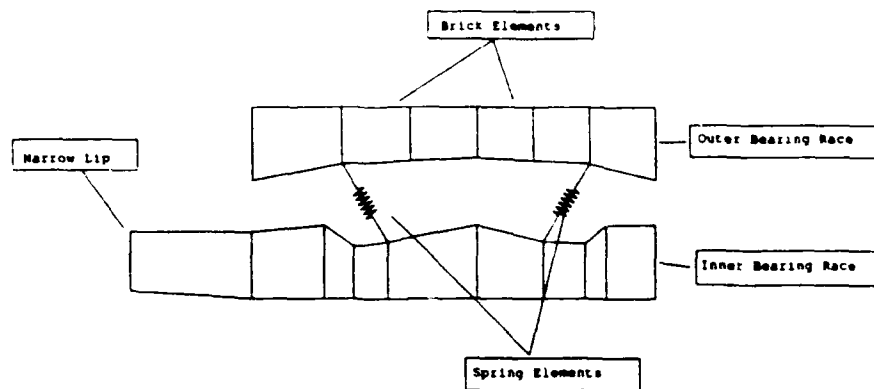


Figure 4-15. Cross sectional view of the double row contact bearing.
Note the narrow lip which attaches to the rotor.

$$K_{eff} = \frac{K_{bearing}}{11.5175} \quad (4.11)$$

Therefore, after obtaining the stiffness value of the needle bearing from the manufacturer, it was divided by a factor of 11.5175 to fit the model [Ref. 14].

8. Gun Body

The gun body is a steel housing which contains the bearings, rotor and stub rotor as shown in Figure 4-16. Since the wall thickness is only 0.5 cm (0.2 inches) and is small compared to its other dimensions, it is represented by thin shells. It is part of the load path between the firing barrels and ground. On either

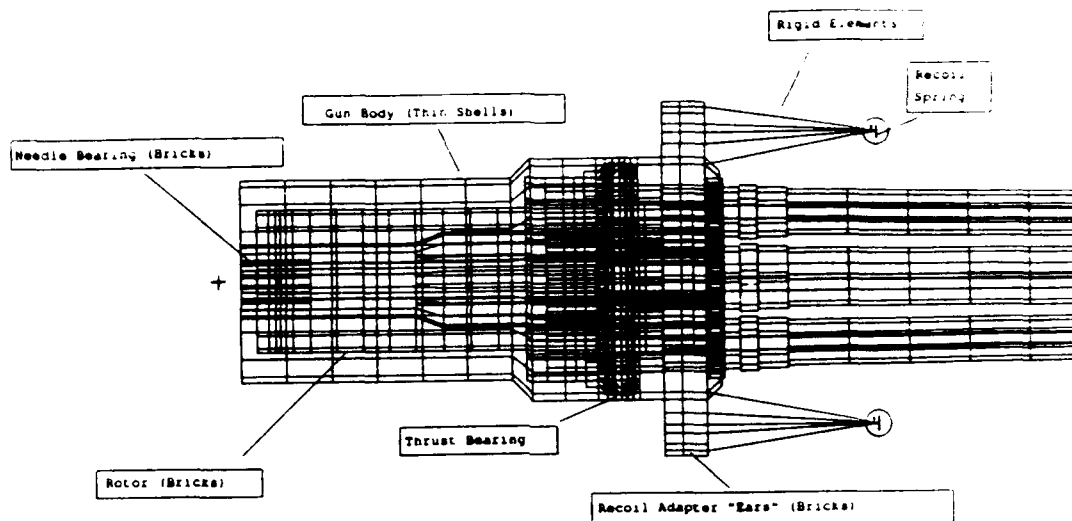


Figure 4-16. Translucent image of the gun body. It shows the relation between the two bearings and the rotor. Also visible are the recoil adapters and the rear support.

side of the gun body, roughly opposite to the double row bearing, are the two recoil adapters. At the rear of the gun body is the third attachment to ground, the ball joint.

9. Recoil Adapters

The two recoil adapters serve to absorb a portion of the forces caused when the gun is fired and then the associated counter-recoil force [Ref. 13]. Figure 4-18 is a photograph of the PHALANX gun on the USS ARKANSAS which shows the construction and mounting of an actual recoil adapter. Since the overall shape

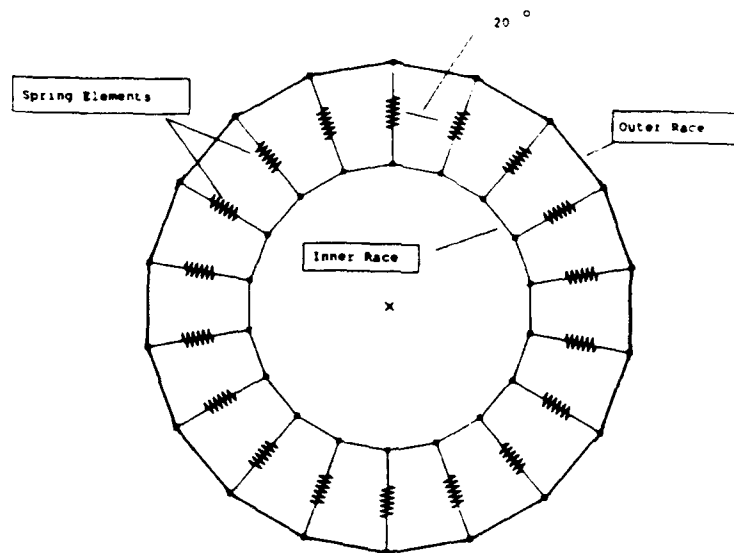


Figure 4-17. Spring placement for the needle bearing.

of the recoil adapter plays a minor role in the dynamics of the gun, it was possible to represent its recoil spring stiffness, placement and attachment to ground simply, but accurately. Looking at Figure 4-16, the recoil adapter's mass and stiffness was modeled using brick elements in the form of "ears" sticking out on either side of the gun body. In order to get the correct placement of the roller, rigid elements were used to connect the brick element ears to the recoil spring. In turn, the recoil spring was connected to a roller. The specifics of the roller will be discussed in the boundary conditions section. The stiffness value for the spring was obtained from a hysteresis curve as shown in Figure 4-19 [Ref. 15]. Here the slope for the upper

and lower branches of the curves was calculated and averaged to get the stiffness value used in the model.

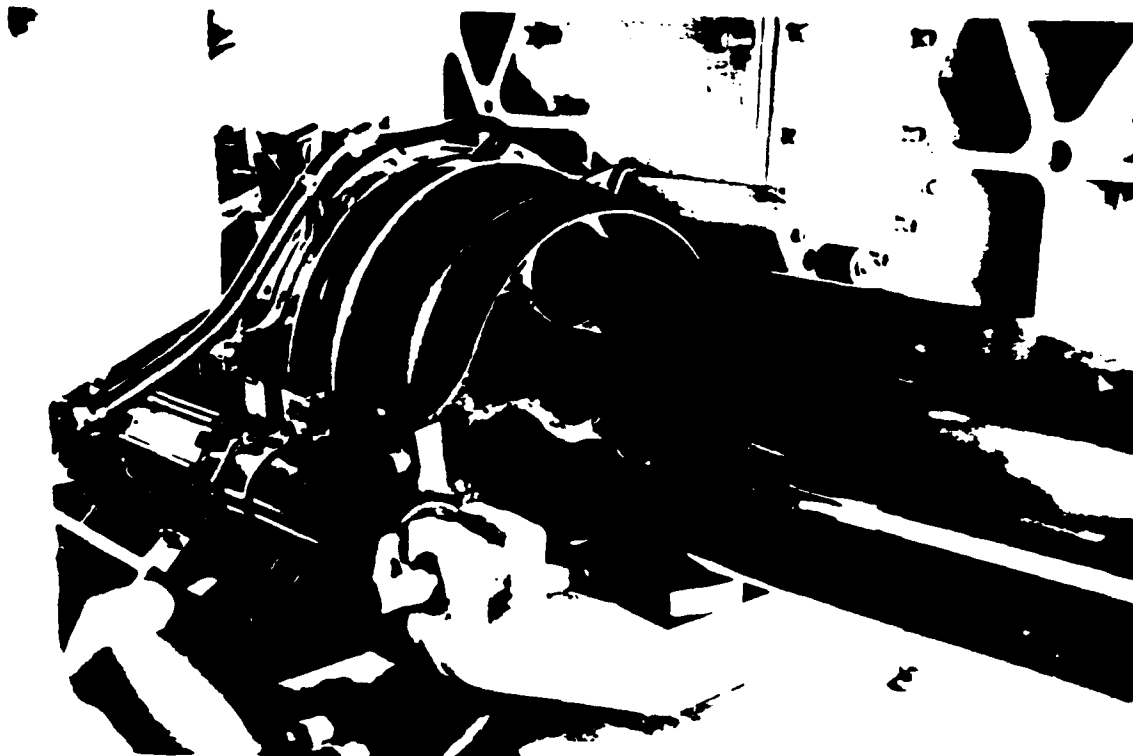


Figure 4-18. Photograph of the gun body. Note the arrangement of the recoil adapters and their construction.

10. Ball Joint

The rear ball joint provides the third support of the tripod supported gun. The geometry of it is displayed in Figure 4-20. It consists of a 3.84 cm (1.5 inch) diameter ball supported by a 9.63 cm (3.79 inches) long rod 2.54 cm (1 inch) in diameter which in turn is attached to the gun mount. The ball fits into a socket mounted on the back of the rear wall of the gun body. When the gun fires, it sets back by about half an inch and oscillates about the new equilibrium point. The ball

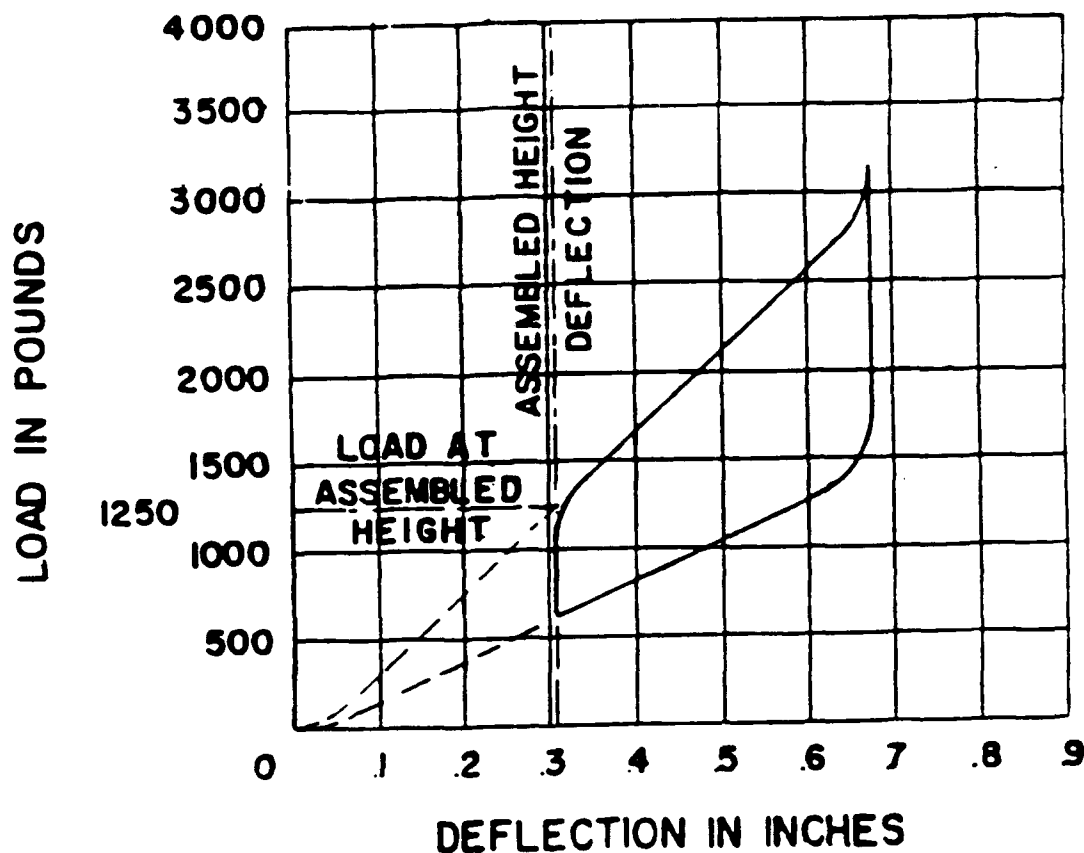


Figure 4-19. Hysteresis curve of the recoil adapter stiffness.

slides into the socket which only provides radial support. Since this is a relatively simple arrangement, a separate side model was built to establish the stiffness of the socket. This stiffness was represented by two springs along the y and z axes perpendicular to the length of the gun thus providing the radial support. The springs were attached to ground on one end while their other end connected to rigid elements that attached to the gun body. These rigid elements represented the support given by the cup to the gun body. Figure 4-21 shows this arrangement in the computer model.

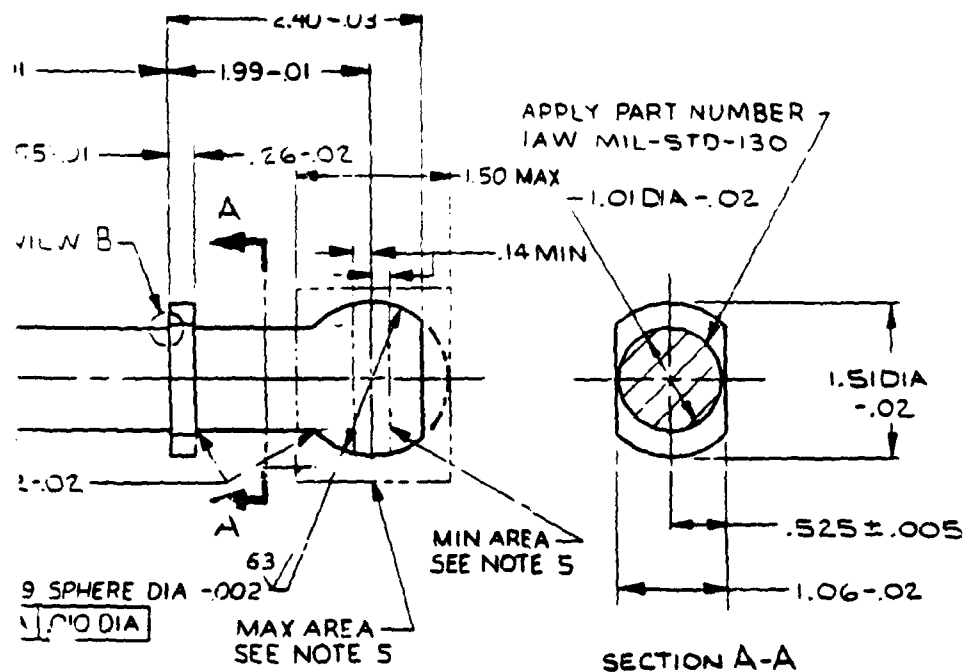


Figure 4-20. Blueprint of the rear ball joint.

C. BOUNDARY CONDITIONS

Having modeled the components of the gun, the next major step is to ensure that the proper boundary conditions are reflected in the model. The boundary conditions define how the components are connected to each other as well as how the whole gun is attached to the gun mount. The next category of boundary conditions that must be determined are the types of degrees of freedom.

As the model stands now, it represents an idealized gun with no worn bearings, or recoil springs and no tolerance between connected components. It may be better than a brand new gun. As mentioned earlier, the barrels are attached to

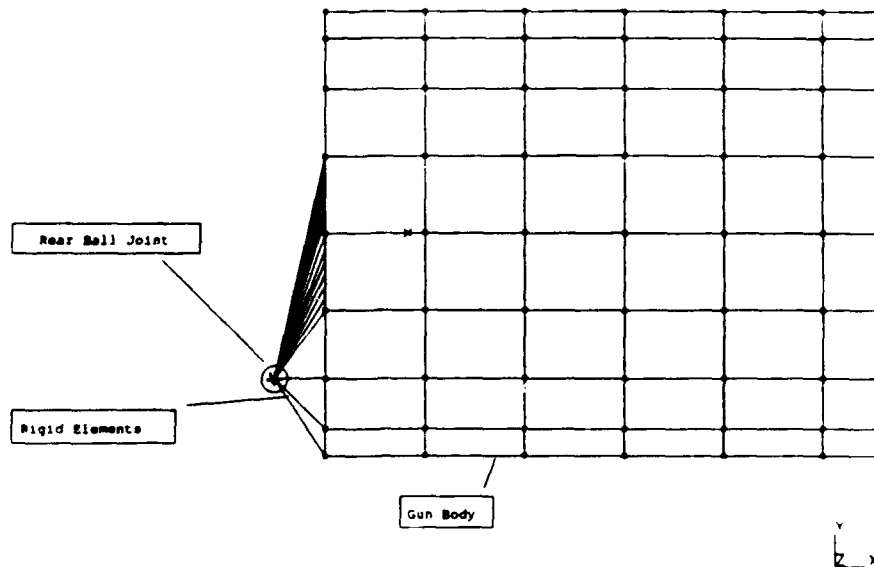


Figure 4-21. Representation of the ball joint in the model.

the clamps, stub rotor and rotor with rigid elements. Figure 4-22 shows an example of a barrel connected to a clamp. The stub rotor is connected to the rotor with rigid elements as well. The rotor is connected to the gun body through the two bearings. The gun body in turn is connected to ground via the recoil adapters and ball joint.

Figure 4-16 expands further on the specific ranges of motion allowed at these three supporting points showing how they were defined in the model. At the two pins which hold the recoil adapters to ground in the real gun, they are allowed to rotate about the z or horizontal axis, but do not rotate or translate in any other direction. To properly represent this condition in the real gun, the node between

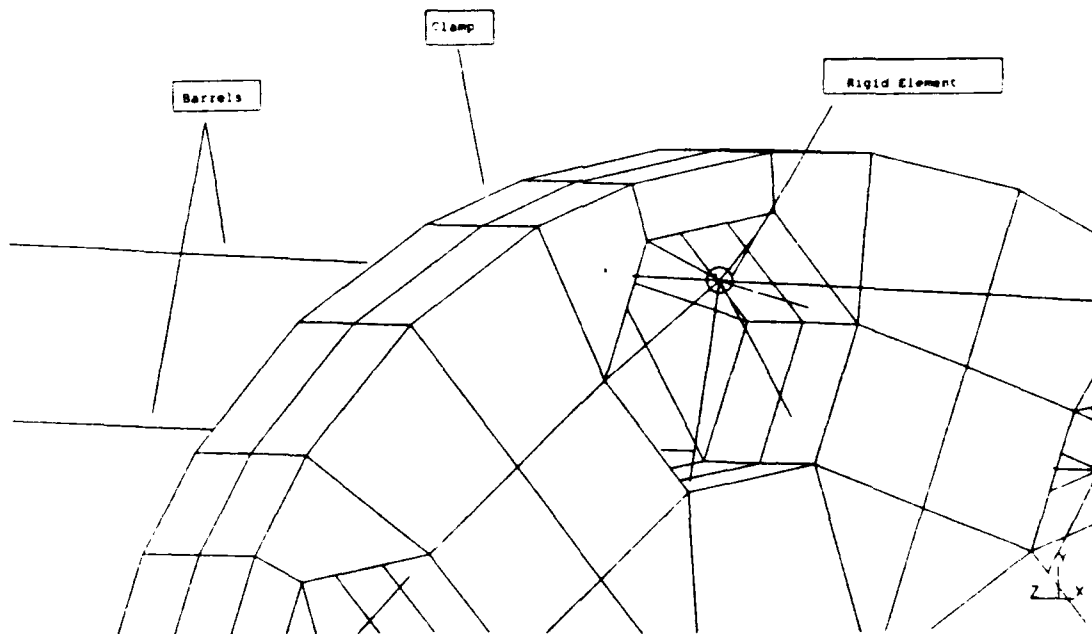


Figure 4-22. Example of rigid elements connecting a barrel to a clamp.

the rigid elements and the springs is allowed to move in the x or axial direction and to rotate about the z axis. The translation in the x direction is necessary in order to allow the springs to be exercised. The springs in turn are attached to ground in order to satisfy the real boundary conditions, albeit broken up into two locations, given the unique representation of the recoil adapters in the model. Motion at the ball joint of the real gun is in the fore-aft or x direction, with the cup providing restraint for translational motion in the y or z directions. All rotations are allowed, however due to the two forward supports this motion would be unlikely. In the computer model, the springs restrict motion in the y and z

directions, thus like the cup, and there are no restrictions for motion in the x direction.

Unlike the real gun, this model does not spin. This is where kinematic and unknown degrees of freedom come into play. The normal mode of rotation about the x axis is prevented. Since the normal modes are being solved without gyroscopics, that is, without an unbalance (centrifugal) excitation, it is restricted in the model by using kinematic degrees of freedom. Four kinematic degrees of freedom were used to restrict the rotation of the rotor inside the gun body. This does not substantially degrade the understanding of the gun's dynamic motion, since the excitation force occurs at the same place and is virtually independent of the rotation. That is, as the rotor is turning and the barrels are sequentially firing, they all fire at the same location. The barrels are not actually rotating in the computer model, but the excitation force is applied at the base of a barrel which is in the proper location to represent each barrel as it fires in the rotating gun. The unknown degrees of freedom correspond to the differential equations solved by the computer. In this model, there are 22,470 degrees of freedom.

D. COMPARISON BETWEEN THE REAL AND MODELED GUN

After completion of the PHALANX gun model, one of the first steps toward validation is to compare its properties with those of the real gun. Based on information provided by Dick Sirola, the properties used for comparison were mass, center of gravity, and moments of inertia for each of the three coordinate axes. This information and their percent difference between the computer model and the real gun is presented in Table 4-2. Further comparisons can be made and the model refined to provide a better match. These small differences are not important to the conclusions reached by this study.

TABLE 4-2. COMPARISON BETWEEN REAL AND MODELED GUN

Comparison							
Mass (kg)		Center of Gravity (cm)			Moment of Inertia (kg-m ²)		
		C.G. _x	C.G. _y	C.G. _z	I _{xx}	I _{yy}	I _{zz}
M61A1	113.5	53.83	0.04	0.0	6796	2.38e ⁵	2.38e ⁵
Model	120.5	55.2	-0.304	-0.053	7240	2.59e ⁵	2.60e ⁵
% Diff.	5.81	2.48	5.75	5.40	6.13	8.01	8.40

Another important area of comparison is to determine whether the actual forces in the gun are linear or non-linear. The computer will only solve the linear problem. Experimental data verifies that the stiffness calculations are linear for the range of barrel tip motion less than ≈ 0.25 cm (0.1 inch) [Ref. 16]. Figure 4-23 shows the test results of muzzle deflection versus a load up to 300 lb applied in the vertical direction at the barrel tip. Since the dispersion data shows that barrel tip displacement is less than ≈ 0.25 cm, the system is considered linear. The linear computer solution is compatible with the experimental data.

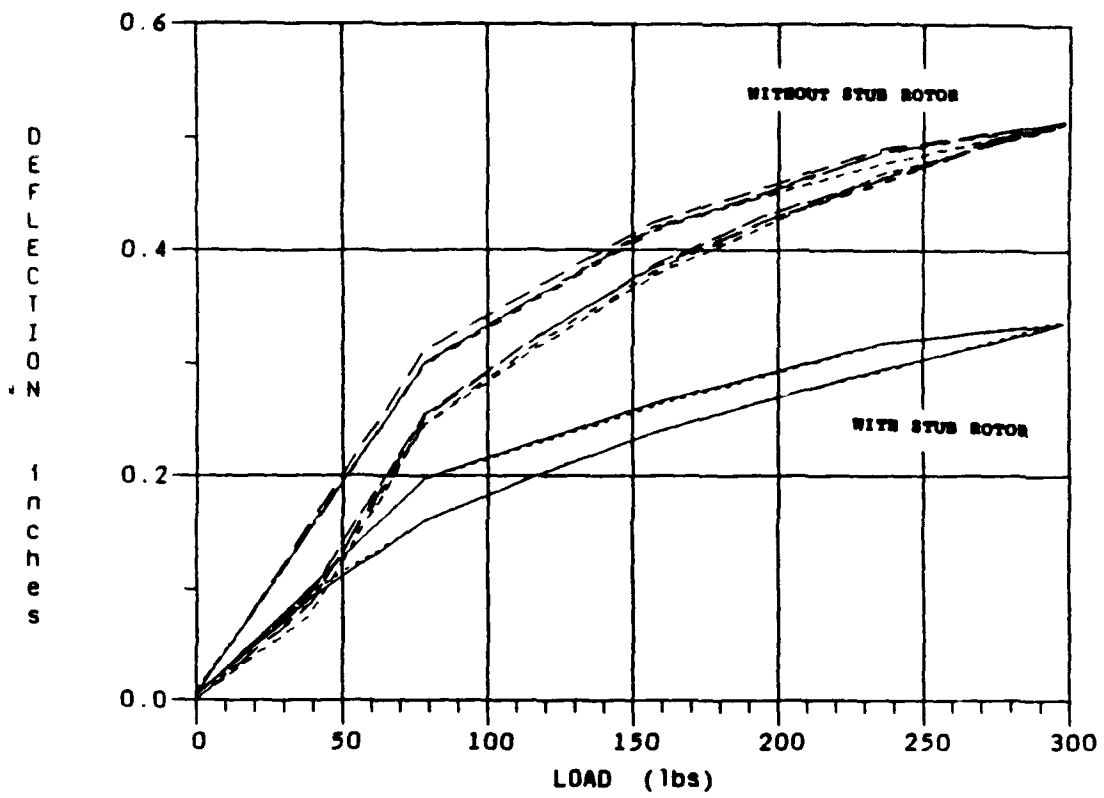


Figure 4-23. Experimental data of muzzle deflection versus load.

V. MODES OF VIBRATION

A. MODES OF VIBRATION OF THE GUN BARRELS

One of the first components of the model to be developed were the gun barrels. Two different levels of modeling detail were used to create two different versions of the barrel. The first, called the advanced barrel, involved the use of 496 brick elements and is shown in Figure 5-1. The brick elements were used to provide better detail in modeling the barrels. The second version, called the simple barrel, used 39 elements with 8 cross sections and is shown in Figure 5-2. The latter version, with its fewer elements, is the best choice for providing a smoother animation picture and keeping the number of degrees of freedom within a manageable budget. The advanced barrel version was kept for comparison purposes so that when future barrel designs are tested using this model of the gun, the most complete finite element modeling technique can be used.

The first component of the PHALANX gun to be received at the Naval Postgraduate School was a single barrel. It provided an opportunity for a validation test of the gun model. The barrel was set up in a mechanical engineering lab, where it was suspended with two low-stiffness cords to determine its normal modes of vibration [Ref. 17]. This method is called the "free-free configuration." If the normal modes were found while the barrel was clamped at its base end, for example, the modes would change to match the clamped boundary conditions and would not represent properties of the barrel above. In the free-free configuration the modes of vibration of the real gun barrel can be determined for use in the computer models.

Using an instrumented hammer, the gun barrel was tapped near its base. The resulting vibrations were recorded opposite the impact point with a single

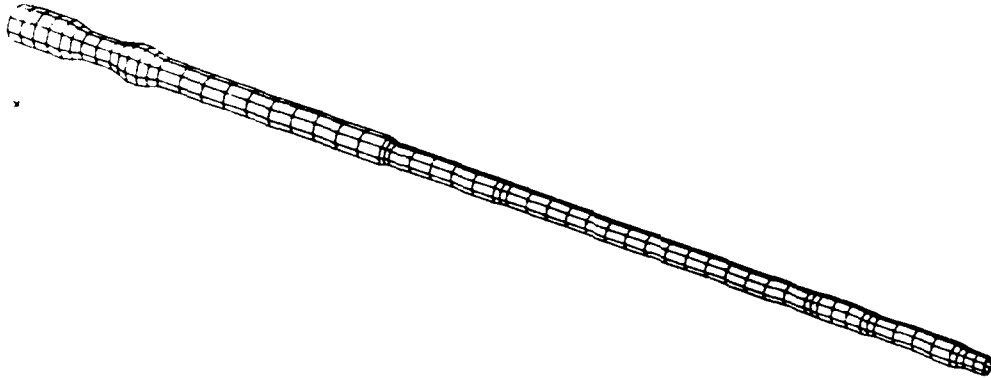


Figure 5-1. A single advanced barrel made of brick elements.

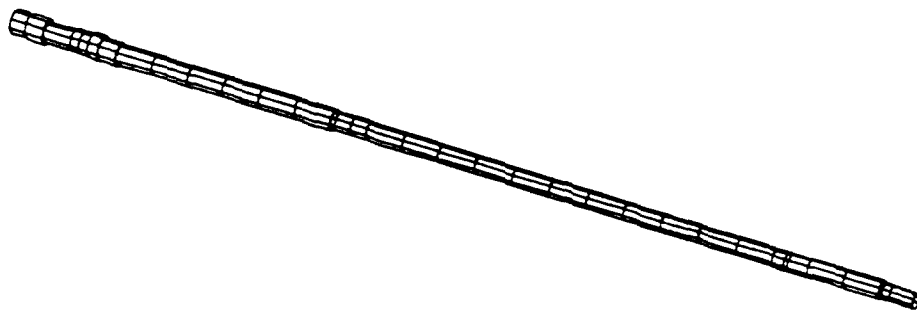


Figure 5-2. A single simple barrel made of beam elements.

transducer or accelerometer. Appendix A shows a plot of the recorded response for frequencies up to 3000 Hz. The excitation force due to the gun firing at a frequency of 75 Hz defines the important frequency range for this problem. The normal modes of vibration of the two versions of the gun barrel were calculated in the free-free configuration. Here, kinematic degrees of freedom were used to simulate the restraints provided by the two low stiffness cords in the experimental set-up. Figure 5-3 shows the first mode of vibration of the advanced barrel and Figure 5-4 shows that of the simple barrel. Table 5-1 lists the experimentally determined modes of vibration of the real barrel and those calculated for the computer models. Figure 5-5 graphically illustrates this data.

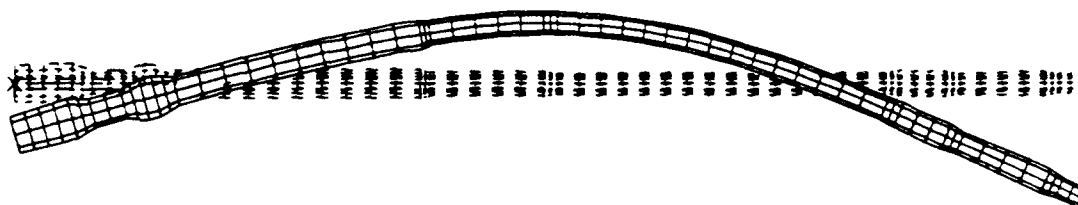


Figure 5-3. The first normal mode of vibration of the advanced barrel.

TABLE 5-1. COMPARISON OF ACTUAL AND MODELED GUN BARRELS

Modes of Vibration		
Experimental Barrel Data	Simple Barrel Data	Advanced Barrel Data
72.8	71.6	64.8
217	224	201
431	455	400
694	744	652
1040	874	809
1428	1111	982
1848	1515	1357
2363	1550	1501
2913	2013	1775

Looking at Figure 5-5, it can be seen that there is good correlation with both models and that of the real barrel over the first four modes of vibration or up through roughly 700 Hz. According to general finite element modeling practice, this agreement of the first four modes suggests that both gun models are validated. The agreement through 700 Hz for both gun models is considered excellent. It is also interesting to note that the simple barrel data matched the experimental barrel data more closely at the higher frequencies than the advanced barrel. This was probably due to the fact that the single layer of brick elements used in the advanced barrel model were not representing beam behavior very well. As

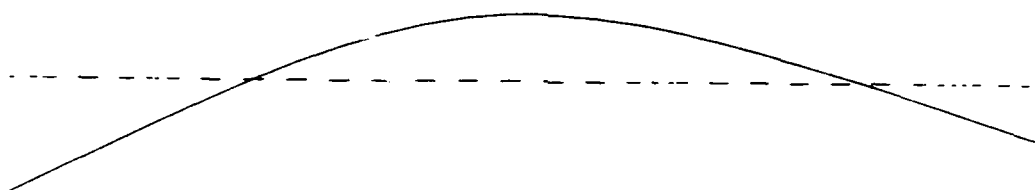


Figure 5-4. The first normal mode of vibration of the simple barrel.

mentioned in the previous chapter, more bricks are required to reflect bending and shear than do beam elements. Therefore, in the case of the advanced barrel, there should at least be two layers of brick elements used to define the barrel's thickness.

B. MODES OF VIBRATION OF THE COMPLETE GUN MODEL

After completion of the PHALANX gun model, its static properties were validated against the actual gun. The next step was to calculate its normal modes of vibration. Table 5-2 lists the first 21 calculated modal frequencies. Upon observing the normal modes, it became apparent that the first mode, which had a frequency around 0.3 Hz, was the normal mode of vibration of rotation about the

Modes of Vibration

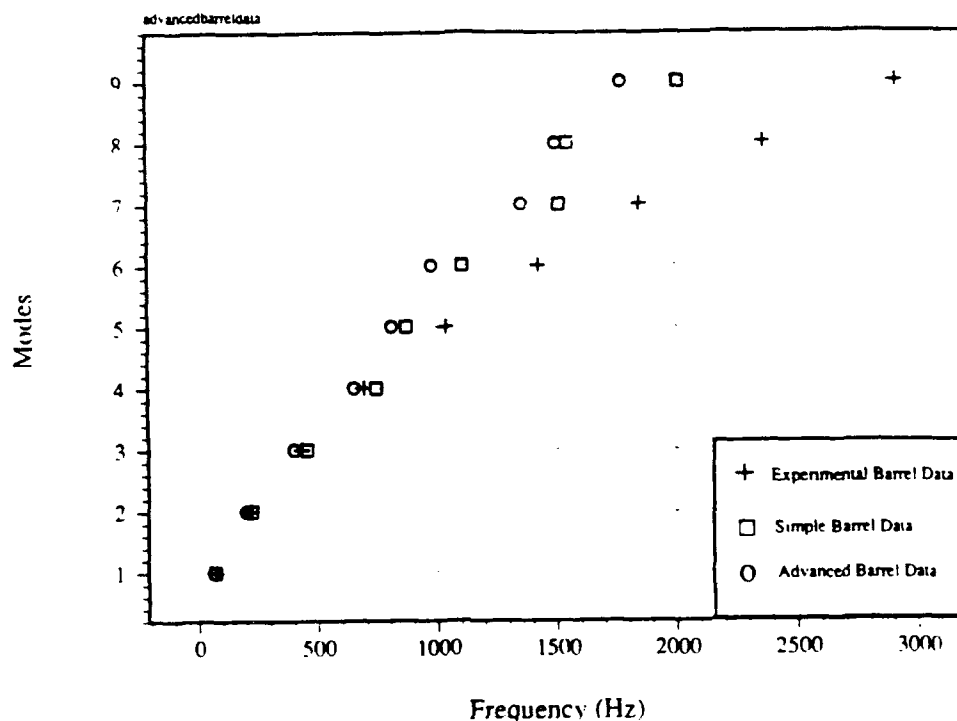


Figure 5-5. Comparison of the modes of vibration of the real barrel versus the two computer models.

lengthwise axis. This is a computational error since the gun barrel assembly is free to spin in the model and does not have any torsional restoring force associated with this motion. Therefore, it has a nonlinear, rigid body rotational mode of vibration of essentially 0.0 Hz. The fact that it was not exactly zero was probably due to the bearing springs not having coincident nodes which creates an unrealistic moment arm (see Chapter VII. Suggestions for Future Work). As mentioned in the previous chapter, the normal modes that are being calculated are those without gyroscopics or an unbalance (centrifugal) excitation. Therefore, the normal modes of the gun were resolved, this time restricting the rotational motion of the rotor, which removed that first torsional mode. Hence, the first 20 flexible modes were

calculated. The periodic force due to the firing of the gun is at a frequency of 75 Hz and lies between modes 6 and 7. A complete pictorial record of all the modes used in the dynamic analysis of the gun appears in Appendix B.

It is also important to note that in the mode shape pictures to follow, the amplitude of the deformation is greatly exaggerated in order to show the general shape of the normal mode and the relative displacements. Correct amplitudes will be found later when the dynamic response of the system is evaluated after driving it with the periodic firing force and values of damping are assigned. Obtaining normal modes is an important step in the process of obtaining displacement information.

TABLE 5-2. MODES OF VIBRATION OF THE PHALANX GUN

Modes of Vibration			
Normal Mode	Frequency (Hz)	Normal Mode	Frequency (Hz)
1	0	12	231
2	14.4	13	242
3	15.5	14	246
4	16.0	15	254
5	35.3	16	254
6	55.3	17	274
7	111	18	274
8	116	19	289
9	129	20	308
10	165	21	309
11	178		

1. First Flexible Mode

The first mode, at a frequency of 14.4 Hz, is considered to be significant in the analysis of the dispersion data. This is the second normal mode in Table 5-2. It appears to be a link between the periodic excitation force and its rotation which may be causing a resulting *whirling* motion of the six-barrel system. Here, the barrels act like an overhung shaft which whips around its center line with the barrel tips tracing a new, larger circle. This type of motion may provide an explanation for dispersion patterns that appear to be a circle of the six individual barrel patterns as mentioned in the first chapter. This motion will be discussed in greater detail in the last chapter.

Figure 5-6 shows a snapshot of this first flexible mode. It primarily consists of a rigid body motion where the barrels are straight and pitch from side to side. The rotor through the barrels move with respect to a stationary gun body. These components are pivoting about the thrust and needle bearings. There is little, if any, fore and aft motion. There is no recoil motion as indicated by the recoil adapter springs which are not exercised. In this mode and all the modes to follow, one component that appears to be "taking a lot of stress" is the rear gun body wall. Its deformation is readily apparent when a transparent picture is taken showing its motion with respect to the rotor, as can be seen in Figure 5-7.

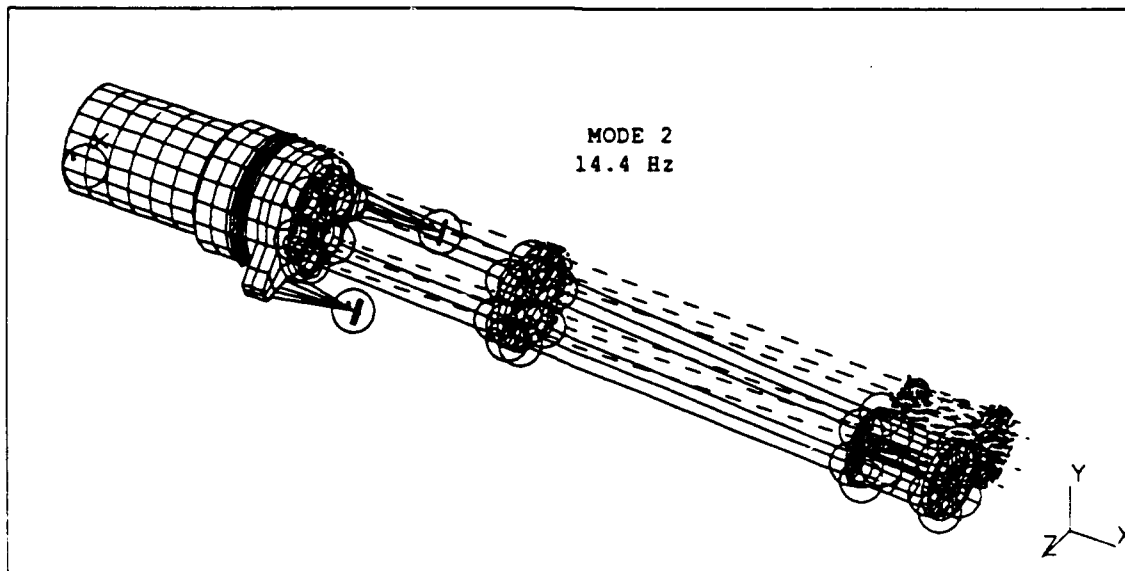


Figure 5-6. Hidden line image of the first flexible mode.

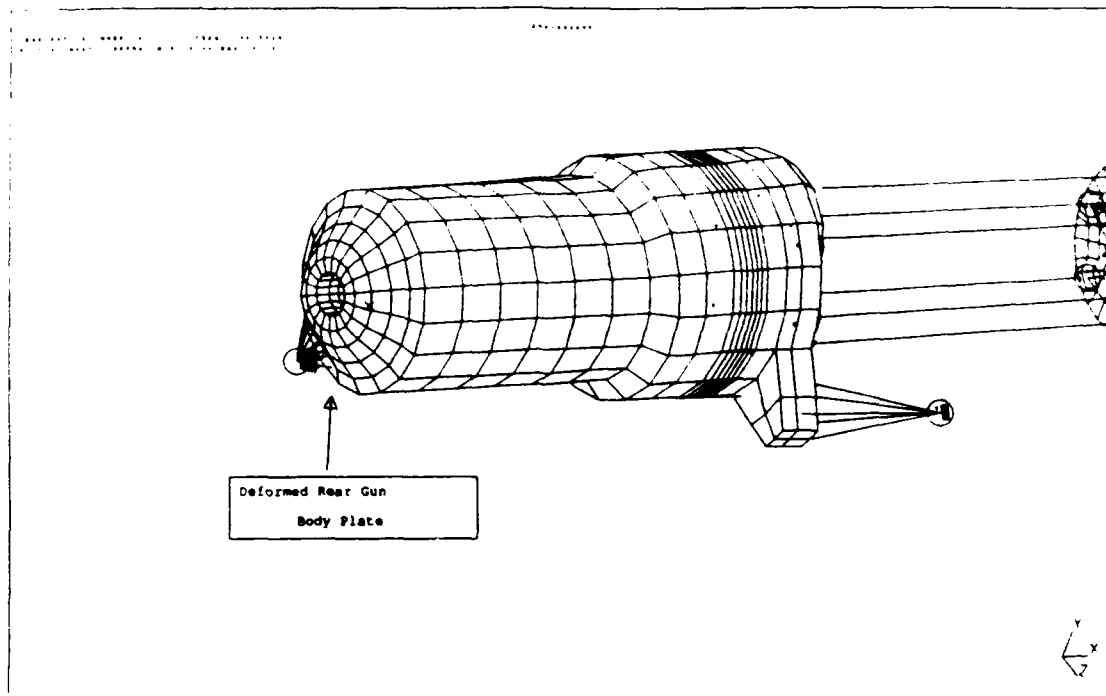


Figure 5-7. Hidden line image showing the deformation of the rear gun body plate.

2. Second Flexible Mode

The second flexible mode, at 15.5 Hz, is a combination of fore and aft motion and pitching of the gun barrel assembly. This is the third normal mode in Table 5-2. Figure 5-8 shows that the barrel assembly remains rigid as it pitches in the vertical plane. At the same time, the whole gun recoils and exercises the recoil adapter springs. It is also apparent that the gun body is also being exercised in this mode for it shows some deformation.

This is one mode where an easy hand calculation can be done in order to ensure that the numerical value of the normal mode frequency is reasonable. Assuming that the rotor, barrel assembly and gun body are rigid, the motion can

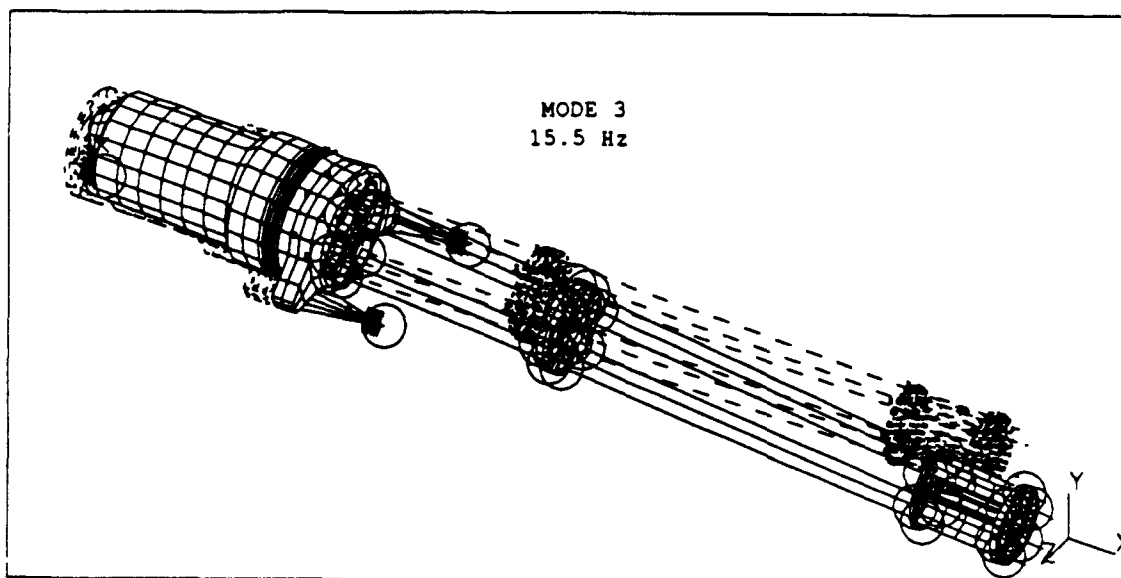


Figure 5-8. Hidden line image of the second flexible mode.

be described as a symmetric mode of the recoil adapters. That is, the whole gun of mass $M = 120$ kg is attached to ground via the two recoil adapter springs as shown in Figure 5-9.

The equation of motion for such a system is

$$M\ddot{x} + 2K_R(x_0 - x) = 0 \quad (5.1)$$

Here, x_0 is the equilibrium position of the lumped mass before it vibrates a distance x along the x axis. $K_R = 590,485$ cN/cm, is the stiffness value for the recoil adapter springs used in the numerical model. From the equation of motion, the normal mode angular frequency of vibration, ω , is

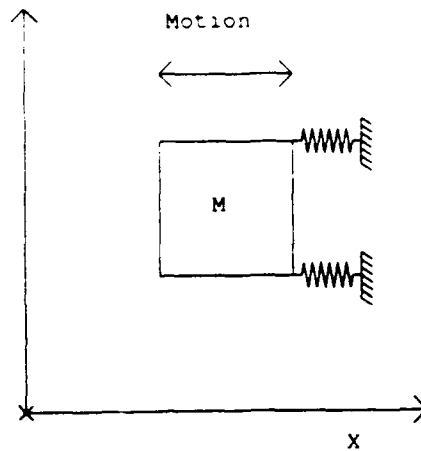


Figure 5-9. Illustration for analytically determining the normal mode frequency of pure recoil motion.

$$\omega^2 = \frac{2K_R}{M} \quad (5.2)$$

Its linear frequency f is therefore

$$f = \frac{1}{2\pi} \sqrt{\frac{2K_R}{M}} \quad (5.3)$$

Now substituting in the numerical values used by the computer, the frequency becomes

$$f = 15.8 \text{ Hz} \quad (5.4)$$

This compares favorably with the model value of $f = 15.5 \text{ Hz}$. The analytic calculation assumed a mode of oscillation purely along the x axis, whereas in the

numerical model, there is a pitching motion as well as the recoil motion which would contribute to the determination of its modal frequency.

3. Third Flexible Mode

The third flexible mode, or fourth normal mode, is similar to the previous mode. A snapshot of its motion is shown in Figure 5-10. Its frequency is only slightly greater at 16.0 Hz. The one apparent difference is that there is less recoil motion than seen in the previous mode. This is evidenced by the lack of deformation in the recoil adapter springs. Its motion is almost a purely pitching motion of the barrel assembly in the vertical direction.

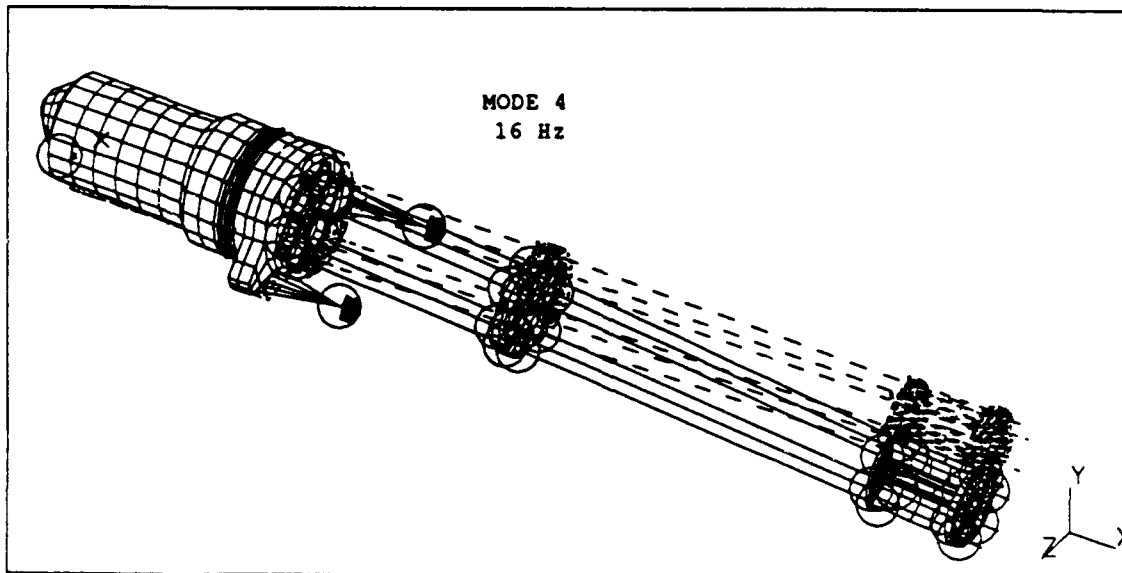


Figure 5-10. Hidden line image of the third flexible mode.

4. Fourth Flexible Mode

The first thing noticeably different in the fourth flexible mode, or fifth normal mode, is the massive deformation of the gun body as displayed in Figure 5-11. The mode of oscillation of the gun body shows a bending node in its mid-section with a normal mode frequency of 35.3 Hz. The gun barrel assembly remains rigid with respect to the thrust and needle bearings. The motion of the barrel assembly appears to be caused solely by the bending of the gun body as it heaves up and down. There is no recoil motion in this mode. It is important again to note the deformation of the rear gun body plate which seems to suggest that its strength would play a crucial role in restricting barrel tip displacement.

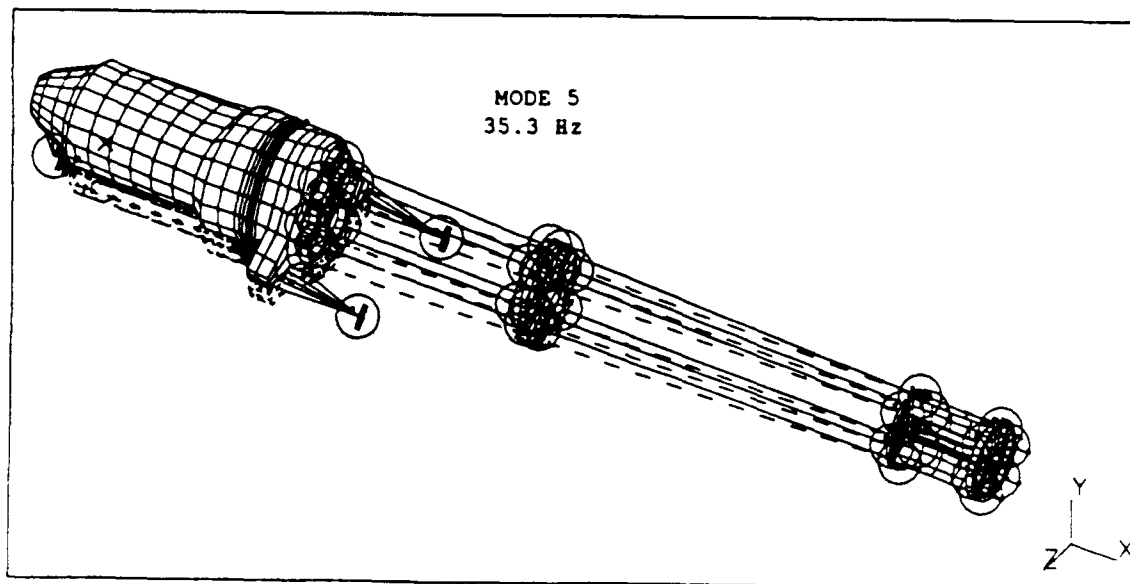


Figure 5-11. Hidden line image of the fourth flexible mode.

5. Fifth Flexible Mode

The fifth flexible mode, or fourth normal mode is at 55.3 Hz. Again it appears to involve a mode of oscillation of the gun body alone as shown in Figure 5-12. However, the gun body oscillation is that of a *breathing* mode where the walls move in and out. Like the previous mode the gun barrel assembly remains stationary with respect to the bearings. So the barrel motion is directly related to the motion of the gun body walls. As the walls breath, the recoil adapters appear to twist in the vertical direction. There is no motion in the fore and aft direction except that caused by gun body oscillation.

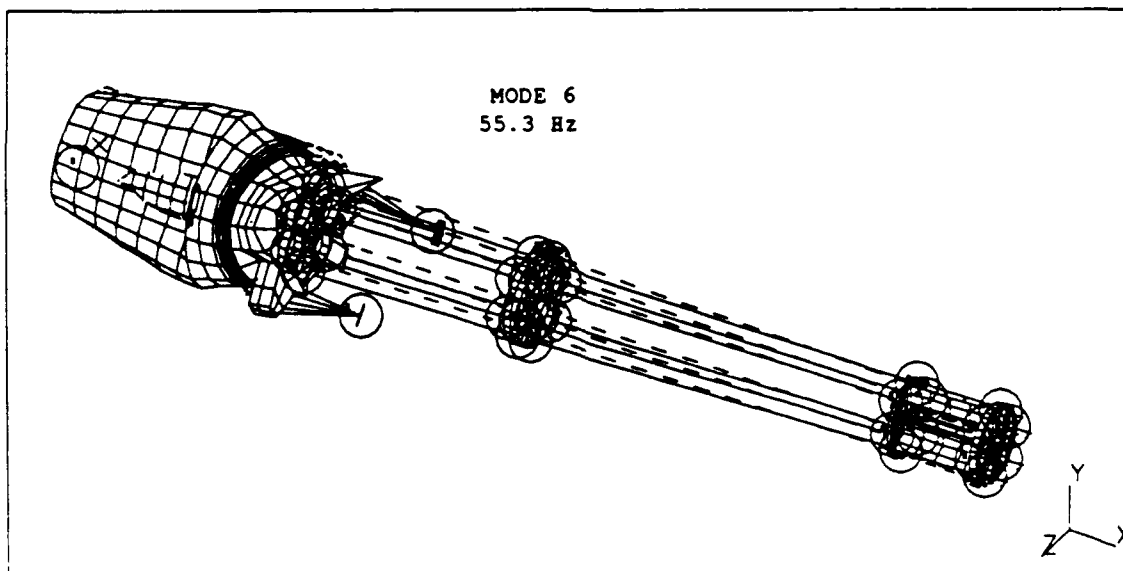


Figure 5-12. Hidden line image of the fifth flexible mode.

6. Sixth Flexible Mode

The final mode to be discussed is the seventh normal mode and is the first mode in which the barrels themselves are exercised. This mode, at 111 Hz, is shown in Figure 5-13. The barrel tips remain parallel to ground as they oscillate about a single bending node located just forward of the mid-barrel clamp. The boundary conditions of the muzzle clamp seems to be vital in relation to barrel tip motion. In the real gun, three of the barrels are *unlocked* in the muzzle clamp while the other three are locked. In this model, all the barrels are rigidly attached or locked to the muzzle clamps. A possible future modification would be to unlock three of the barrels in the muzzle clamp and simulate the effect of a gap around them using spring elements. The difficulty would come in determining the stiffness values of the springs since this is a nonlinear problem. A new version of I-DEAS, called the Master Series, is able to simulate the effect of a gap or tolerance. After the real gun is set up or-sight, then tests can be performed to determine the proper stiffness values. This vibrational mode of the barrels with clamps seems to exhibit the behavior of a *deep flange beam* which is different than the six barrels represented as a single beam. A deep flange beam tends to shear like the barrels in the model rather than bend like a beam.

Looking at the rest of the gun, there is massive deformation of the gun body with a single bending mode in the middle. The rotor essentially remains parallel to ground as the gun body and barrels flex. There is no recoil motion associated with this normal mode.

C. MODAL TRUNCATION

With 22,470 degrees of freedom, there are an equal number of normal modes of vibration. Solving for all of these normal modes is unnecessary, but would defeat the purpose of reducing the complex model into relatively simple normal modes. The System Dynamics Analysis module, to be discussed further in the next

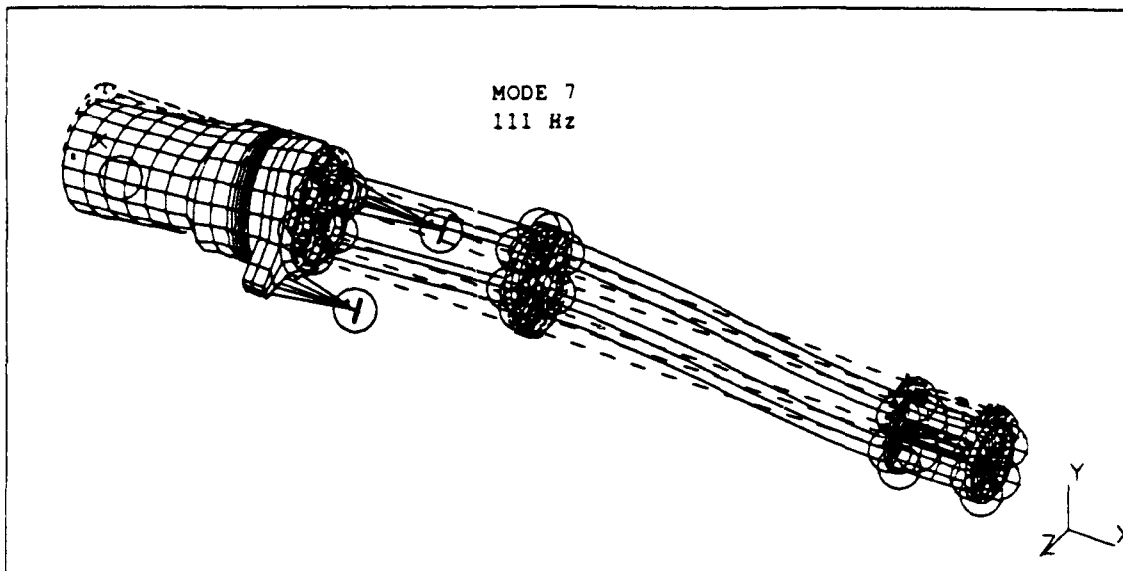


Figure 5-13. Hidden line image of the sixth flexible mode.

chapter, calculates the dynamic response of a system by first solving for the modes of vibration. Instead of using the 22,470 *physical* degrees of freedom, it can describe the response using the first 20 flexible modes of Table 5-2.

According to generally accepted finite element modeling practice, the number of normal modes that should be carried through for a dynamic response analysis are those that fall within twice the excitation frequency. Since the gun's principal excitation frequency is 75 Hz, the modes through 150 Hz should be calculated. By solving for the first 20 modes, up to a frequency of 309 Hz then this criteria is more than satisfied.

VI. DRIVING AND DAMPING OF THE PHALANX GUN

A. DYNAMIC ANALYSIS OF THE GUN MODEL

Having completed a modal analysis of the PHALANX gun model, the next step, as outlined in Chapter III, is to perform a forced response analysis of the gun. The excitation forces caused by the bullets recoil and estimates of damping in the gun are applied. The resulting response, such as barrel tip displacement, can then be determined and compared to experimental data. The most prominent normal mode can be found to describe the actual motion of the gun when firing. With the completion of these steps, a *working* model of the PHALANX gun has been created. The factors which contribute to dispersion can be studied systematically, and potential solutions to problems can be tested to provide an additional source of information to the PHALANX program office. Various components can be "swapped" out to evaluate modified components, and the resulting effects on gun performance predicted prior to any hardware tests. This is the first finite element model of its kind ever constructed of the PHALANX gun, and the possibilities for its use are only limited by imagination.

The I-DEAS computer code evaluates a structure's response to applied forces in the computer module called System Dynamics Analysis (SYSTAN). The method used by SYSTAN is to first develop a *modal component model* of the structure. That is, a certain number of normal modes of a structure are calculated and stored as a new modal model of the structure which is then used to calculate the dynamic response. Other methods can be used, such as directly integrating the equation of motion

$$\underline{F} = [\underline{M}]\ddot{\underline{X}} + [\underline{C}]\dot{\underline{X}} + [\underline{K}]\underline{X} \quad (6.1)$$

Here, column matrices are represented with underlines and square matrices with

brackets. \underline{F} represents the applied forces and their direction on each degree of freedom in the system. $[M]$ is the modal mass matrix that was obtained through the process of transforming to normal coordinates described in Chapter III. Each of the i th matrix elements is a measure of how much mass is participating in the i th normal mode. Similarly, $[K]$ is the modal stiffness matrix and is a measure of the stiffness occurring in each of the normal modes. $[C]$ is the associated damping for and between each degree of freedom. The displacements, velocities and accelerations for each degree of freedom are represented by \underline{X} , $\dot{\underline{X}}$, and $\ddot{\underline{X}}$ respectively. However, when there is a structure with many degrees of freedom, like the PHALANX gun model with 22,470, it becomes apparent that the calculations required are memory and time consuming. Reducing the number of physical degrees of freedom, \underline{X} , from 22,470 to 20 modal degrees of freedom, \underline{x} , greatly reduces the complexity of the model. In order to accomplish this reduction, a transformation to normal coordinates diagonalizes the mass, stiffness and damping matrices of the equation of motion as discussed in Chapter III. Reductions which do not diagonalize are also possible, but will not be discussed here. The equation of motion can then be written as

$$\underline{F} = \begin{bmatrix} \mathbf{M}_{11} & 0 & . & . \\ 0 & \mathbf{M}_{22} & 0 & . \\ . & 0 & . & 0 \\ . & . & 0 & \mathbf{M}_{ij} \end{bmatrix} \ddot{\underline{x}} + \begin{bmatrix} \mathbf{C}_{11} & 0 & . & . \\ 0 & \mathbf{C}_{22} & 0 & . \\ . & 0 & . & 0 \\ . & . & 0 & \mathbf{C}_{ij} \end{bmatrix} \dot{\underline{x}} + \begin{bmatrix} \mathbf{K}_{11} & 0 & . & . \\ 0 & \mathbf{K}_{22} & 0 & . \\ . & 0 & . & 0 \\ . & . & 0 & \mathbf{K}_{ij} \end{bmatrix} \underline{x} \quad (6.2)$$

This equation is similar to the diagonalized equation of motion (3.60), developed in Chapter III, except that now a damping matrix $[C]$ and an excitation force \underline{F} have been added. Damping is necessary when evaluating a dynamic response in order to simulate the effects of energy dissipation in each normal mode. Otherwise, the motion of a structure will continue to grow unbounded as the excitation force is applied. In (6.2) and in SYSTAN, the damping is assumed to be viscous damping proportional to the velocity of the structure simulating the effects of friction. With

the matrices diagonalized, and hence uncoupled, the equations of motion are easily solved. [Ref. 11]

The conversion can then be made back to the physical degrees of freedom through the relation

$$\underline{X} = [\Phi] \underline{x} \quad , \quad (6.3)$$

where $[\Phi]$ represents the spatial and temporal parts of the mode shape as discussed in Chapter III. Each column of this matrix is an eigenvector ϕ^i which corresponds to each modal degree of freedom. [Ref. 11]

B. DAMPING IN THE PHALANX GUN

Damping in the PHALANX gun model is defined as Rayleigh or proportional damping. Since the diagonalized modal mass and stiffness matrices were obtained without the velocity damping term in the equation of motion, then the damping matrix $[C]$ is not diagonalized. Instead, the damping coefficients are defined by the relation

$$C = \alpha K + \beta M \quad . \quad (6.4)$$

Diagonalizing this matrix yields

$$\begin{aligned} \phi^T C \phi &= \alpha \phi^T K \phi + \beta \phi^T M \phi \\ &= \alpha [K] + \beta [M] \quad , \end{aligned} \quad (6.5)$$

where $[K]$ and $[M]$ are now diagonalized matrices. Substituting these relations back into the equation of motion gives

$$\underline{F} = [M] \ddot{\underline{x}} + [K] \underline{x} + (\alpha [K] + \beta [M]) \dot{\underline{x}} \quad . \quad (6.6)$$

The quantity in parenthesis is called modal damping and it was this quantity that was assigned a numerical value in the gun model. The correct modal damping values, α and β , can only be determined by measurements on the actual system being modeled. Therefore, damping is associated with each normal mode and not

with each element in the gun model. To more accurately represent damping of the real gun, damping would have to be defined in terms of two physical points, such as a dashpot in the recoil adapter, and not just with each mode. Each mode itself is not a pure motion as well. For example, the recoil mode has a certain amount of pitching associated with it, so an additional value of damping should be assigned to this additional motion. In the absence of measurements, the particular components of the gun involved in each normal mode can be used to estimate damping. Damping values were assigned based on knowledge of how the components are assembled, for example, welded or bolted components have certain damping, while the barrels alone have only small damping as observed in the modal vibration tests and the recoil adapter springs are intentionally damped by the manufacturer, as described by a hysteresis plot.

In the SYSTAN module, damping is defined as a percent of *critical* damping. To clarify further, the effects of damping are associated with three physically distinct cases. These cases are derived from the equation of motion (6.2) where an exponential function of the form

$$X = e^{qt} \quad , \quad (6.7)$$

was used as a solution with the driving force set to zero. The equation of motion for the first mode is then

$$M_{11} \frac{d^2}{dt^2} e^{qt} + C_{11} \frac{d}{dt} e^{qt} + K_{11} e^{qt} = 0 \quad . \quad (6.8)$$

Performing the necessary derivatives and canceling the factors of e^{qt} yields the quadratic equation

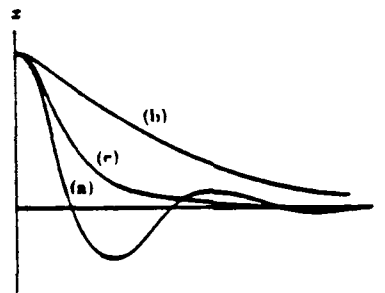
$$M_{11} q^2 + C_{11} q + K_{11} = 0 \quad . \quad (6.9)$$

Solving for q using the quadratic formula gives

$$q = \frac{-C_{11} \pm (C_{11}^2 - 4M_{11}K_{11})^{\frac{1}{2}}}{2M_{11}} \quad . \quad (6.10)$$

The three different damping cases are then determined from the value of the discriminant $C_{11}^2 - 4M_{11}K_{11}$. *Overdamping* occurs for the case where $C_{11}^2 - 4M_{11}K_{11} > 0$. In this case there is an exponential type of decay. Given an initial displacement, the structure does not oscillate about its equilibrium position as shown in Figure 6-1(b). The *critical damped* case occurs when $C_{11}^2 - 4M_{11}K_{11} = 0$. Like overdamping, critical damping does not oscillate, but dampens out asymptotically as shown in Figure 6-1(c). Finally, the *underdamped* case occurs when $C_{11}^2 - 4M_{11}K_{11} < 0$ where the structure oscillates about its equilibrium point sinusoidally, but eventually dampens out as shown in Figure 6-1(a). [Ref. 18]

THE DAMPED HARMONIC OSCILLATOR



Return of harmonic oscillator to equilibrium. (a) Underdamped. (b) Overdamped.
(c) Critically damped.

Figure 6-1. Graphs of displacement for the three case of damping.

When determining a damping value based on knowledge of how the components are connected, experts in the industry have accepted general empirical values until more information is obtained. Modes involving welded parts are assumed to have damping values of around 1 percent of critical damping whereas bolted structures have values between 3 and 5 percent. For clamped components, 2 percent is an accepted value. Since most of the components are clamped in the gun, 2 percent was used for most of the modes. [Ref. 11]

A second case estimates the modal damping value for a single gun barrel. Only this component has been observed while measuring the modal vibration. While obtaining the normal modes of vibration of the single gun barrel by tapping it with the instrumented hammer, it was observed to have a very low damping value. It was observed to have a damping value of less than 1 percent in the free-free configuration. The damping value used in the computer model was raised to 2 percent to reflect the fact that each gun barrel is clamped at its base, middle and end points.

Another component that has experimental damping information available are the two recoil adapters. A hysteresis plot provided by Martin Marietta for the two recoil adapters is shown in Figure 6-2 [Ref. 15]. It shows the loading force applied to the recoil springs for one cycle on the vertical axis and the resulting deflection on the horizontal axis. The upper branch reflects the initial loading and the lower branch the return to battery. The area contained within the two branches is the energy dissipated per cycle, $E_D = 4.34 \times 10^3 \text{ N}\cdot\text{cm}$ (384 *lb\cdot in*). The damping coefficient, C_{hyst} , is then determined from the equation

$$E_D = \pi C_{hyst} |x|^2 \omega \quad , \quad (6.11)$$

where, x is the amplitude of oscillation about its driven equilibrium point estimated by the mid-point in the hysteresis plot, or $x = 0.4 \text{ cm}$ (0.15 in). After the first few rounds are fired, the gun sets back about 1.3 cm (0.5 in), and then

oscillates about this new equilibrium position until the gun stops firing. It never returns to battery between shots like other naval guns. The angular frequency of oscillation of the recoil mode $\omega = 30\pi / s$. Rearranging and solving for C_{hyst} yields

$$C_{hyst} = \frac{E_d}{\pi |x|^2 \omega} = 91.6 \frac{N}{cm / s} \quad (6.12)$$

The damping coefficient, $\gamma = C_{hyst} / C_{crit}$, used by the computer code is expressed as a percentage of critical damping, C_{crit} where

$$C_{crit}^2 = 4mK \quad , \quad (6.13)$$

m is the mass of the gun, and K is the stiffness of the recoil adapters. Substituting values into this equation gives

$$C_{crit} = 2.38 \times 10^2 \frac{N}{cm / s} \quad , \quad (6.14)$$

so that γ can now be calculated as

$$\gamma = \frac{C_{hyst}}{C_{crit}} = 0.39 \quad (6.15)$$

The value for γ in (6.15) is consistent with the actual damping value used in the design of the recoil adapters, $\gamma = 0.33$, as provided by Martin Marietta [Ref. 19]. A damping coefficient which approaches critical damping, $\gamma \rightarrow 1$, gives a more optimum return to equilibrium after the excitation force has stopped. In the computer model a damping value of $\gamma = 0.33$ was used for this mode. The recoil mode, referred to in Chapter V as the third flexible mode of vibration at 15.5 Hz, shows the gun sliding fore and aft exercising the recoil adapter springs with a slight pitching of the barrels in the vertical plane. This is the only mode using a damping value other than 2 percent. The purpose of the recoil adapters is to dissipate some of the force caused by the firing rounds and to couple the remaining force to the ship. Allowing a gun to recoil even a few calibers greatly reduces the

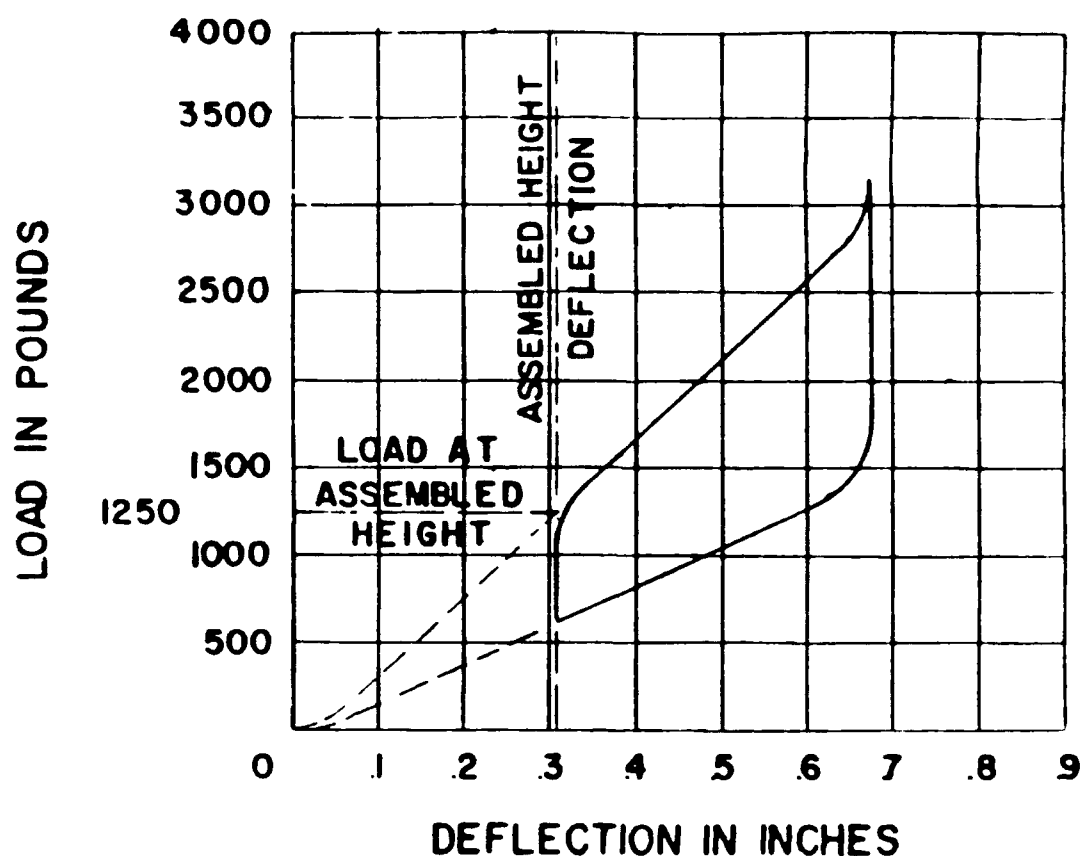


Figure 6-2. Hysteresis plot of the recoil adapter springs.

force of recoil transmitted to the mount so that a much lighter gun mount can be used.

Table 6-1 lists the damping values applied to each normal mode of vibration used in the PHALANX gun model. Most of the damping values used in the model are crude estimates based on information derived without the actual gun on sight. Further experimental tests should be performed allowing for further refinement of the damping values.

TABLE 6-1. MODAL DAMPING VALUES

Damping of the Modes of Vibration			
Normal Mode	Damping (γ)	Normal Mode	Damping (γ)
1	0	12	0.02
2 (yaw)	0.02	13	0.02
3 (recoil, pitch)	0.33	14	0.02
4 (pitch)	0.02	15	0.02
5 (gun body mode)	0.02	16	0.02
6 (gun body mode)	0.02	17	0.02
7 (barrel bending)	0.02	18	0.02
8	0.02	19	0.02
9	0.02	20	0.02
10	0.02	21	0.02
11	0.02		

C. DRIVING THE PHALANX GUN

The principal excitation force of the PHALANX gun is the repeated firing of the rounds. Only one barrel shoots at a time, so that a firing rate of 4500 shots per minute gives the frequency of the excitation force 75 Hz. The experimentally determined force on the breech for a single shot lasts roughly 2.3 milliseconds as displayed in Table 6-2 and plotted in Figure 6-3 [Ref. 15].

TABLE 6-2. FORCE ON GUN BREECH

Force of Single Shot on Breech			
Time (milliseconds)	Force (lb)	Time (millisecond)	Force (lb)
0.05	8.74×10^2	0.80	2.85×10^4
0.10	1.26×10^3	0.85	3.02×10^4
0.15	1.72×10^3	0.90	3.12×10^4
0.20	2.33×10^3	0.95	3.16×10^4
0.25	3.12×10^3	1.00	3.13×10^4
0.30	4.14×10^3	1.05	3.02×10^4
0.35	5.45×10^3	1.15	2.59×10^4
0.40	7.11×10^3	1.25	2.02×10^4
0.45	9.17×10^3	1.45	1.16×10^4
0.50	1.17×10^4	1.65	7.68×10^3
0.55	1.45×10^4	1.85	5.57×10^3
0.60	1.76×10^4	2.05	4.29×10^3
0.65	2.08×10^4	2.25	3.46×10^3
0.70	2.37×10^4	2.31	3.26×10^3
0.75	2.64×10^4		

A typical missile engagement burst lasts for only a few seconds up to a maximum of 5 seconds before the barrels deteriorate due to the high temperature. Therefore, a driving force of one hundred shots was constructed. Due to the sharpness of the firing "spike" compared to the length of time between shots, 13.3 milliseconds at 75 Hz, it was necessary to determine more data points for each shot in order to increase the resolution of the response. A function was fit to the available data in Figure 6-3, as shown in Figure 6-4. The function's representation

Force on Breech

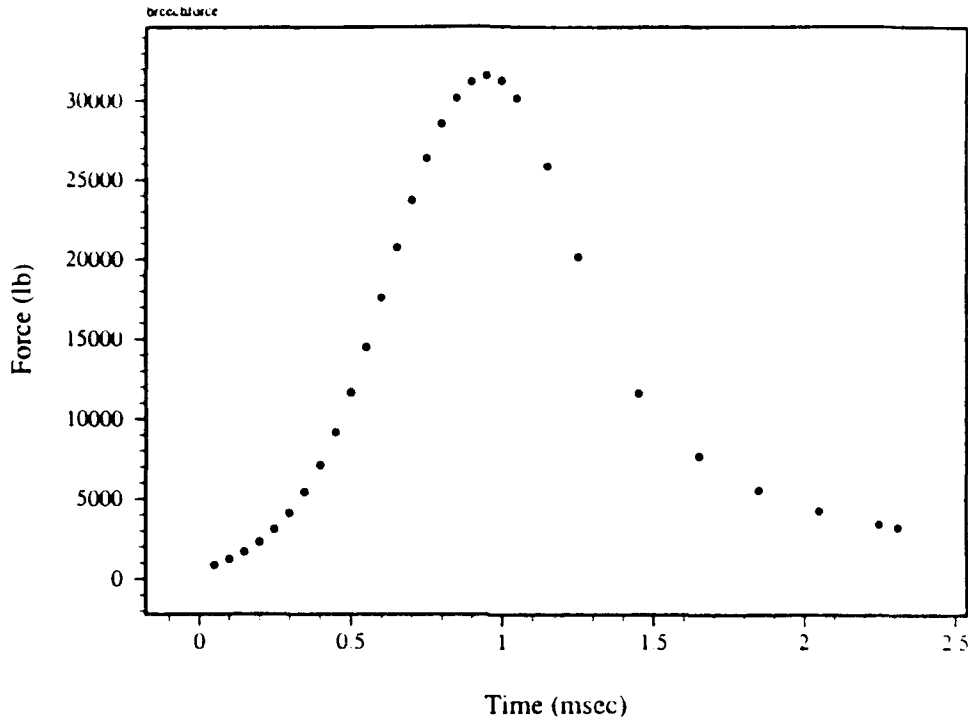


Figure 6-3. Plot of the force on the breech from a single shot [Ref. 15].

of the first 3 shots is shown in Figure 6-5 with dots representing the experimental data points described above. The function was used in SYSTAN to create a forcing function using 26,400 data points over a one hundred shot burst. The 26,400 evenly spaced points are spaced at intervals of 0.05 milliseconds to provide a good representation of each 2.3 millisecond shot. The number of data points used is then determined as

$$\text{Number of points} = \frac{1.3 \text{ seconds}}{0.05 \text{ milliseconds}} \approx 26,400 \quad (6.16)$$

where, 1.3 seconds is the length of time for a 100 shot burst.

Force on Breech

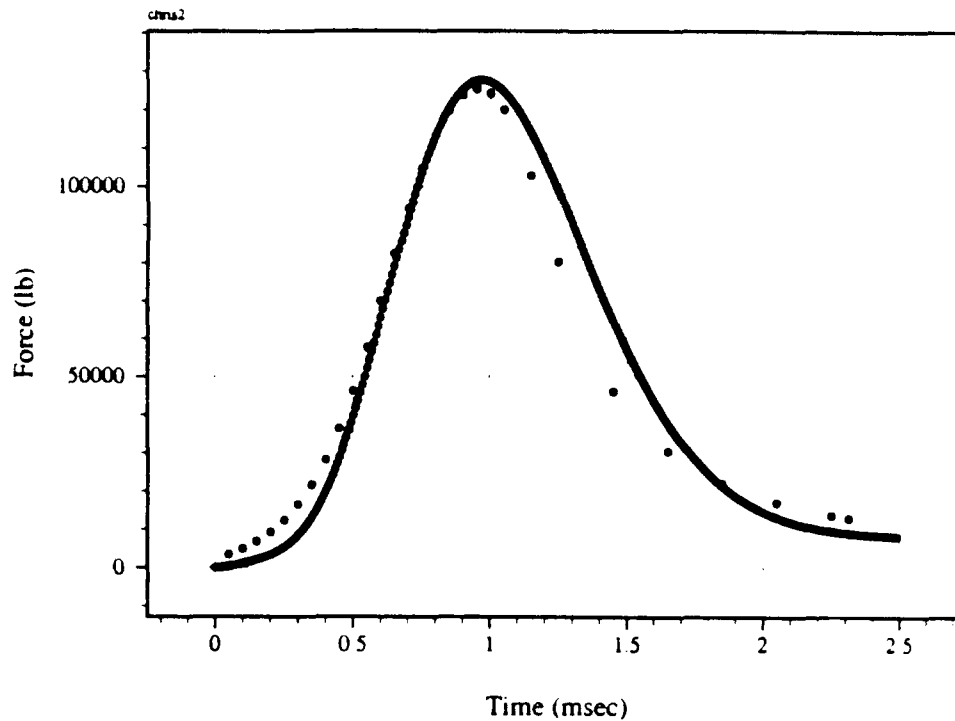


Figure 6-4. Plot of the function used to approximate the single shot data.

A single shot by itself is broad band and is comprised of many frequencies. It is like an impulse or delta function. The firing of a single shot by the gun model, would be expected to excite many normal modes of vibration over a wide frequency range. However, the gun is never used in the single shot mode, so this case is irrelevant. A long series of shots is no longer broad band, but has a fundamental frequency of 75 Hz. This type of excitation force would be expected to excite fewer modes in a small range around 75 Hz.

A burst of shots is applied at the base of the firing barrel located approximately between 10 and 12 degrees from top dead center. The firing sequence was first designed for the older firing rate of 3000 shots per minute. In this case, the round was ignited at this off-center position so that when the barrel

Force on Breech

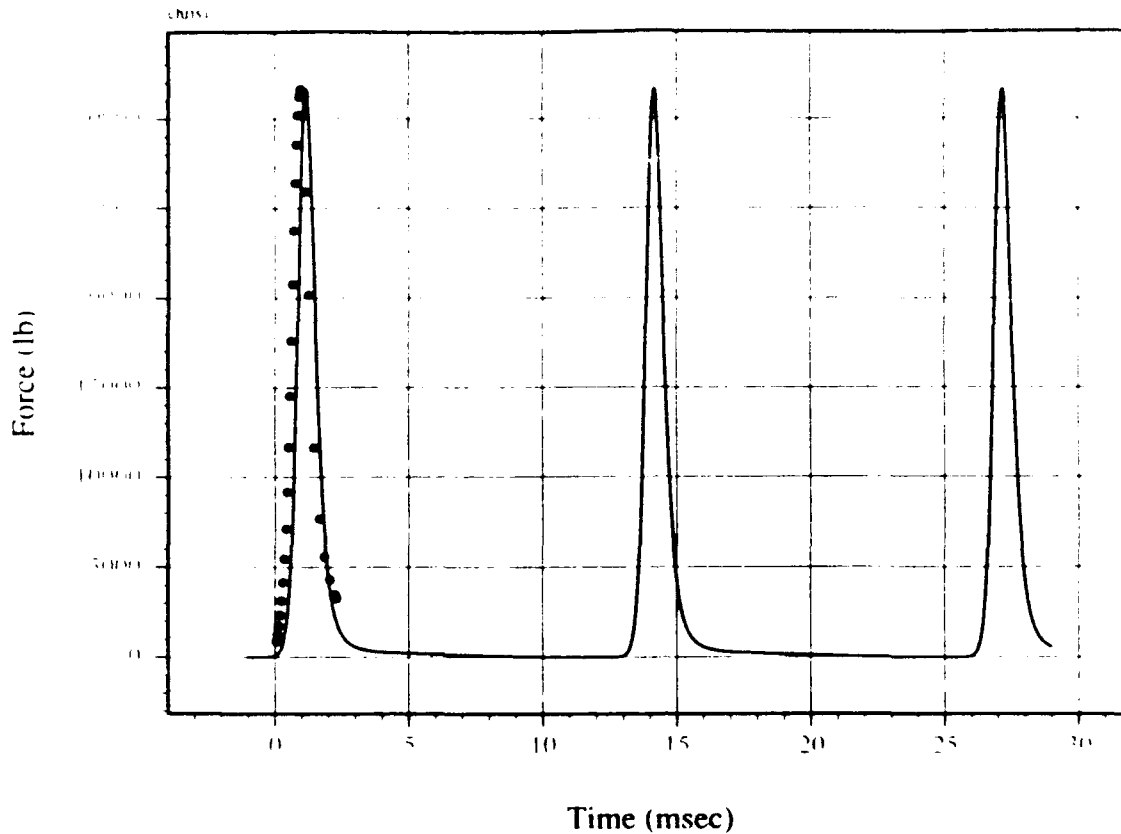


Figure 6-5. The function's approximation for the first 3 shots.

reached the top, the round would just be leaving the barrel. However, the firing rate has been changed to 4500 shots per minute without an adjustment being made to the igniting point. Because of the higher rotation rate of the barrel assembly, the bullet leaves the barrel approximately 14 degrees *past* top dead center. The time varying magnitude of the firing force is applied to the gun over a 20 degree arc. To simulate this off-center firing force, the barrels were moved 10 degrees from the top. The gun model barrels can be rotated to any point along this 20 degree arc, and the firing force reapplied. The barrel tip motion can then be recalculated. This is an approach being taken by Martin Marietta. It has not been possible to continuously rotate the barrels in the numerical model while applying

the firing force. The current arrangement gives a good approximation. It appears that there is a way to "trick" the computer code into simulating the effects of rotation, but this is currently beyond the scope of the current work. Exploring this improvement is recommended as a further refinement of the model.

A possible complication in applying the firing force to the gun is the fact that it may be a *follower force* problem. That is, as the barrel assembly becomes displaced from its center line, for whatever reason, the firing force ought to be applied to the gun in this displaced position. The combination of this displacement and normal firing would add other, currently unpredictable, effects on the barrel tip motion. The following force problem is probably best suited to be described analytically. Preliminary steps in this direction have been taken by Professor Gordis.

Another force acting on the gun arises from the rotating barrels. The rotation rate of the six-barrel system is $12.5 \text{ Hz} = 75 \text{ Hz} / 6 \text{ barrels}$. This motion can play an important role in gun dynamics since there is a nearly resonant normal mode of vibration at 14.4 Hz . This normal mode describes a pitching motion of the barrels and may contribute to the dispersion pattern if excited.

When the rotating barrels are displaced from their center line, they will cause excitation. A perturbing force that could cause a displacement would be a weight imbalance between the barrels. The mass of a barrel may vary by as much as 0.227 kg (0.5 lb) away from the average weight of 8 kg (18 lb). This imbalance would cause the barrel cluster to bend slightly as they rotate. This displacement could also start when the barrel cluster kicks up as the gun first fired. The kicking up is caused by the placement of the recoil adapters and the rear ball joint in relation to the point of application of the firing force. Displacement is created due to the imbalance of the firing point and the three supports. Any of these causes leads to excitation of a physical motion called gyroscopic "whirl." The near resonance of the barrel rotation rate and the first flexible mode of vibration

appears sufficient to excite this pitching mode and greatly affect dispersion. Furthermore, a non-preloaded thrust bearing, as is used in the PHALANX gun, is considered to be a root cause of gyroscopic whirl [Ref. 20]. Gyroscopic whirl will be further discussed in a latter section. There are a variety of "causes" for dispersion that may feed upon others. If one could determine the primary causes then it may be possible to prevent or limit others.

Another excitation force on the gun is the torque exerted on the barrel as each round spins up as it travels along the barrel. The barrel lands have a right-hand exponential gain twist which rotates the penetrator to a rotation rate of 120,000 revolutions per minute (2,000 revolutions/ second) as it leaves the barrel [Ref. 21]. The torque to achieve this rotation rate can be calculated by first determining its rate of angular acceleration,

$$\dot{\omega} = \frac{\omega_f - \omega_o}{t_s} \quad , \quad (6.17)$$

where, ω_f is the final rotation rate, ω_o is the initial rotation rate, and t_s is the time that the round travels the length of the barrel. Substituting the values in yields

$$\dot{\omega} = 5.46 \times 10^6 \frac{\text{radians}}{\text{second}^2} \quad .$$

The torque applied by the barrel on the round to achieve this rotation rate can be calculated using the following relation,

$$F_b = \frac{I \dot{\omega}}{a} \quad , \quad (6.18)$$

where I is the moment of inertia of a cylinder which approximates that of the round, and a is the inner radius of the barrel. I is determined according to the relation

$$I = \frac{m_r a^2}{2} \quad , \quad (6.19)$$

where m_r is the mass of the round. I is calculated to be

$$I = \frac{(0.071 \text{ kg} \times 10 \text{ mm})^2}{2} = 3.55 \times 10^{-6} \text{ kg m}^2$$

Substituting this value into equation (6.18) gives

$$F_b = 435.6 \text{ lb}$$

showing a significant force on the barrels. This type of force may be difficult to simulate with this model due to its variation in location with time, and is similar to the rotating barrel problem.

Other possible forces include an imbalanced load on the gun with heavy preshot rounds on one side and the lighter expended casings on the other. Also, the act of loading a round is not insignificant and would add an impulsing torque to the gun assembly. Furthermore, the actual rate of firing varies since the hydraulic motor which rotates the barrel assembly, and determines the firing rate, varies its speed by as much as ± 50 revolutions per minute. These variations could occur as sudden rotation speed shifts resulting in a torque or "jerk" on the barrel assembly.

The modeling of the PHALANX gun in this study ends at the three supporting fixtures. Other factors affecting the gun's motion from beyond these points are not being simulated, but may also play a role in the actual dispersion. The gun mount will rarely be in a stationary position when attempting to shoot down targets moving at speeds on the order of a few Mach. The gun can slew at a maximum rate of 92 degrees per second in elevation and 126 degrees per second in train or rotation. This motion, may serve as a perturbing force to start the gyroscopic whirl mentioned earlier. The whole gun mount is mounted on a set of shock absorbers whose purpose is to limit the shock wave of a close-order explosion. The vibrating gun interacting with these shock mounts may merit future consideration.

In an actual gun, all of these forces may play a role in the observed dispersion pattern. Some of these forces may be added to the current gun model analysis, but this study only addresses the role played by the most significant force of the gun firing.

D. RESPONSE OF THE GUN MODEL

While driving the gun model with a one hundred shot forcing function, the resulting response of the top barrel tip was evaluated to its translation along each of the three coordinate axes. Shown in Figure 6-6 is the amplitude of the barrel tip's motion along the x-axis in the fore-aft direction versus time. The plot shows that the gun immediately sets back by roughly 1.27 cm (0.5 in) after the first shot is fired. It then begins to oscillate about its new equilibrium position by roughly 0.80 cm (0.32 in) at a frequency between 15 to 20 Hz as one or more of the lower order modes is excited. It appears to reach a steady-state oscillation near the end of the burst of shots. When the firing is complete after 1.3 seconds time on the horizontal axis, the gun moves forward to its initial position and vibrates like an underdamped harmonic oscillator. During excitation, the displacement versus time shows an irregular pattern of jagged peaks indicating excitation of several normal modes. Understanding which normal modes are involved in the response will provide the greatest benefit in predicting the dispersion pattern. The determination of these modes will be provided by a frequency analysis which will be the subject of the next section.

The important barrel tip displacement in the vertical direction is shown in Figure 6-7. The barrel tip can be seen to pitch upward significantly after the first shot, and then approach steady-state oscillation near the end of the firing burst. The peak-to-trough barrel tip displacement measured near the steady-state motion is about 2.5 mm (0.1 in) and gives the observed 1.64 milliradian dispersion for a 1.52 m long barrel. The first 20 to 30 shots of the firing burst have a much greater

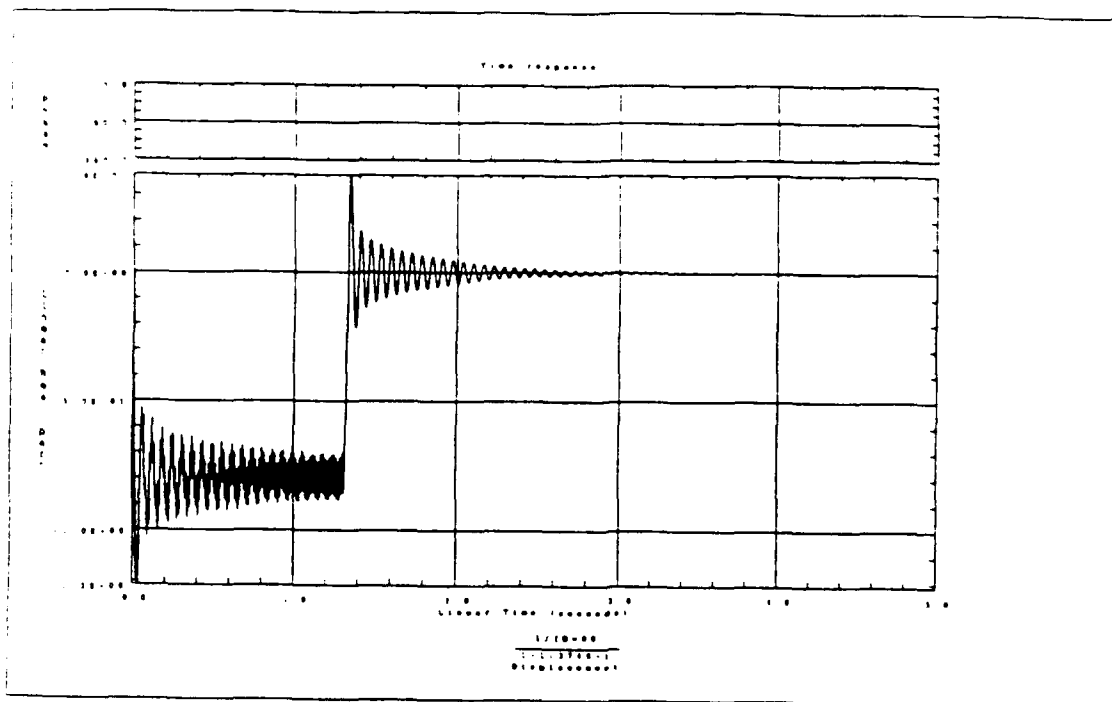


Figure 6-6. Response plot of the barrel tip in the fore-aft direction (x-plane).

dispersion pattern than the last 20 to 30 shots. No data is currently available for comparison to this modeled phenomenon. Since the recoil normal mode of vibration at 15.5 Hz has an associated pitching motion, it appears that this motion is important for predicting the dispersion pattern. Unlike the response in the fore-aft direction, this vertical response appears to involve only a single mode with a frequency of oscillation between 15 to 20 Hz. The barrel tip displacement corresponds to an angle of 1.64 milliradian movement which represents a significant start in quantifying the amount of dispersion associated with barrel tip motion.

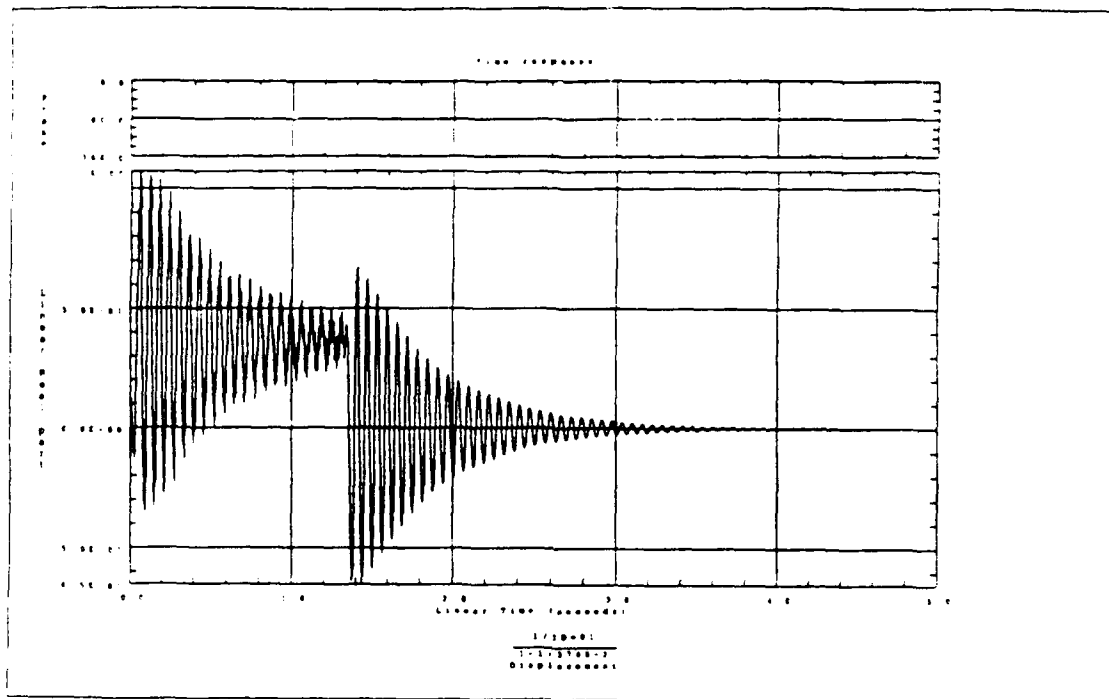


Figure 6-7. Response plot of the barrel tip in the vertical direction (y-plane).

Figure 6-8 shows barrel tip translation along the z-axis, or side-to-side motion. The amplitude of motion is noticeably less than in the vertical plane and demonstrates the relative strengths of the moment arms about the center of gravity. In the vertical plane, there is a larger moment arm from the firing point to the recoil adapter pivot points than there is in the z-plane so that greater displacement in the y-plane is expected. The off-center firing force causes a larger displacement in one direction than in the other. This shows that actual dispersion should be broken down into components in the two transverse dimensions x and z. Based on this analysis, the Naval Surface Warfare Center, Dahlgren, and Martin Marietta have now begun to describe their observed dispersion patterns as

elliptically shaped [Ref. 22]. The maximum barrel tip displacement in the z direction is about 5.10 mm (0.20 in), and settles into a steady-state displacement of about 2 mm (0.08 in). The response in the z -plane appears to be multimode which is similar to that of the x -plane response. The response and ring down show beats which suggests that the multimode response involves two normal modes whose frequencies are close together. Recall that the response of a structure is just the summation of the excited normal modes of vibration as given by

$$\underline{X} = [\Phi] \underline{x} \quad . \quad (6.20)$$

The beating appearing in this response plot indicates that the normal modes excited have similar damping. The multiple normal modes excited in the x -plane apparently had different damping. More will be discovered in the next section on this topic using the frequency response plots.

E. FREQUENCY RESPONSE FUNCTIONS

The previously discussed response plots are important for ensuring that the finite element model appears to be a close approximation of the real structure. It is a check on the assumptions made during the modeling process. However, it is more important to understand the normal modes involved in the response. In this way, it is possible to pinpoint causes of large amplitude displacements of the structure. A structure's response to an excitation depends on the magnitude of the excitation force, the frequency of the excitation force, the point of application and damping. Large displacements can occur if the frequency of the excitation is near that of a normal mode of vibration. This process is called *resonance*. Here it is possible to get large structural displacements even though the magnitude of the excitation may be small. If the magnitude of the driving force is large, then the structural deformation will also be large. It is also important whether the point of application of the driving force is at a node of the mode shape or at an antinode. If applied at a node the response is less than if the force was applied at an antinode.

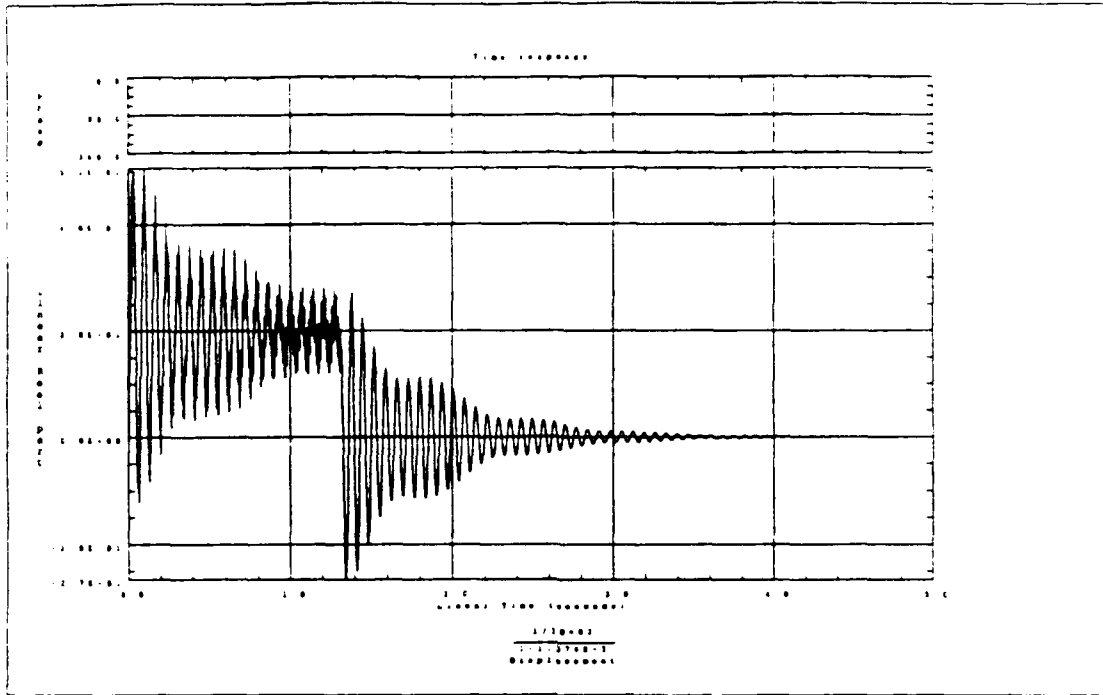


Figure 6-8. Response plot of the barrel tip in the horizontal direction (z-plane).

Therefore, frequency response functions and modal analysis are crucial in diagnosing the barrel tip displacement of the PHALANX gun.

One of the best tools for understanding which normal modes are involved in a forced response is called the frequency response function (FRF). This function is obtained by applying an input force at one point in the structure and measuring the response such as displacement at another point. The FRF is then the ratio of the response divided by the input. In this study, three FRF's were obtained, one for response of the barrel tip motion along each coordinate axis. Mathematically, they appear as

$$\frac{X_{3748}(\omega)}{F_{x1165}(\omega)}, \frac{Y_{3748}(\omega)}{F_{x1165}(\omega)}, \frac{Z_{3748}(\omega)}{F_{x1165}(\omega)} \quad (6.21)$$

In these three functions, the numerator stands for the displacement in the respective direction at node number 3748 which is at the tip of the firing barrel. The denominator represents the driving force function along the x (fore-aft) axis applied at node number 1165 at the base of the firing barrel. To determine the FRF, the frequency of the force is swept from zero to a high value. The FRF appears as a series of spikes which are resonant with the normal modes of vibration. The height of the spikes depends on the magnitude of excitation and the width of the peaks depends on the damping associated with that normal mode. A wider spike has a larger damping value. This FRF is complex since both amplitude and phase of oscillation are involved. [Ref. 11]

Figure 6-9 is a FRF of the gun response along the x direction at the barrel tip. As expected from the transient plot in Figure 6-6, there is a multimode response involving the first flexible mode at 14.4 Hz and second at 15.5 Hz which are being excited. The second mode is much more excited than the first based on the height of the two peaks. This is expected since the second mode is the recoil mode, while the first is a rigid body pitching mode. It appears also that no other modes are being excited. The next three or four modes involve the deformation of the gun body, and do not appear to be excited. This may be because the point of application of the driving force is at the rotor which is suspended by the recoil bearings.

The next FRF is shown in Figure 6-10 describing the barrel tip response in the y direction. It appears to verify the transient response in that this is a single mode excitation. The mode that appears to be excited is the recoil mode mixed with some pitching motion. This is identified as the second mode due to the fact that its normal mode motion is in the vertical plane, and that the spike is fairly wide suggesting that it uses the higher damping value of 0.33 rather than the others at 0.2.

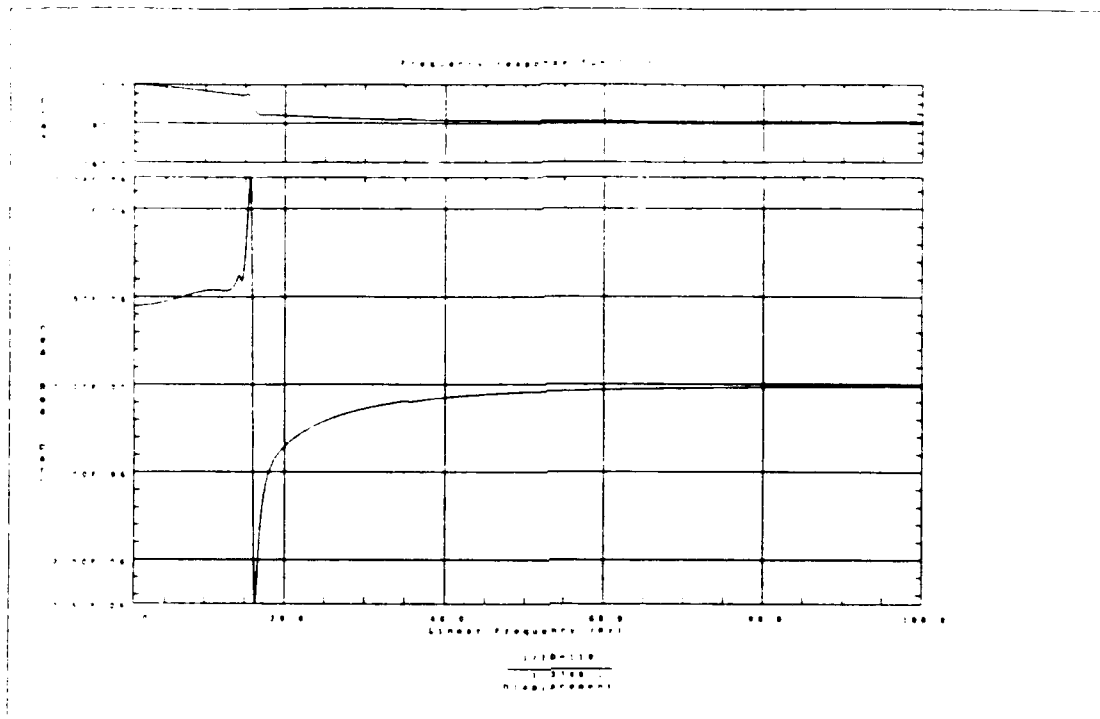


Figure 6-9. Frequency response function of the barrel tip in the x direction.

The last FRF shown in Figure 6-11 is that of the barrel tip in the z direction. As mentioned earlier, the response plot of Figure 6-8 showed that the phenomenon of beating was occurring. Studying the FRF, it appears that the first flexible mode at 14.4 Hz and third flexible mode at 16.0 Hz are being excited. These two modes have similar damping values allowing them to interfere and beat. Beating occurs when two modes are closely spaced in frequency and amplitude as seen here. The amplitudes were different in the x direction case, so that beating could be seen. The two modes involved in the z direction FRF are more closely excited to the same amplitude than in the x direction where only one mode was predominantly excited.

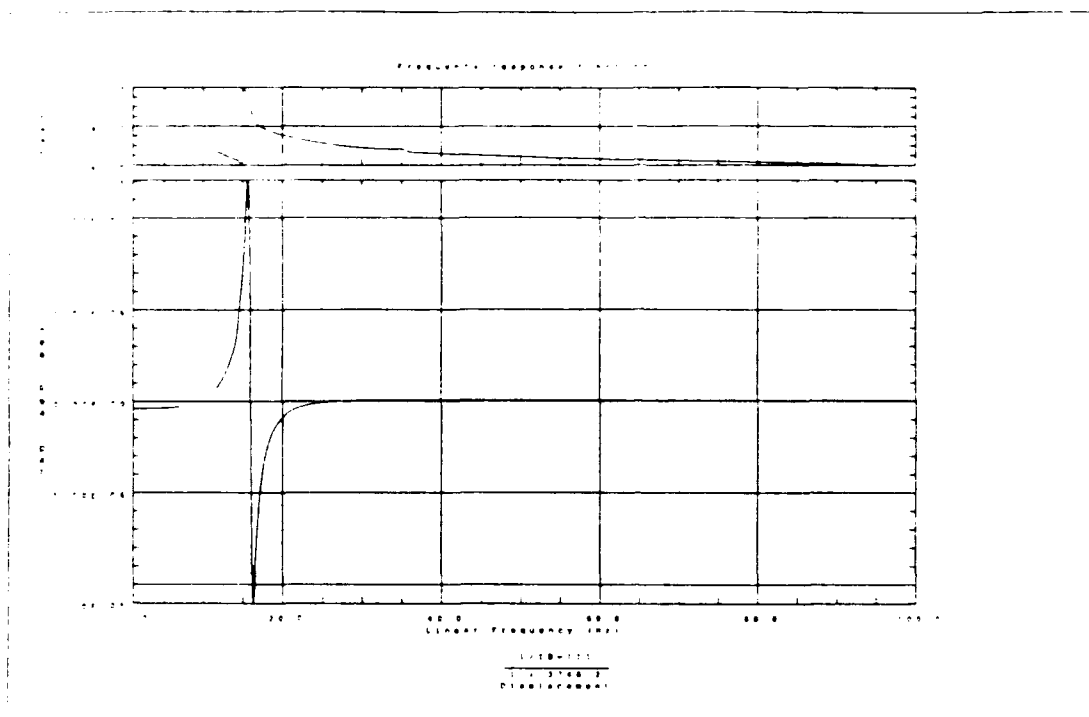


Figure 6-10. Frequency Response Function of the barrel tip in the y direction.

F. OTHER FACTORS AFFECTING DISPERSION

In addition to the resonance described above, other physical phenomenon such as gyroscopic whirl and rotor imbalance may contribute to dispersion. Gyroscopic whirl is a self-excited vibration that occurs when there is a tangential force normal to the axial direction of a rotating shaft. At some critical speed, the whirl instability will overcome any stabilizing forces, such as those provided by bearings. The amplitude of the whirl motion will only be limited by nonlinear stabilizing forces. This type of motion is common in machinery that has an overhanging shaft such as that shown in Figure 6-12. In this figure, the two rear supports can be thought of as the rear needle bearing and the forward thrust

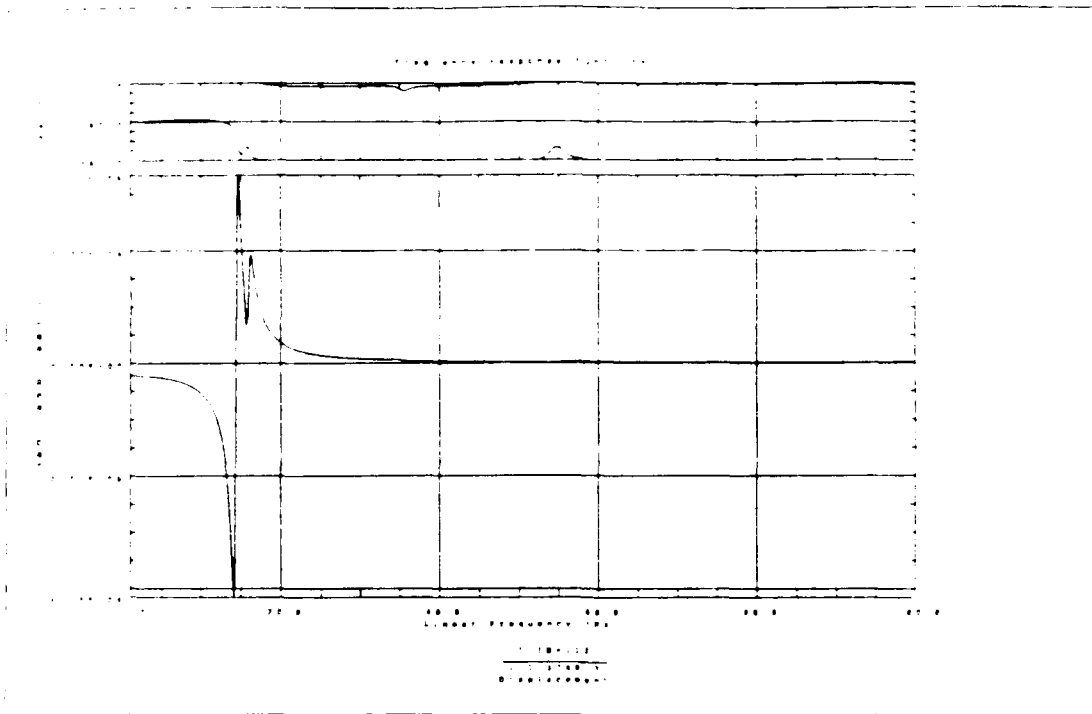


Figure 6-11. Frequency Response Function of the barrel tip in the z direction.

bearing. The mass of the disc at the end of the shaft represents the gun barrels and clamps. The PHALANX gun system is similar to that of an overhung shaft. This fact combined with the knowledge that the thrust bearing is not preloaded are two key requirements for the onset of whirling. The principal excitation force of the firing gun induces several moment arms which would lead to forces normal to the axis of rotation. These indications coupled with the data on PHALANX dispersion, such as the pattern shown in Figure 6-13, strongly implies that whirling is occurring. The speed of the whirl is usually close to that of the rotating shaft, and accounts for the fact that each barrel appears to shoot in the same direction on each cycle. Discussions with Stan Wilson of Port Hueneme indicates

that field experience supports this possibility [Ref. 23]. When an old thrust bearing was replaced with a new one, the dispersion pattern improved substantially. This would seem to indicate that the stabilizing forces of a new thrust bearing can limit the onset of whirl [Ref. 20]

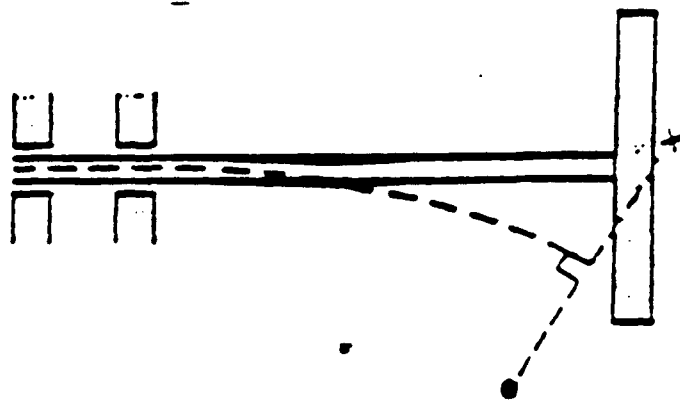


Figure 6-12. Representation of a hung shaft demonstrating the concept of gyroscopic whirl.

Rotor imbalance is another phenomenon found in rotating machinery which could lead to barrel tip displacement. If the principal axis of rotation does not coincide with a fixed line in space, then wobbling may occur. This rotational instability can be caused by machining tolerances or mass asymmetries. Once started it can aggravate other sources of vibration when rotational speeds are high, as in the PHALANX gun. The imbalance is significant since it determines the

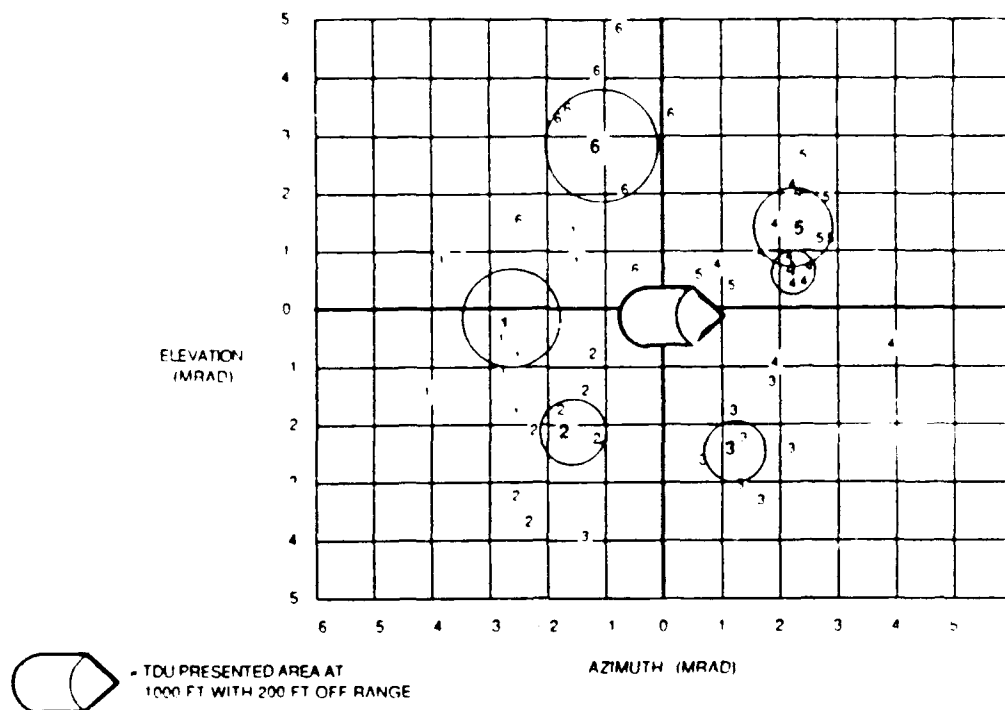


Figure 6-13. A dispersion pattern of the PHALANX gun. This particular pattern leads to assuming that whirl is occurring.

degree to which any bending or flexural mode of vibration is excited. At a critical speed, corresponding to a resonant frequency of the system, the rotor modal response becomes a maximum. When a rotor spins at a speed near its critical speed, it tends to adopt the shape of the normal mode that is excited. The amount of rotor displacement depends on damping in the system as well as the modal components of the imbalance. This modal component of imbalance may be reduced by adding a number of correctional tuning masses that would shift the normal mode frequency away from a critical speed.

VII. SUGGESTIONS FOR FUTURE WORK

A. REFINING THE GUN MODEL

The current PHALANX gun model is a first cut at attempting to understand the gun's complex dynamic behavior. It was decided early that it was better to go through the complete simulation cycle from finite element modeling to calculating its dynamic response, rather than getting caught up in trying to make a perfect model without ever calculating its response. In this way, the whole process was validated and demonstrated to be a useful tool in understanding the dispersion as well as modifying various components to see how the real gun could be improved. Now that the modeling process is understood from start to finish, and valuable experience obtained along the way, certain recommendations stand out as the next logical steps in continuing this research.

The first recommendation is to refine the gun model. The purpose of this refinement is primarily to reduce the number of degrees of freedom so that the model would have a smoother animation picture and a quicker solve time. The model should be simplified while retaining pertinent characteristics. This would serve to better illustrate the dynamic behavior of the gun's mode shapes and lead to more insight as to how the dispersion pattern is being formed. Currently, the animation picture is slow and lurches from one frame to the next. The second purpose behind further refinements was to choose better elements to capture even finer details of the gun's behavior. Now that the real gun is better understood, some components of the gun should have elements that model bending and torsional behavior with beams and thin shells whereas others should have bricks to model elasticity without any preferred direction. Neither of these elements can perform both functions. Next, the gun's boundary conditions are now better

understood; some barrels in the muzzle clamp are constrained while others are unconstrained. After attending the barrel optimization conference in Burlington, Vermont, May 26th and 27th, 1993, the consensus was to firmly clamp all the barrels. This modification could easily be evaluated with the current gun model. Finally, some of the currently modeled components, such as the recoil adapters, could be more accurately represented.

1. Muzzle and Mid-Barrel Clamps

In an effort to reduce the degrees of freedom of the model, the muzzle clamp could be further simplified. Currently the muzzle clamp shown in Figure 3-9 has brick elements representing the plates and thin shells representing the webbed meshing connecting the two. This arrangement is good for representing the inertial properties of the clamp, but the bricks themselves do not add much to the model other than increasing its complexity. Since it is unlikely that clamp shear plays a significant role in the gun's dynamic behavior, such elements that model shearing well are not necessary. Bricks, beams and shells would be important if this model was used to understand the gun's thermodynamic behavior, but that is currently not the case. Instead it is proposed that the bricks be replaced by a lumped mass located at the center of gravity of the muzzle clamp plates. This lumped mass is an "element" choice in I-DEAS where a structure's mass and inertia can be defined at a geometric point. The lumped mass can then be connected to the barrels via rigid elements. Figure 7-1 shows this proposed arrangement. These rigid elements are massless and do not flex, but they are effective in attaching two structures together. In this case, the barrels are attached to the lumped mass. This will serve the purpose of defining the appropriate boundary conditions. Some barrels could be connected while others are not in order to model the current gun in the fleet. Alternately they all could be easily connected together to test the proposed gun design. What is lost in this

representation is the bending behavior of the plates. It is uncertain if this behavior is important to model or not, but experiments could be performed on the real gun at the Naval Postgraduate School to resolve this question. In a separate finite element model of the muzzle clamp, the first flexible normal mode of vibration occurred at about 500 Hz and is far from the excitation force frequency of 75 Hz. It is unlikely that this mode is being excited. If this did not turn out to be the case and the mode is excited, thin shells could be used to represent the muzzle clamp plates vice lumped masses and rigid elements. Few degrees of freedom would be added to the model, since they would still be "cheaper" to use than bricks and have the benefit of bending behavior. The mid-barrel clamp would be modeled like the muzzle clamp plate.

What is important about the muzzle and mid-barrel clamps is how they determine the boundary conditions on the barrels. Currently three of the barrels have their rotations taken out at the muzzle clamp while the other three are allowed to rotate. At the mid-barrel clamp the barrels are rigidly attached. It has been proposed that the PHALANX gun would be improved if its barrels were all rigidly constrained at the muzzle clamp like that of the 30 mm GOALKEEPER gun [Ref. 21]. This particular gun has a smaller dispersion pattern than the PHALANX gun. Therefore, it is not so important that the clamps are geometrically correct, but that they are dynamically correct.

2. Gun Body Housing

The next area of finite element refining is that of the gun body housing. Its current representation can be seen in Figure 3-6. The model could be improved if there was better matching of the degrees of freedom between the thin shells of the gun body and the bricks of the thrust bearing. The thin shells have six degrees of freedom while the bricks have three. This creates a possible boundary condition problem and appears to manifest itself in the extreme distortion of the gun body in

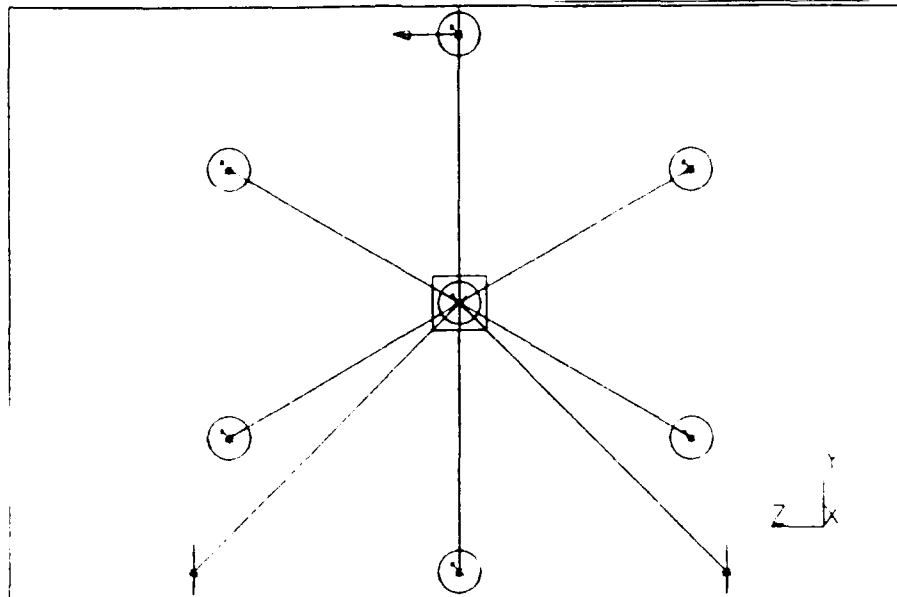


Figure 7-1. Recommended modification for representing the muzzle clamp. This figure shows a lumped mass connected to the barrels via rigid elements.

front of the thrust bearing. Instead of obtaining the continuous dynamic behavior of the gun body, it has been broken up into two distinct parts with the thrust bearing serving as the divider. The forward part of the gun body acts like a short drum, anchored at the thrust bearing. By itself, its finite element representation is too coarse and leads to unrealistic modeling behavior. This behavior appears in the higher order modes of vibration. If the forward gun body is coupled to the rear gun body, as it should be, then its finite element representation is not too coarse and no further refinements are needed.

How is this continuity achieved? The brick elements used to represent the thrust bearing should be replaced by beam elements. In I-DEAS, a beam element's cross-section can be defined in as much detail as desired. The inner and outer race, as shown in Figure 3-15, could be defined as a beam cross-section. By replacing the bricks with beams, the degrees of freedom are then matched with the thin shells, since beams also have six degrees of freedom. Therefore, the rear gun body and forward gun body are now coupled and continuous dynamic behavior would be achieved.

In making this transition to beam elements, the springs used to model the ball bearings would also have to be modified. Now rigid elements would be used to extend from the centroid of the inner and outer races to a common, coincident point between them. The springs would be co-located, one for radial stiffness, axial stiffness and torsional stiffness. This refinement would also serve the purpose of removing any moment arms that currently exist in the model due to the finite distance the springs extend between the inner and outer race.

More attention could be used when modeling the details of the gun body housing. Currently, it is represented as a cylinder, whereas in reality, there are many intricate details that might be important to model more accurately. For example, the ammunition chuting and a hydraulic motor coupled to the gun drive could be better studied now that the gun is on-sight.

3. Rotor

The rotor is a cylindrical component represented with brick elements as shown in Figure 3-16. The dynamics of the rotor are not critical to understanding the gun, but could be better represented by a lumped mass and inertia properties while keeping a portion of the brick elements for use in attaching to the thrust and needle bearings. In this way, the degrees of freedom of the model are reduced, while preserving the load path from the excitation force to ground. The bricks

would be important if there was some concern that shear forces were causing it to deform, or if thermodynamic properties were being modeled. Since neither of these characteristics are being modeled, the use of brick elements for the whole rotor is unnecessary. The portions used to couple the barrel assembly to the bearings should be kept, and should be connected via rigid elements to a lumped mass at its center of gravity.

4. Stub Rotor

The stub rotor, constructed much like the muzzle clamp as Figure 3-11 shows, with webbing between two plates, could be further improved by dividing the single row of bricks for each plate into two rows. The stub rotor is a critical component in the dynamics of the gun, perhaps more so than any other component. Its rigidity is important in determining how much the gun barrels will displace and has been experimentally studied by Martin Marietta to calculate its characteristics [Ref. 16]. The component should be modeled using more elements instead of fewer elements. By including two rows of elements, its bending behavior can be better represented. One aspect of the stub rotor and barrel clamps that is difficult to model is the nonlinear effects that gaps play in the gun dynamics. The current version of I-DEAS does not allow this option, but a new release will allow the nonlinear gaps to be modeled.

5. Recoil Adapters

The recoil adapters have been the most challenging components to model. The current model defined them in terms of "ears" that stood out on either side of the gun body that were connected to ground via rigid elements and recoil springs as shown in Figure 3-16. The "ears" were solely used to represent the adapter's mass and to model the correct geometric position of the attachments. The model could be simplified if the "ears" were replaced with lumped mass elements. In

addition, the rigid elements could connect the gun body to the springs directly while maintaining the correct offset of the pivot points. These changes are needed in order to provide better coupling of the recoil springs to the gun body. As discussed earlier, problems occur when there is a discontinuity between degrees of freedom of elements. In this case, it occurs between the thin shells of the body to the bricks of the "ears." This recommendation is better than trying to accurately model the recoil adapters. It is likely that little would be gained for such detailed modeling and would significantly add to the model's complexity.

B. VALIDATION OF THE MODEL THROUGH TESTING

After constructing the finite element model of the gun and obtaining its normal modes, the next logical step would be to compare both the mode shapes and their associated frequency with those of the real gun. However, it was only until late in this study that a M61A1 PHALANX gun was received at the school. After proper mounting, a modal analysis of the gun could then be performed and the results compared to the model. The equipment already exists on-sight for this type of testing. In addition to testing the whole gun as one unit, it could be broken down into a barrel cluster and gun body which would then be tested separately. In this way, discrepancies could be localized to determine which components needed to be better modeled.

Another comparison that can be made using the real gun is that of finding the proper damping values. Although the damping value of the recoil adapters was provided by Martin Marietta and verified through analytical means in Chapter VI, it would be useful to obtain these values experimentally. It is uncertain whether the damping values vary much from one adapter to another, or the effect wear plays on them. More importantly though, all other normal modes of the gun were estimated to have a damping value of two percent. The damping values of the gun model could be correlated with the real gun during its modal analysis.

As mentioned earlier, it is also uncertain how much free play exists in the gun and the amount each component contributes to the total. This information could also be determined experimentally. Individual components of the gun should be weighed in order to provide another means of comparison so that the modeling could be improved.

C. ADDITIONAL MODELING

1. Modifying the Existing Firing Force

In an effort to get through a complete modeling cycle, there were many variations of the existing firing force that were put off until a later time. One of the modifications which would certainly add to the accuracy of the model is to ramp up the firing force. The real gun does not immediately jump to a firing rate of 4500 shots per minute. This could be accomplished by spacing out the firing impulses for the first ten to twenty shots according to data available from the Naval Surface Warfare Center in Dahlgren or Port Hueneme. Further modifications would be to model the different firing rates themselves. This study only looked at the firing rate of 4500 shots per minute. However, the existing PHALANX gun can select a rate of fire of either 3000 or 4500 shots per minute. There has been a proposal to investigate a firing rate of 6000 shots per minute. If the mass of the penetrator were to change or if the penetrator's velocity were modified, the firing force would change and could easily be modeled. The gun is capable of longer engagements and longer bursts of shots. Longer firing bursts should be modeled. An additional and perhaps important firing force to model would be that of an occasional misfire. In this case, the gun has a chance to translate forward after the misfire and then be slammed back as the next round is fired.

2. Adding Additional Forces

In this study, only the firing force was represented. The impulse of loading each round may also affect the gun. In discussions with Martin Marietta, this force is not insignificant since the round has a tight fit in the barrel. This loading force is applied as the barrel passes through its lowest point of circular motion. While the frequency of the loading force must be the same as the firing rate, the phase relation may allow it to add to or subtract from the firing force.

The effects of rotation can also be modeled in I-DEAS. Here the damping matrix is modified to represent the effect of rotation. Even though the modeled gun is not rotating, it can be "tricked" into producing the same dynamic results as if it were rotating by modifying its damping matrix. This involves adding off-diagonal terms in the viscous damping matrix. The normal modes of vibration are then resolved as before, and the excitation forces applied. This technique is only good for one frequency, and the model will have to be resolved for each different firing rate.

Another force to model is the variation in rotation of the gun by adding an impulse perpendicular to its axial length. Even though this force may be small, its effect could be large since it might be a contributing perturbation to significant dynamic forces such as whirl.

3. Additional Modeling

With the current PHALANX gun model partially validated, it is possible to move on and use it as a tool. The U. S. Navy is interested in the possibility of reducing the PHALANX gun's dispersion by constructing a gun barrel restraint like the one shown in Figure 7-2. This structure will be clamped at its base to the isogrid of the gun mount. The other end will use a radial bearing to clamp onto the gun barrels. Its purpose is to restrict the most extreme motions of the barrel cluster. A finite element analysis has not been used to date to study the motion of

this structure and optimize its design. The blueprints have been received, and the Naval Postgraduate School is poised to take on this task [Ref. 24]. The computer model will be able to study the mode shapes of this combined system and check if there is any problem resonant frequencies. By studying the mode shapes, it will be possible to determine the best location to clamp the bearings. This system can be driven and damped to calculate the new barrel tip displacements. The muzzle restraint structure could be modified in various ways to find its optimum design and placement.

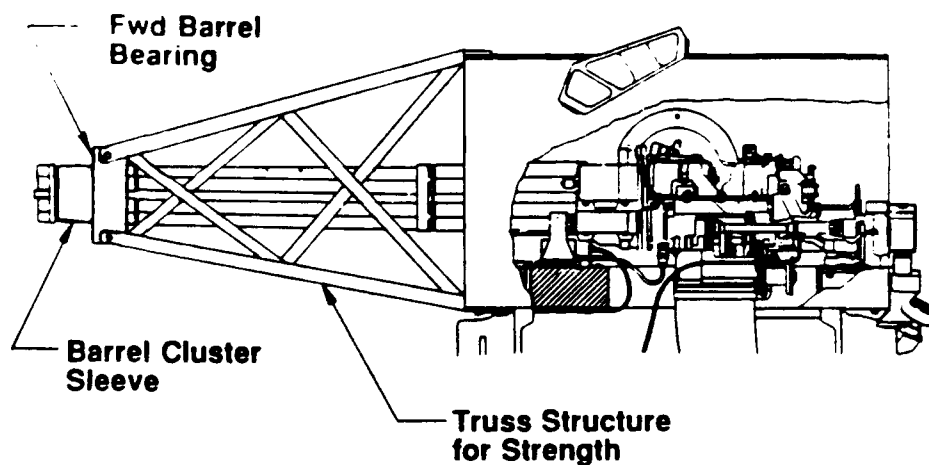


Figure 7-2. Proposed assembly of the PHALANX muzzle restraint [Ref. 24].

Another modeling task is to swap out the current set of finite element barrels in exchange for the proposed optimized barrels. This will help determine

whether the new barrels will pitch more than the old ones. The new barrels will be much heavier, nearly 18 kg (39 lb) compared to the current 8 kg (18 lb) barrels. They will be much longer, roughly 200 cm (79 in) compared to the current 152 cm (59 in) barrel length. The effect of this extra weight and length on the gun mount and its dispersion has not been modeled to date. The NPS model would be an excellent tool for making this analysis. The firing force would have to be modified to take into account the extra recoil force associated with the heavier enhanced-lethality projectile designed to be used by these barrels. It has a greater mass of 0.290 kg (0.64 lb) than the old projectile mass of 0.245 kg (0.54 kg), and will be fired at a greater velocity increasing the specific impulse on the gun mount. An additional modeling step would be to use the proposed muzzle restraint, as described above, with these new barrels and solve for its dynamic response.

VIII. CONCLUSIONS

Using a finite element model to understand the complex dynamics of the PHALANX gun has made possible new areas of analysis and component design. This has been the first effort to use the sophisticated I-DEAS computer code to study the gun. According to the Naval Surface Warfare Centers in Dahlgren and Port Hueneme, it has also been the most "technologically advanced" modeling research of this important weapon system [Ref. 25]. Not only does it provide a thorough and detailed model of the gun where various driving forces can be applied and the barrel tip response calculated, but it is a working tool to assist the PHALANX program. In particular, each individual component of the gun can be studied in detail to understand how much it affects the overall dispersion. This is an especially important tool today when budget limitations allow only modest improvements to be made to the gun. Furthermore, new components can be tested and their performance predicted before any actual hardware tests. This can be applied to the proposed muzzle restraint and set of optimized barrels, before any prototypes are ever constructed. The cost saving and, not to mention, time saving aspects of this method provides an invaluable resource to the program. This type of research may not have been carried out before by private industry or the U. S. Navy because the computer code is expensive and has only been made easily accessible in the past few years. The Naval Postgraduate School receives an educational discount to obtain an on-sight license for the code. In addition, the high concentration of professors with doctorates and U. S. Navy officer/students makes for a unique and productive environment. The school has been proposed as the center of all future modeling research of the PHALANX gun [Ref. 26]. In summary, the U. S. Navy is now using state-of-the-art technology to understand and improve old technology in a cost saving way.

The primary goal of this study has been to construct an accurate finite element model of the PHALANX gun and demonstrate the potential of such a sophisticated computer code. This goal has been achieved. Parts of the model have been validated with the real gun, and the results of this study have been presented to the several organizations involved in improving the PHALANX gun [Ref. 21]. The model is poised to take on most of the new design changes that the group proposes. The model is now considered an integral part of the decision making process. With an actual gun on-sight, the model can be completely verified.

Although the primary purpose of constructing this finite element gun model has been achieved, some preliminary analysis was conducted along the way. One of the first areas of concern to be noticed was the gun's normal mode of vibration around 14 Hz. This first flexible mode with associated pitching motion would contribute to dispersion, if it is sufficiently excited. The gun rotates at a frequency of 12.5 Hz making this rotational force a contender for exciting this mode. Frequency response functions taken of the barrel tip indicates that this mode is being excited by the principal driving force, of the gun firing. This discovery was somewhat unexpected, but upon analysis of the moment arm created from the driving force and the gun mounting positions, it is reasonable that it is excited. As the gun fires, the moment arm causes the gun to rock back and pitch upward coupling the firing recoil into other planes of motion. Fourier transforms performed of actual dispersion tests appear to correlate this 14 Hz normal mode [Ref. 22].

As far as design analysis of the gun, the most critical component contributing to dispersion was revealed by this study as the double angular contact bearing, or thrust bearing. When various bearing stiffness values were tested, the effect on barrel tip displacement was significant. Confirmation of this fact came from the field where the dispersion pattern improved tremendously as a worn thrust bearing was replaced with a new one [Ref. 23]. No data is available on the rate of wear of the thrust bearing. In fact, the bearing itself is not inspected while on ships, but

only when the gun is returned for depot level maintenance. The fact that the bearing is not pre-loaded is a leading cause of the physical effect known as whirl that occurs on an overhung shaft as in the PHALANX gun. Dispersion data also suggests the possibility that whirl is occurring. The addition of the new, heavier and longer barrels may significantly aggravate whirl and counteract any dispersion improvements achieved by the new barrels, especially if the bearing is not redesigned to support these new barrels. Unfortunately, this appears to be the case. Not only would the added torque of the new barrels lead to a greater amount of whirl, but it would probably cause a greater amount of wear on the bearing which would further worsen the problem.

One of the first validation tests of the gun model was to drive it with the principal driving force of the rounds firing. In the response plots shown in Chapter VI, the firing gun barrel acted as predicted. That is, the gun set back the observed 1.27 cm and oscillated about this new equilibrium point. Barrel tip displacement in the pitch and yaw directions corresponds well with the observed 2 milliradian dispersion. Elliptical dispersion patterns were also predicted for the first time.

In this first finite element study of the PHALANX gun, the potential for its future use has been documented in this effort. It is a cost effective tool that has been designed to help the U. S. Navy not only understand the current gun's complex dynamics, but those of any future gun as well. As a ship's last layer of defense, the PHALANX gun provides a valuable function for the ship and her crew. This is especially true in the near future where the U. S. Navy has extended its operating envelope into new environments, where the last layer of defense may be the first layer.

APPENDIX A. GUN BARREL NORMAL MODES

The following graphs are experimental data of the normal modes of a single PHALANX gun barrel. The barrel was suspended by two low stiffness cords and tapped with an instrumented hammer. The resulting vibrational information was recorded with a transducer mounted on the opposite side of the hammer impact point. The normal mode frequencies were determined through 3000 Hz and appear as spikes in the following graphs.

X=72.75 Hz
Ya=16.8167 dB

FREQ RESP
20.0

dB

-60.0

10

FREQ RESP
160

Phase

Deg

-480

10

3AVG

0%OVL

FR/EX

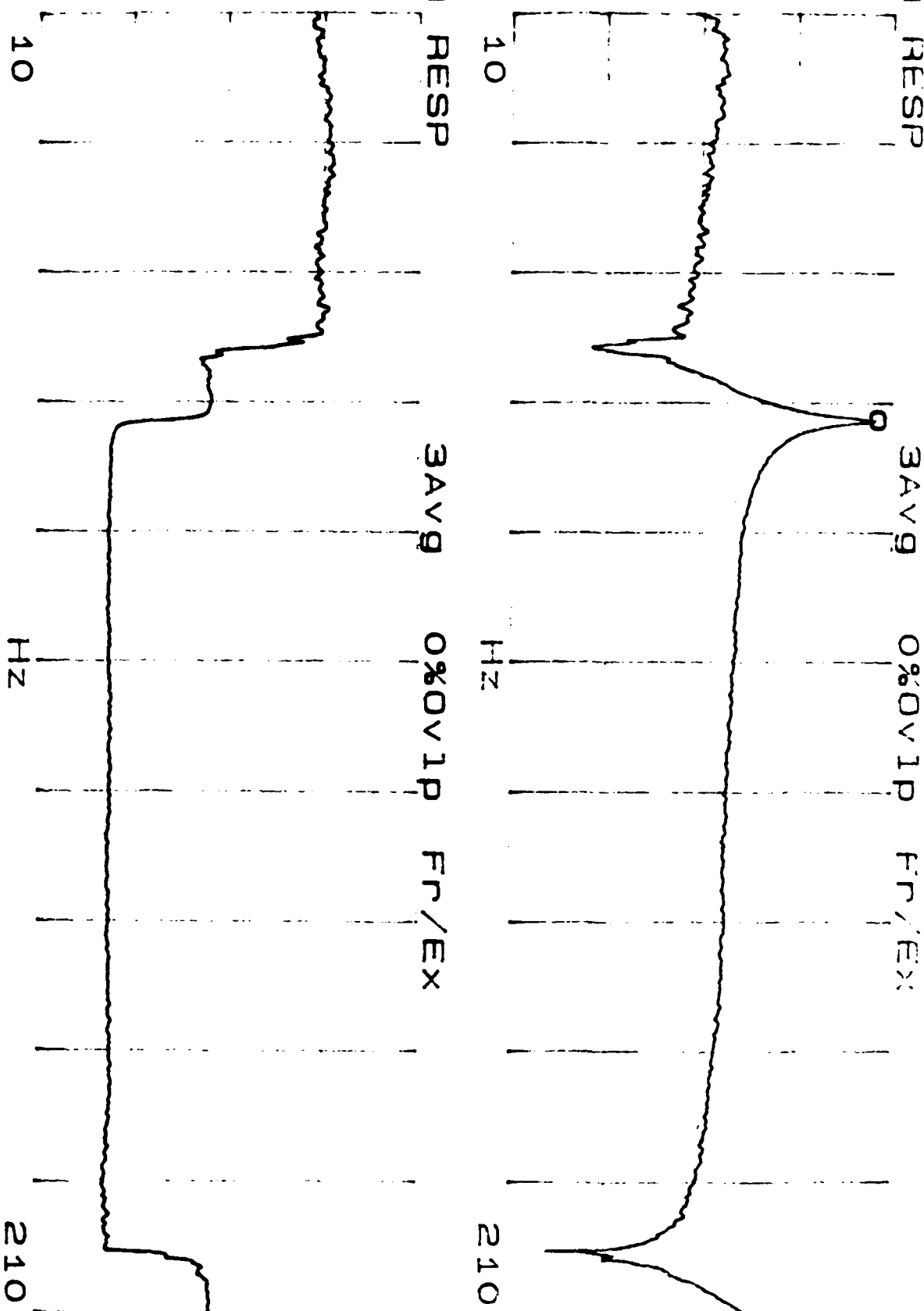
Hz

210

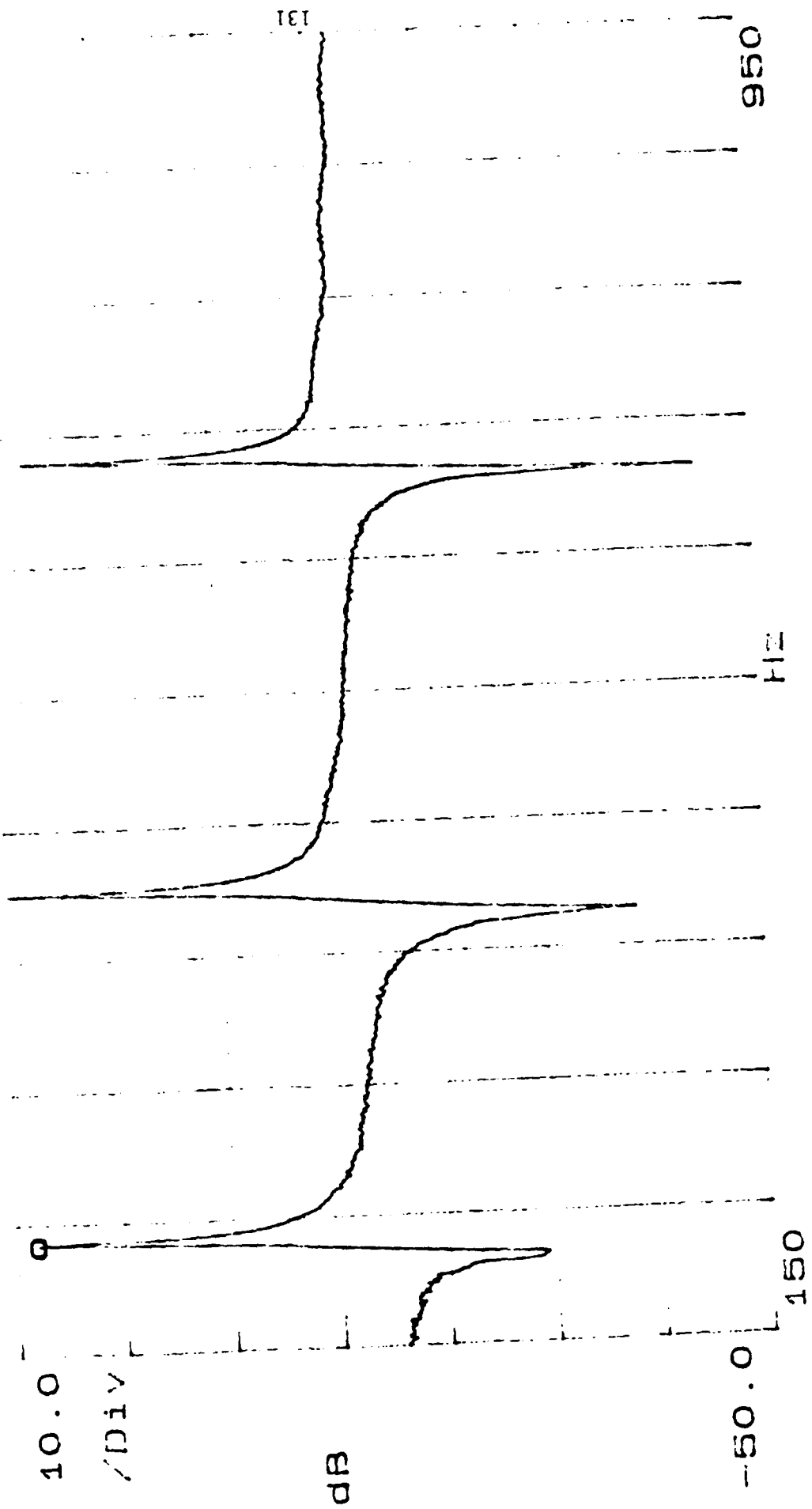
130

Hz

210



X=217 HZ 0729 dB
Ya=18.0729 dB
FREQ RESP
30.0



X=1.01KHZ

dB

Ya=-13.595

ERRQ HRSR

30.0

3AV9 0%OVLP PR.128

10.0

1019

dB

132

50.0

2K

1K

2K

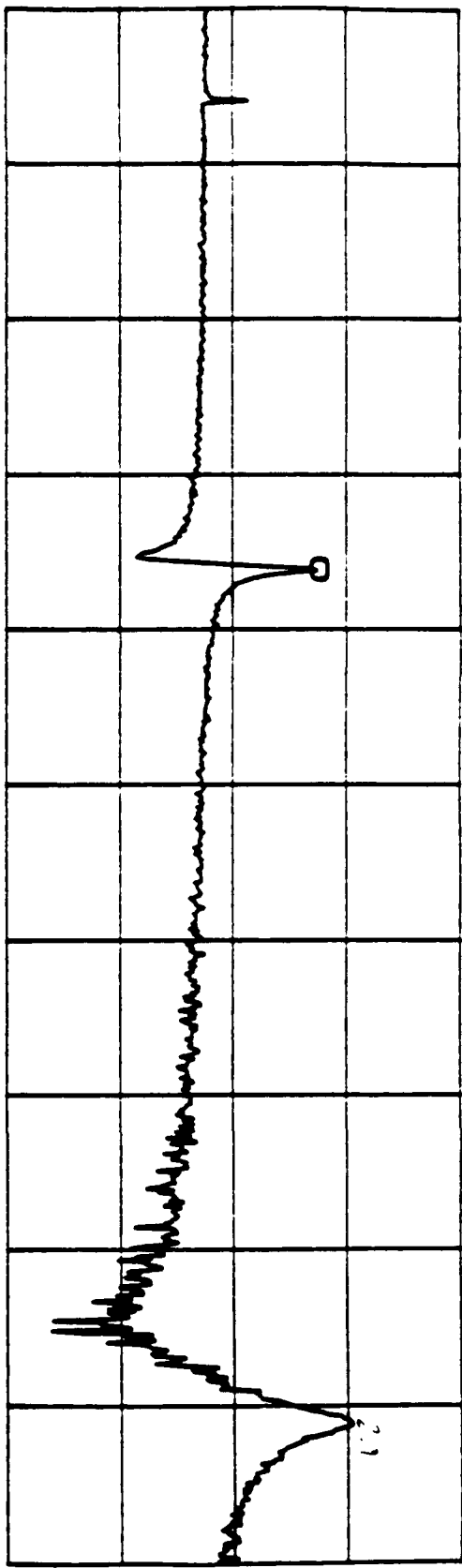
X=2.3625KHz
Ya=3.87844 dB

FREQ RESP
24.0

3Avg 0%OVLP Ff/EX

dB

-40.0



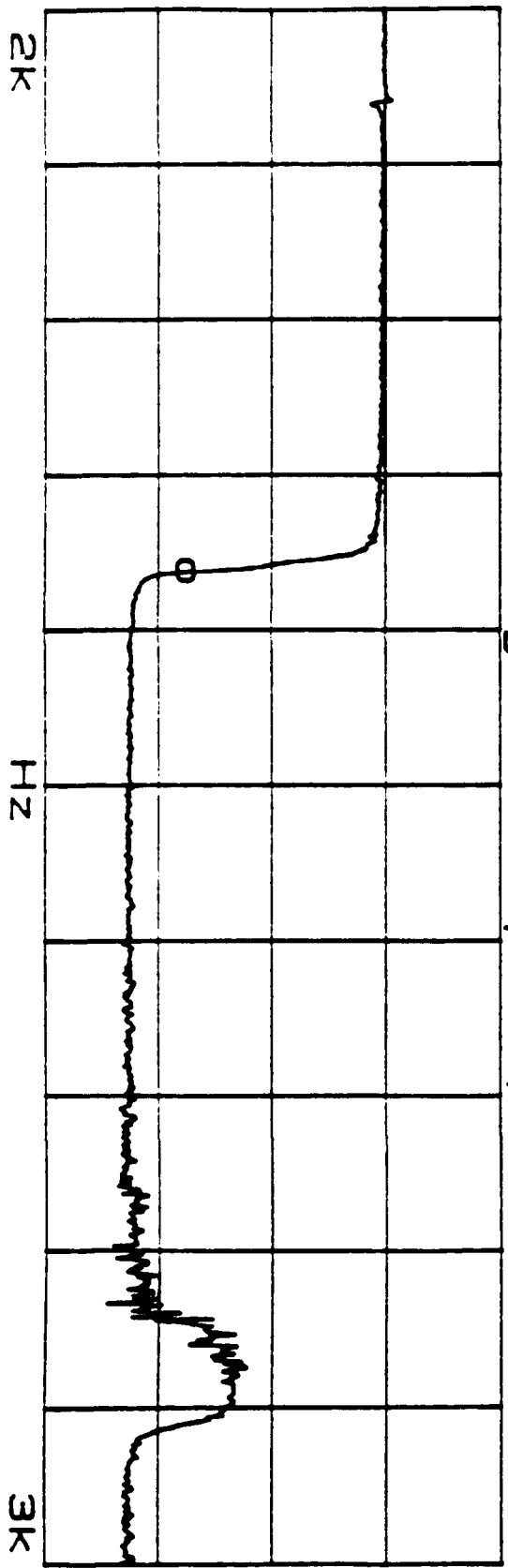
Yb=-285.31 Deg
FREQ RESP
160

3Avg 0%OVLP Ff/EX

Phase

Deg

-480



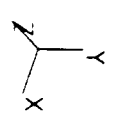
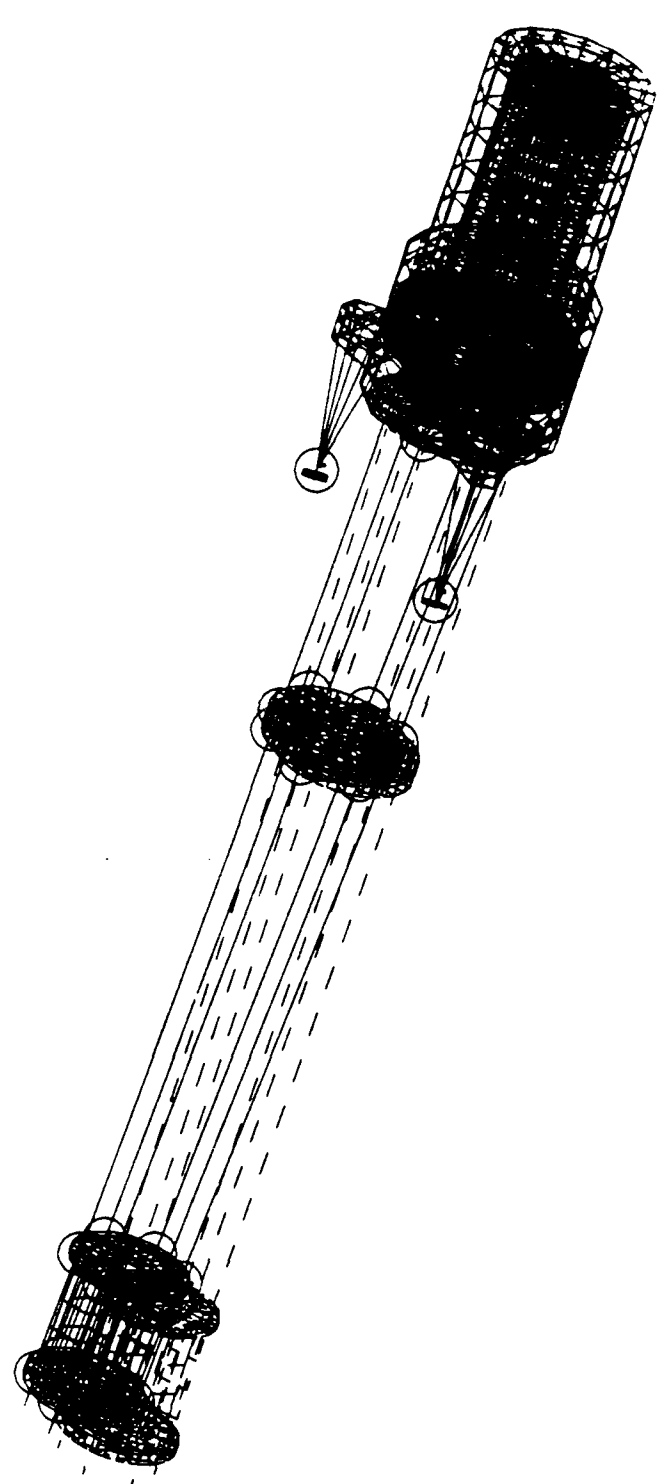
APPENDIX B. GUN MODEL MODE SHAPES

The following pictures are snapshots of the mode shapes used in the dynamic analysis of the gun. There are 20 flexible modes listed in ascending order by frequency.

Figure 1. A schematic diagram of a system for the study of the interaction of a laser beam with a plasma. The diagram shows a laser beam (1) entering a plasma (2) from the left. The beam is focused by a lens (3) onto a target (4). The target is a small, cylindrical object. The plasma is a large, cylindrical volume. The beam is shown as a series of parallel lines. The plasma is shown as a shaded region. The target is shown as a small circle. The lens is shown as a series of curved lines.

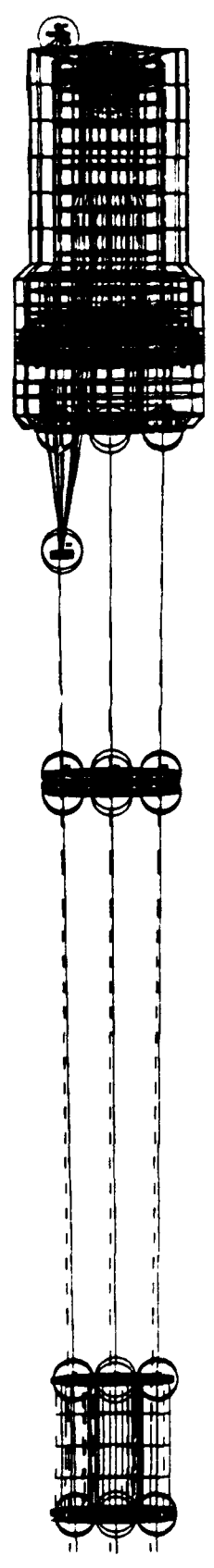
Figure 1

The diagram shows a laser beam (1) entering a plasma (2) from the left. The beam is focused by a lens (3) onto a target (4). The target is a small, cylindrical object. The plasma is a large, cylindrical volume. The beam is shown as a series of parallel lines. The plasma is shown as a shaded region. The target is shown as a small circle. The lens is shown as a series of curved lines.



1. A. ...
 2. ...
 3. ...
 4. ...
 5. ...
 6. ...
 7. ...
 8. ...
 9. ...
 10. ...
 11. ...
 12. ...
 13. ...
 14. ...
 15. ...
 16. ...
 17. ...
 18. ...
 19. ...
 20. ...
 21. ...
 22. ...
 23. ...
 24. ...
 25. ...
 26. ...
 27. ...
 28. ...
 29. ...
 30. ...
 31. ...
 32. ...
 33. ...
 34. ...
 35. ...
 36. ...
 37. ...
 38. ...
 39. ...
 40. ...
 41. ...
 42. ...
 43. ...
 44. ...
 45. ...
 46. ...
 47. ...
 48. ...
 49. ...
 50. ...
 51. ...
 52. ...
 53. ...
 54. ...
 55. ...
 56. ...
 57. ...
 58. ...
 59. ...
 60. ...
 61. ...
 62. ...
 63. ...
 64. ...
 65. ...
 66. ...
 67. ...
 68. ...
 69. ...
 70. ...
 71. ...
 72. ...
 73. ...
 74. ...
 75. ...
 76. ...
 77. ...
 78. ...
 79. ...
 80. ...
 81. ...
 82. ...
 83. ...
 84. ...
 85. ...
 86. ...
 87. ...
 88. ...
 89. ...
 90. ...
 91. ...
 92. ...
 93. ...
 94. ...
 95. ...
 96. ...
 97. ...
 98. ...
 99. ...
 100. ...

1. ...
 2. ...
 3. ...
 4. ...
 5. ...
 6. ...
 7. ...
 8. ...
 9. ...
 10. ...
 11. ...
 12. ...
 13. ...
 14. ...
 15. ...
 16. ...
 17. ...
 18. ...
 19. ...
 20. ...
 21. ...
 22. ...
 23. ...
 24. ...
 25. ...
 26. ...
 27. ...
 28. ...
 29. ...
 30. ...
 31. ...
 32. ...
 33. ...
 34. ...
 35. ...
 36. ...
 37. ...
 38. ...
 39. ...
 40. ...
 41. ...
 42. ...
 43. ...
 44. ...
 45. ...
 46. ...
 47. ...
 48. ...
 49. ...
 50. ...
 51. ...
 52. ...
 53. ...
 54. ...
 55. ...
 56. ...
 57. ...
 58. ...
 59. ...
 60. ...
 61. ...
 62. ...
 63. ...
 64. ...
 65. ...
 66. ...
 67. ...
 68. ...
 69. ...
 70. ...
 71. ...
 72. ...
 73. ...
 74. ...
 75. ...
 76. ...
 77. ...
 78. ...
 79. ...
 80. ...
 81. ...
 82. ...
 83. ...
 84. ...
 85. ...
 86. ...
 87. ...
 88. ...
 89. ...
 90. ...
 91. ...
 92. ...
 93. ...
 94. ...
 95. ...
 96. ...
 97. ...
 98. ...
 99. ...
 100. ...

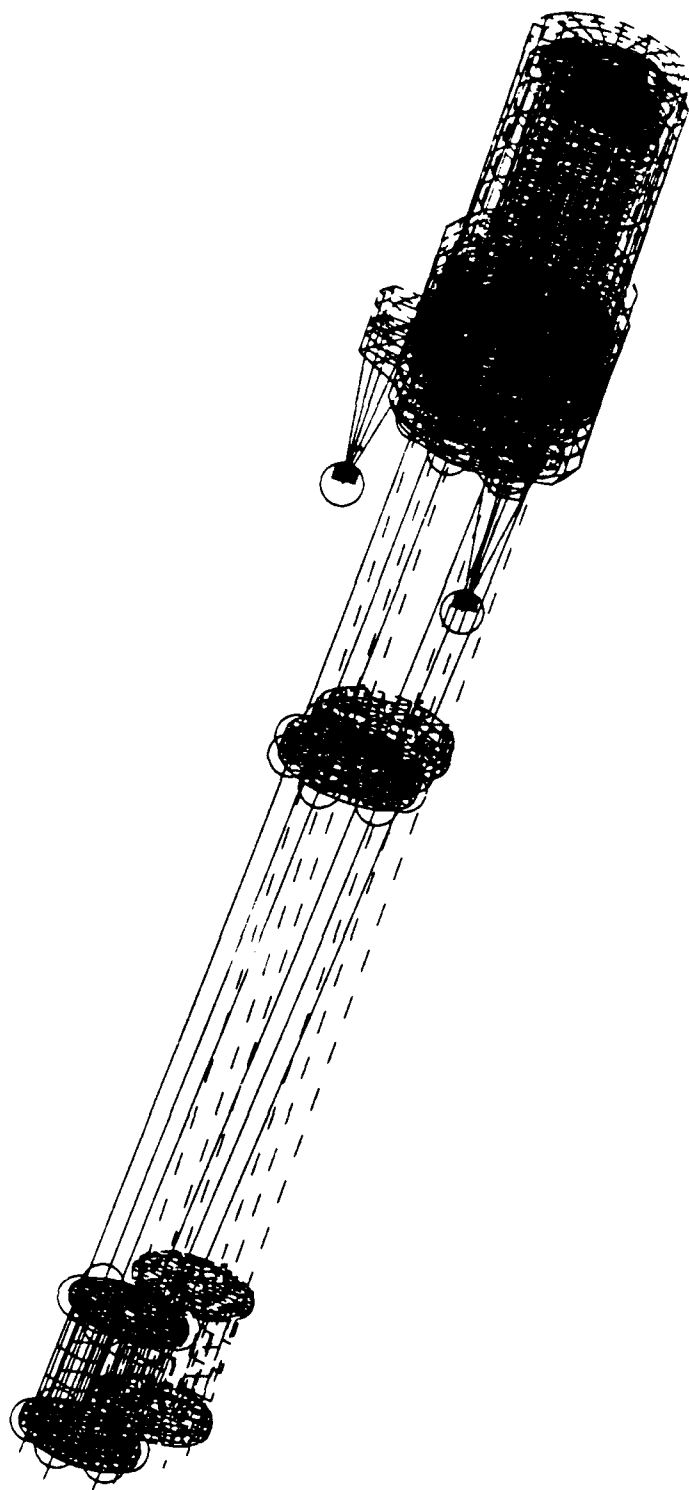


Y
 X

[illegible]

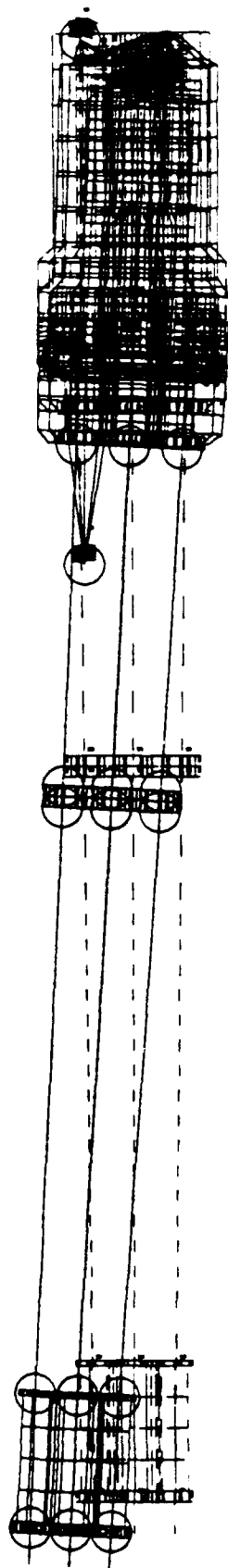
As of 10:01 AM, 9/19/2019, 5419

1. **NAME** : _____
2. **ADDRESS** : _____
3. **PHONE** : _____
4. **DATE** : _____

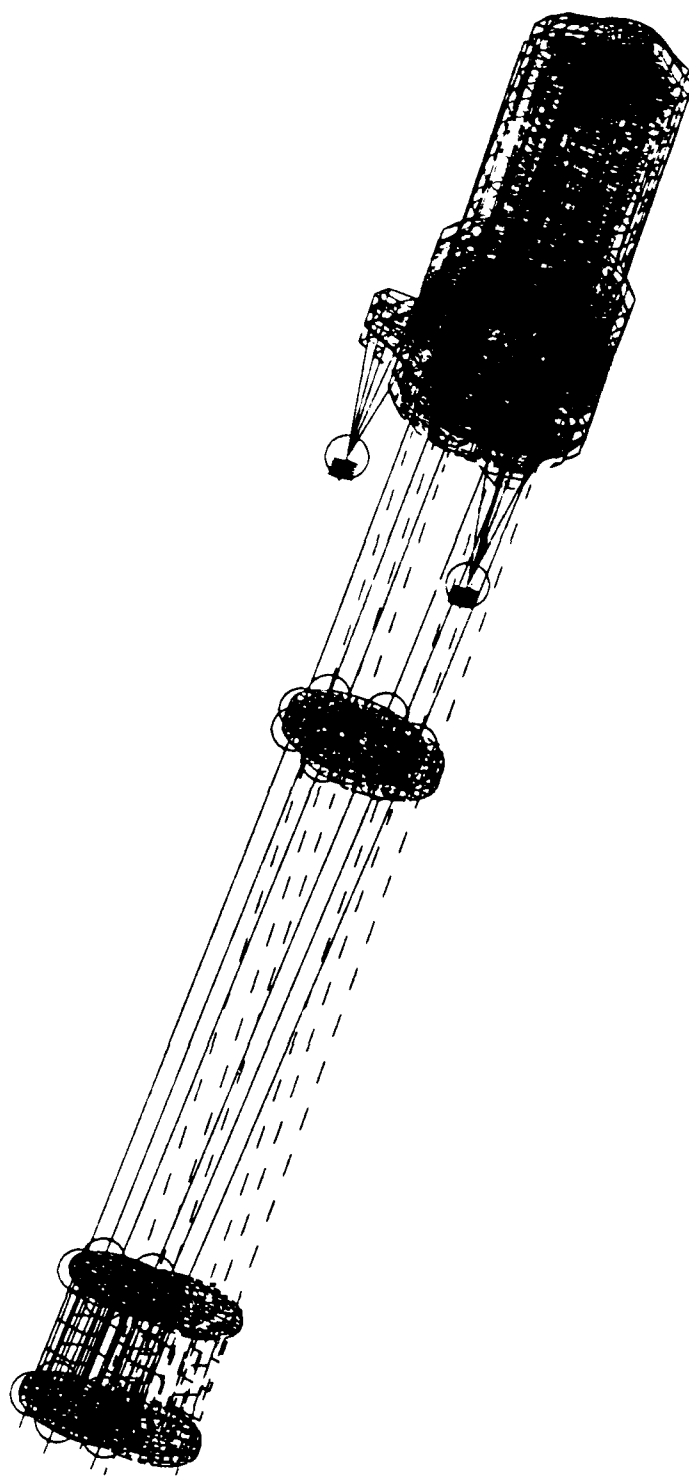


1. The first part of the diagram shows a cross-section of a structure with a central vertical axis. The structure is composed of several layers of material, with the outermost layer being the most dense. The central axis is marked with a vertical line, and the layers are labeled with letters A, B, C, D, E, F, G, H, I, J, K, L, M, N, O, P, Q, R, S, T, U, V, W, X, Y, Z.

2. The second part of the diagram shows a cross-section of a structure with a central vertical axis. The structure is composed of several layers of material, with the outermost layer being the most dense. The central axis is marked with a vertical line, and the layers are labeled with letters A, B, C, D, E, F, G, H, I, J, K, L, M, N, O, P, Q, R, S, T, U, V, W, X, Y, Z.



Y
 X



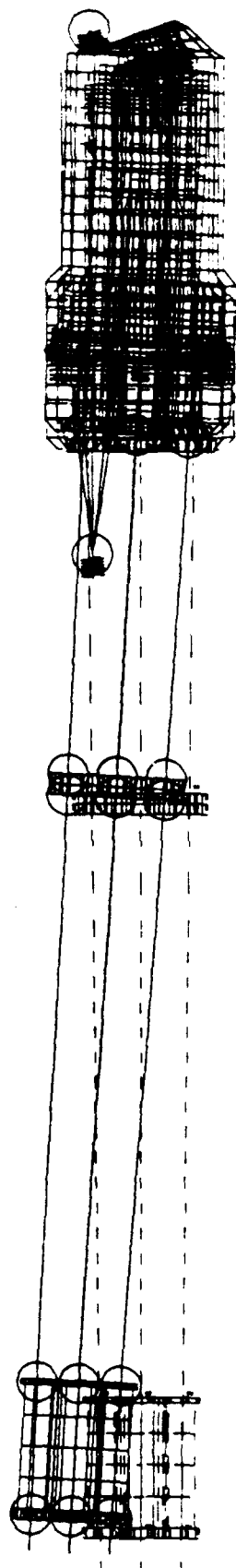
1. The purpose of this study is to determine the effect of the various parameters on the performance of the system. The parameters considered are the wavelength of the light, the diameter of the lens, the distance between the lens and the sensor, and the angle of incidence of the light. The results of the study are presented in the following table.

2. The first parameter considered is the wavelength of the light. The results show that the performance of the system is highest for wavelengths between 400 nm and 600 nm. The performance is lowest for wavelengths below 400 nm and above 600 nm.

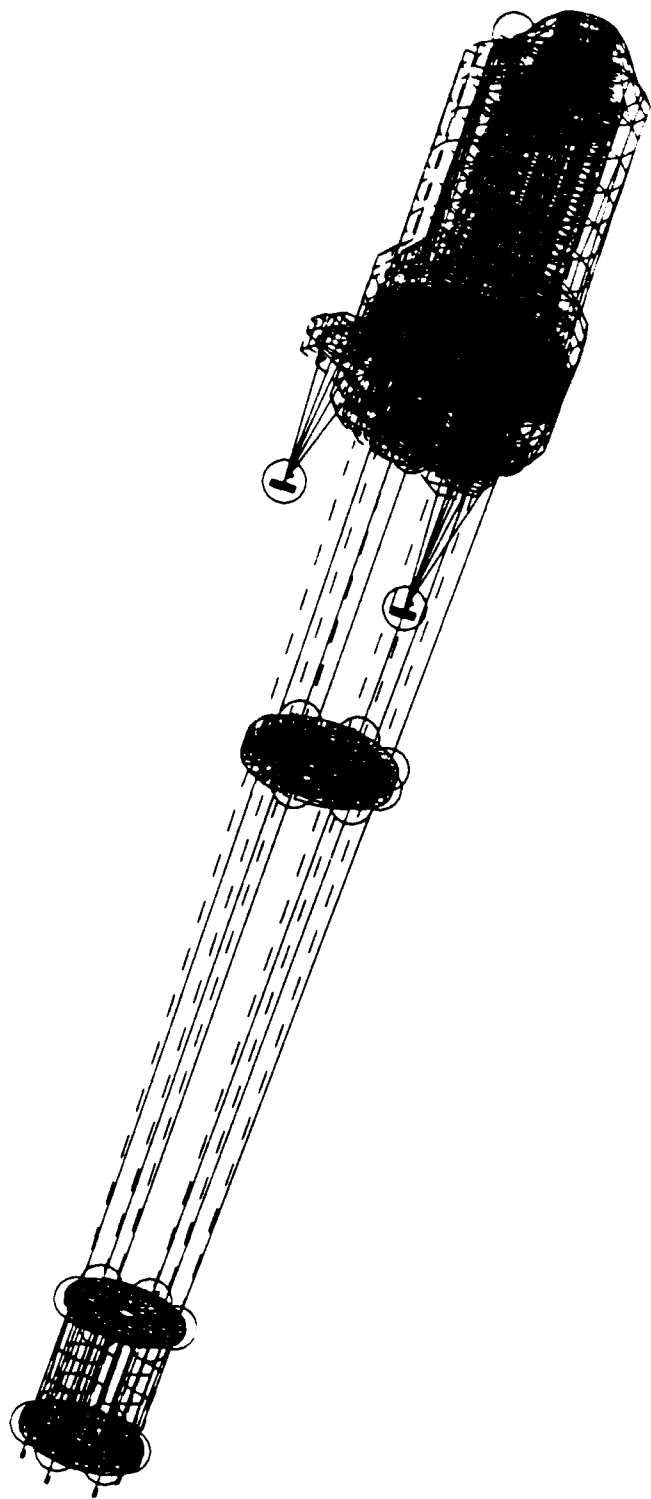
3. The second parameter considered is the diameter of the lens. The results show that the performance of the system is highest for a lens diameter of 10 mm. The performance is lowest for a lens diameter of 5 mm and 15 mm.

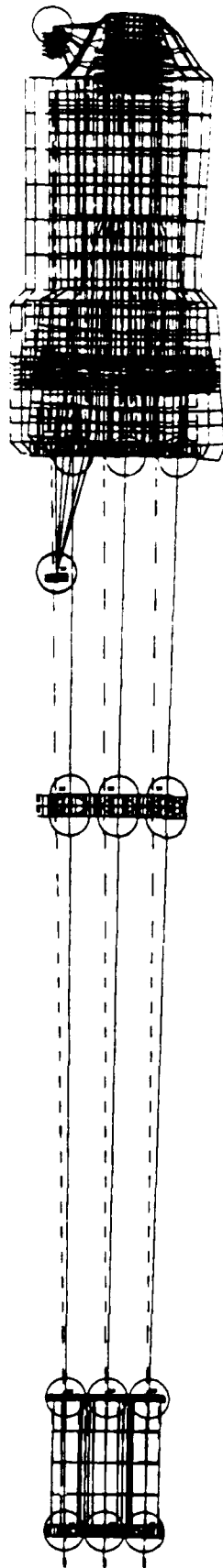
4. The third parameter considered is the distance between the lens and the sensor. The results show that the performance of the system is highest for a distance of 10 cm. The performance is lowest for a distance of 5 cm and 15 cm.

5. The fourth parameter considered is the angle of incidence of the light. The results show that the performance of the system is highest for an angle of incidence of 0 degrees. The performance is lowest for an angle of incidence of 30 degrees and 60 degrees.



X
7
Y

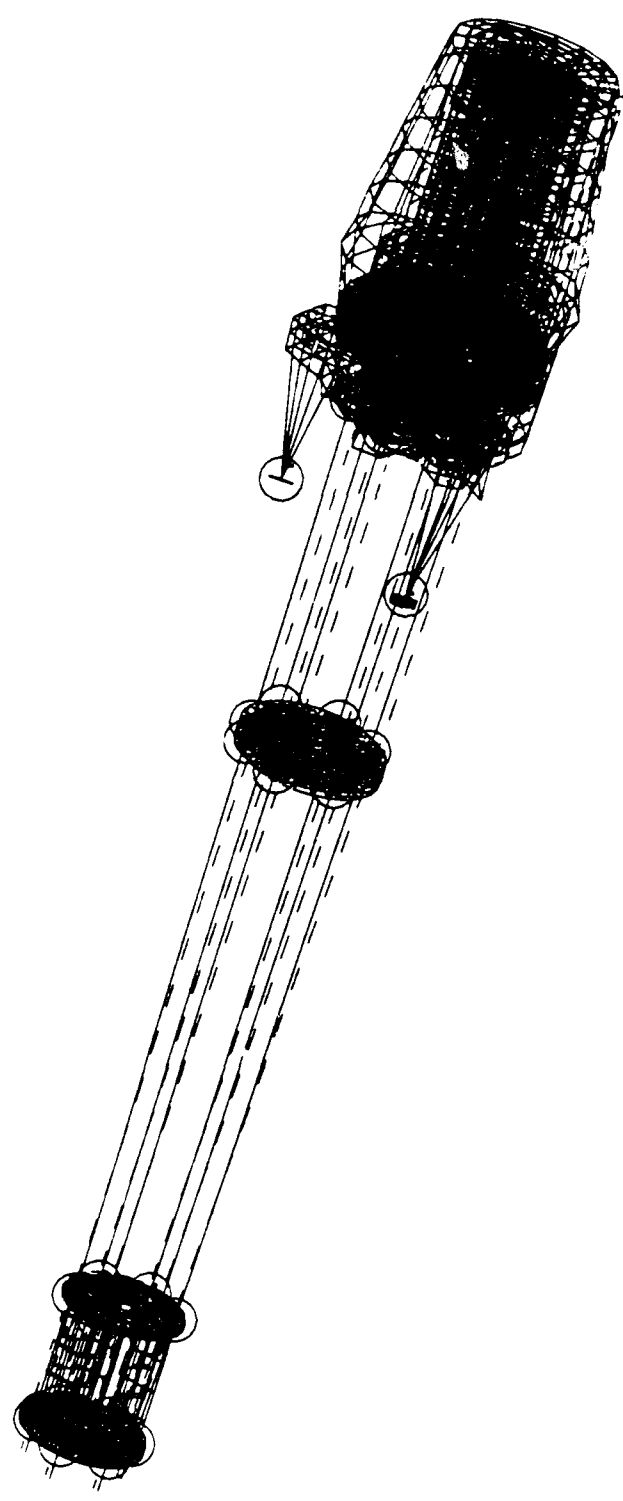




X
Y

1. The first part of the diagram shows a cross-section of a cylindrical object with a grid pattern. The grid is composed of lines that are slightly curved, suggesting a non-cylindrical shape or a specific coordinate system. The object is labeled with '1' and '2' at the top and bottom respectively.

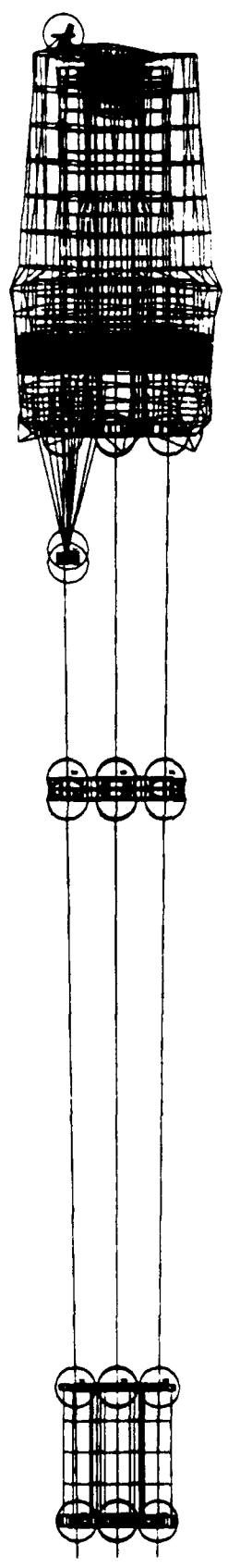
2. The second part of the diagram shows a similar cross-section, but with a different grid pattern. The lines are more pronounced and form a distinct shape. This part is labeled with '3' and '4' at the top and bottom respectively.



1. The first part of the document is a description of the system. It is a system for the control of a machine. The system is designed to be used in a factory or in a workshop. It is a system for the control of a machine. The system is designed to be used in a factory or in a workshop.

2. The second part of the document is a description of the system. It is a system for the control of a machine. The system is designed to be used in a factory or in a workshop. It is a system for the control of a machine. The system is designed to be used in a factory or in a workshop.

3. The third part of the document is a description of the system. It is a system for the control of a machine. The system is designed to be used in a factory or in a workshop. It is a system for the control of a machine. The system is designed to be used in a factory or in a workshop.



x
 y
 z

09:03:41

Unit 0 : CM

Model 1 Bin: 1-MAIN

Associated Worker: 26-WORKING SET26

Associated Worker: 26-WORKING SET26

...

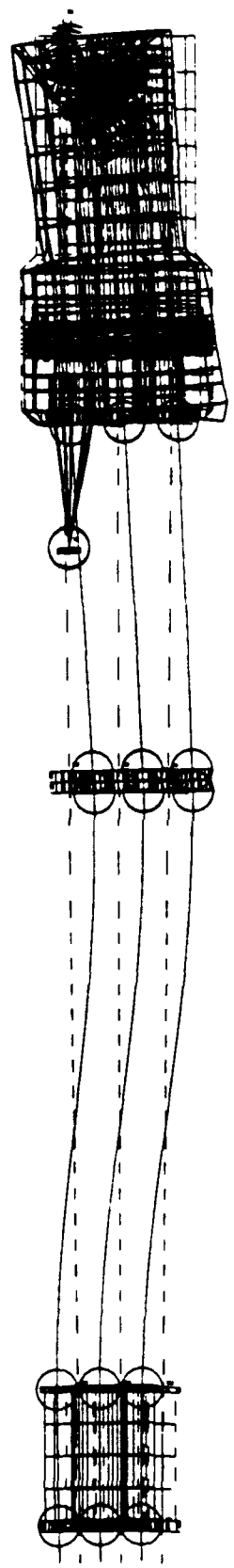


1. The first part of the diagram shows a cross-section of a structure with a grid-like pattern. The grid is composed of horizontal and vertical lines, forming a series of squares. The structure is labeled with 'A' at the top and 'B' at the bottom.

2. The second part of the diagram shows a cross-section of a structure with a grid-like pattern. The grid is composed of horizontal and vertical lines, forming a series of squares. The structure is labeled with 'A' at the top and 'B' at the bottom.

3. The third part of the diagram shows a cross-section of a structure with a grid-like pattern. The grid is composed of horizontal and vertical lines, forming a series of squares. The structure is labeled with 'A' at the top and 'B' at the bottom.

4. The fourth part of the diagram shows a cross-section of a structure with a grid-like pattern. The grid is composed of horizontal and vertical lines, forming a series of squares. The structure is labeled with 'A' at the top and 'B' at the bottom.



X
 Y

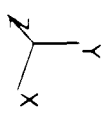
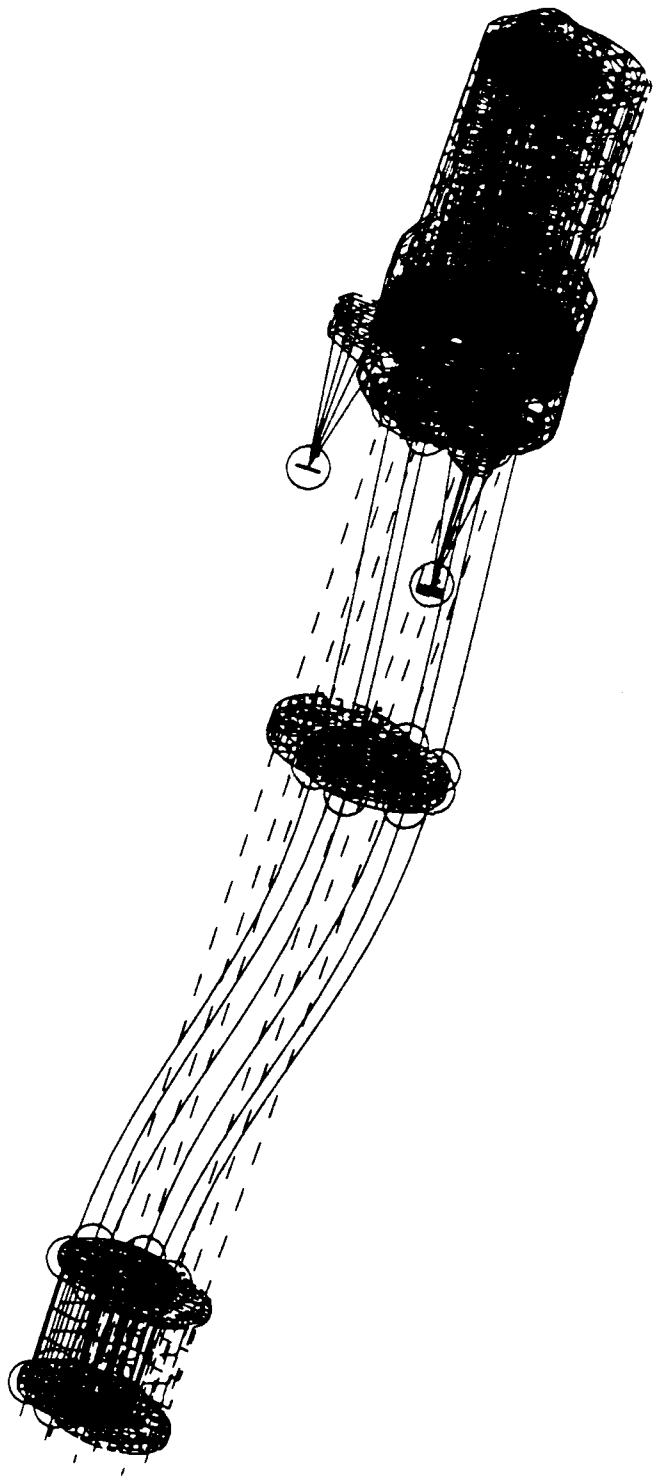
1. The first part of the paper is devoted to a description of the physical system under consideration. The system consists of a set of particles moving in a magnetic field. The particles are assumed to be identical and to have a constant mass and charge. The magnetic field is assumed to be uniform and to be directed along the z-axis. The particles are assumed to be moving in the xy-plane. The first part of the paper is devoted to a description of the physical system under consideration. The system consists of a set of particles moving in a magnetic field. The particles are assumed to be identical and to have a constant mass and charge. The magnetic field is assumed to be uniform and to be directed along the z-axis. The particles are assumed to be moving in the xy-plane.

2. The second part of the paper is devoted to a description of the mathematical model used in the calculations. The model is based on the assumption that the particles are moving in a magnetic field. The particles are assumed to be identical and to have a constant mass and charge. The magnetic field is assumed to be uniform and to be directed along the z-axis. The particles are assumed to be moving in the xy-plane.

3. The third part of the paper is devoted to a description of the results of the calculations. The results show that the particles move in a helical path around the z-axis. The radius of the helix is determined by the initial conditions of the particles. The period of the helical motion is determined by the mass and charge of the particles and the strength of the magnetic field.

4. The fourth part of the paper is devoted to a discussion of the physical significance of the results. The results show that the particles move in a helical path around the z-axis. This is a well-known result in classical electrodynamics. The results also show that the radius of the helix is determined by the initial conditions of the particles. This is also a well-known result. The period of the helical motion is determined by the mass and charge of the particles and the strength of the magnetic field. This is also a well-known result.

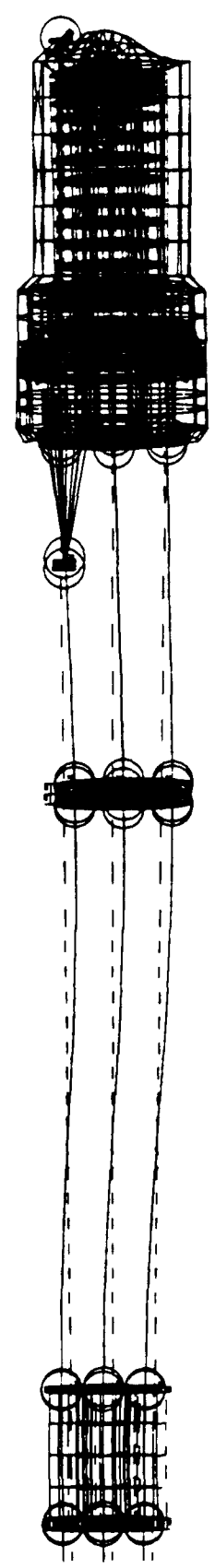
5. The fifth part of the paper is devoted to a conclusion. The results of the calculations show that the particles move in a helical path around the z-axis. The radius of the helix is determined by the initial conditions of the particles. The period of the helical motion is determined by the mass and charge of the particles and the strength of the magnetic field.



1. The first part of the document is a description of the system. It is a system for the control of a large number of small, independent, and mobile units. The system is designed to be used in a variety of environments, including urban, suburban, and rural areas. The system is designed to be used in a variety of environments, including urban, suburban, and rural areas.

2. The second part of the document is a description of the system. It is a system for the control of a large number of small, independent, and mobile units. The system is designed to be used in a variety of environments, including urban, suburban, and rural areas. The system is designed to be used in a variety of environments, including urban, suburban, and rural areas.

3. The third part of the document is a description of the system. It is a system for the control of a large number of small, independent, and mobile units. The system is designed to be used in a variety of environments, including urban, suburban, and rural areas. The system is designed to be used in a variety of environments, including urban, suburban, and rural areas.

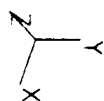
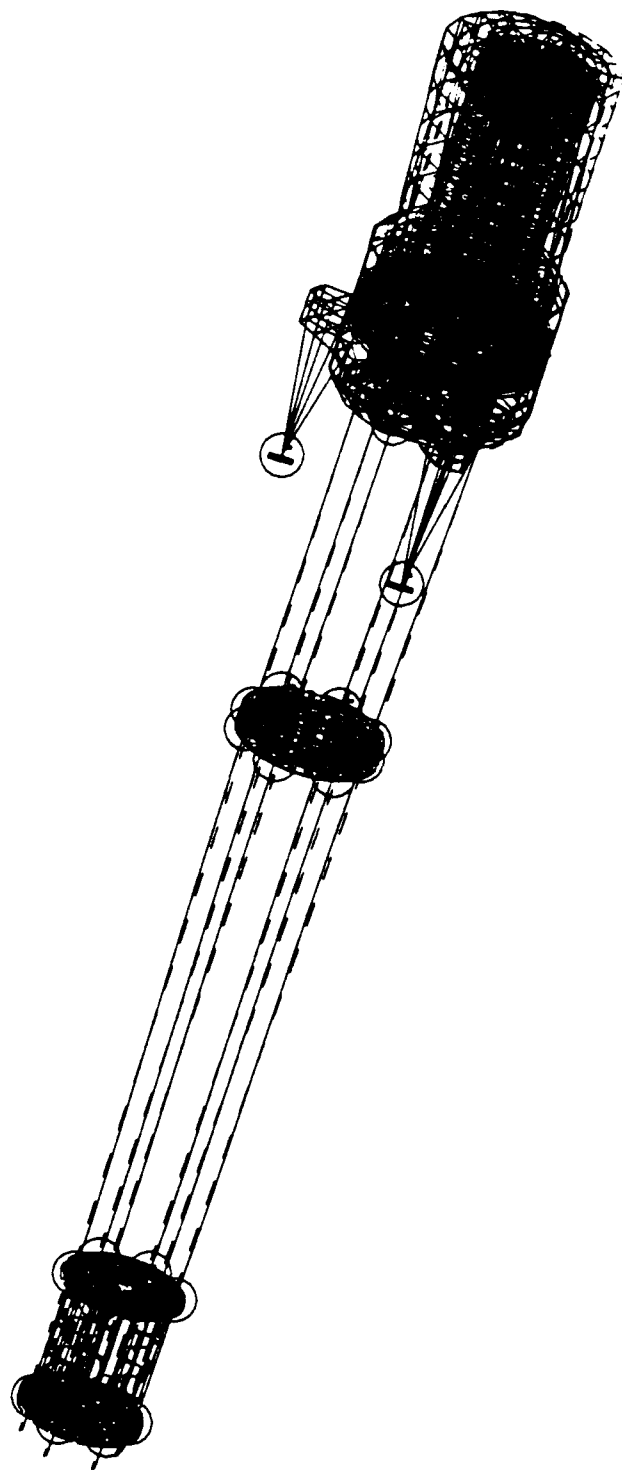


X
 Y

1. The first part of the paper is devoted to a review of the existing literature on the subject of the stability of the motion of a rigid body in a fluid. The second part is devoted to the study of the stability of the motion of a rigid body in a fluid. The third part is devoted to the study of the stability of the motion of a rigid body in a fluid.

2. The first part of the paper is devoted to a review of the existing literature on the subject of the stability of the motion of a rigid body in a fluid. The second part is devoted to the study of the stability of the motion of a rigid body in a fluid. The third part is devoted to the study of the stability of the motion of a rigid body in a fluid.

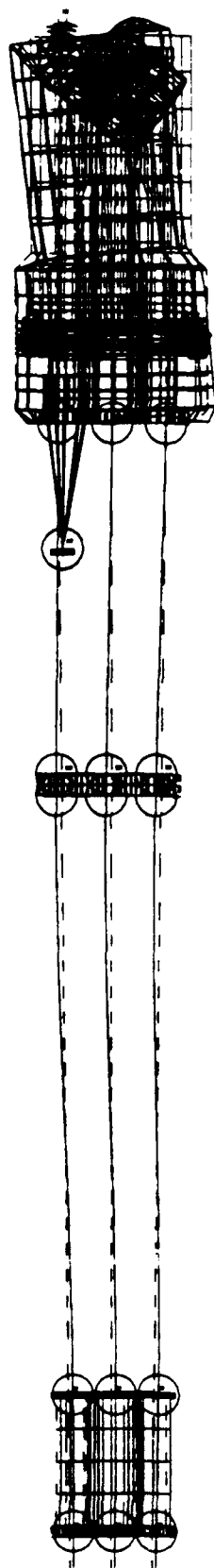
3. The first part of the paper is devoted to a review of the existing literature on the subject of the stability of the motion of a rigid body in a fluid. The second part is devoted to the study of the stability of the motion of a rigid body in a fluid. The third part is devoted to the study of the stability of the motion of a rigid body in a fluid.



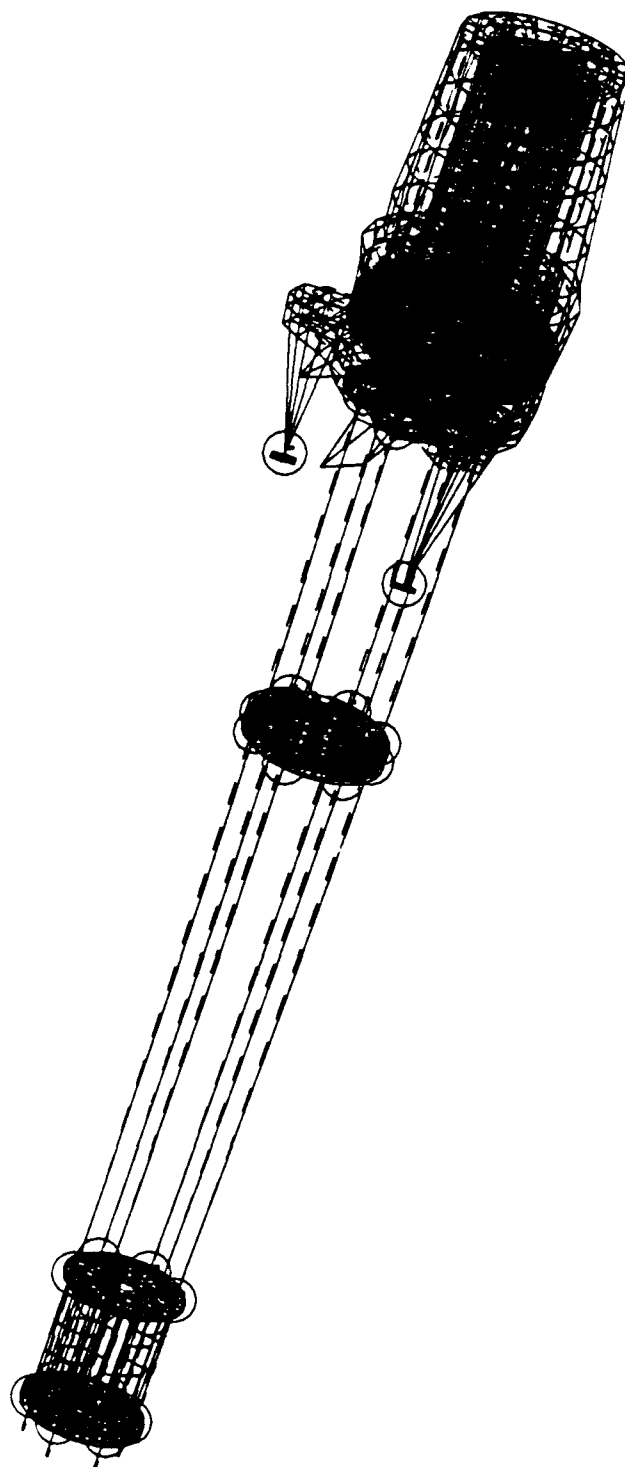
100

The diagrams illustrate the stages of mitosis:

- a**: Prophase, showing a cell with a prominent nucleus and nucleolus.
- b**: Metaphase, showing chromosomes aligned at the equatorial plate.
- c**: Anaphase, showing sister chromatids separating and moving toward opposite poles.
- d**: Telophase and cytokinesis, showing the formation of two new nuclei and the division of the cell.

[illegible]

✕

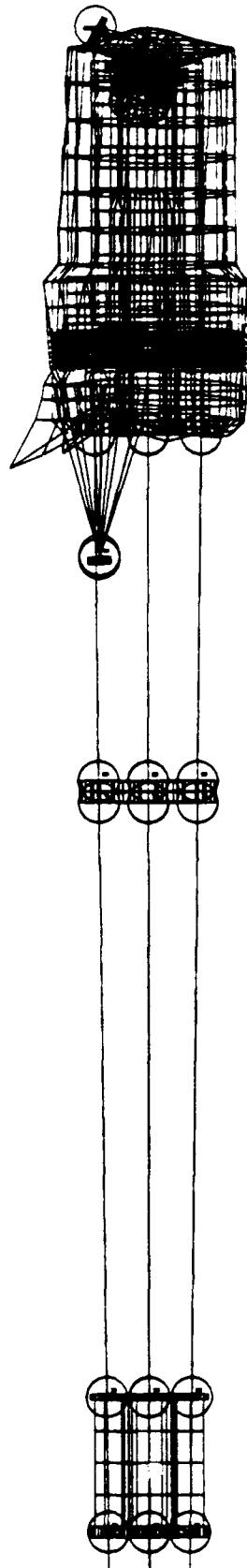


1. The purpose of this study is to determine the effect of the cable arrangement on the stability of the system. The study is conducted using a finite element analysis (FEA) method. The results of the analysis are presented in the following table.

Case	Stability Factor	Displacement (mm)	Stress (MPa)
1	1.2	10	100
2	1.5	15	150
3	1.8	20	200
4	2.1	25	250
5	2.4	30	300

2. The results of the analysis show that the stability factor increases as the displacement and stress increase. This indicates that the system becomes more stable as the displacement and stress increase. The results also show that the displacement and stress increase as the cable arrangement changes. This indicates that the cable arrangement has a significant effect on the stability of the system.

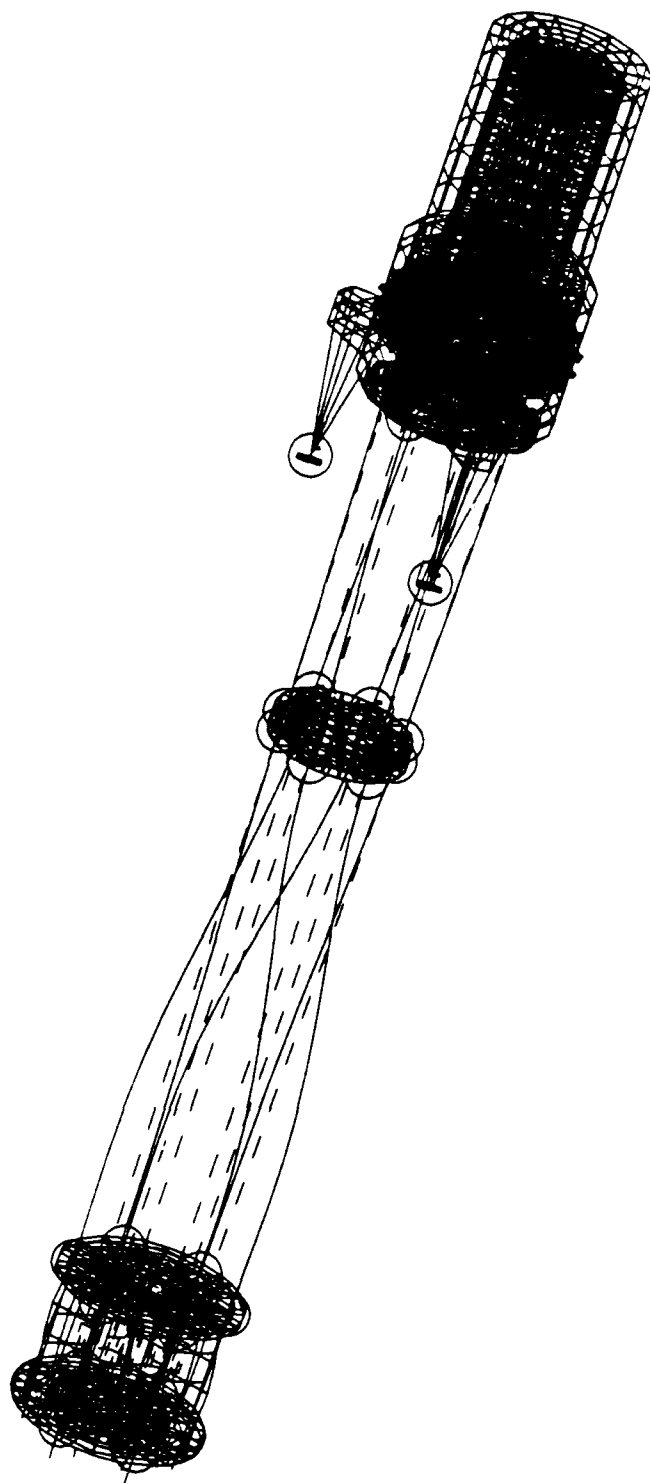
3. The study concludes that the cable arrangement has a significant effect on the stability of the system. The results of the analysis show that the stability factor increases as the displacement and stress increase. This indicates that the system becomes more stable as the displacement and stress increase. The results also show that the displacement and stress increase as the cable arrangement changes. This indicates that the cable arrangement has a significant effect on the stability of the system.

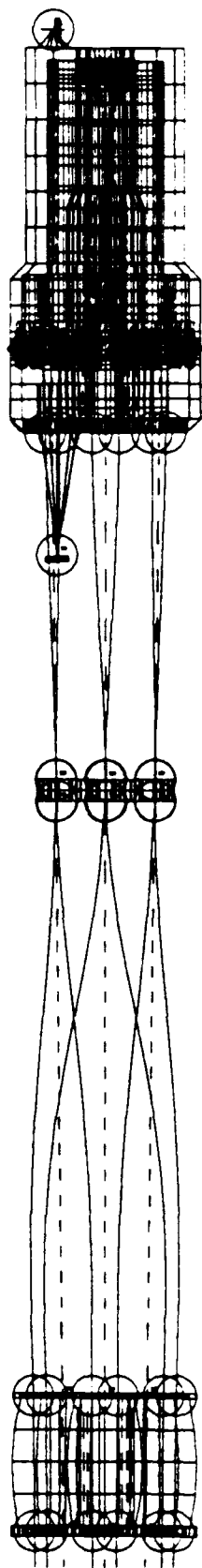


x
7
y

1. *Figure 1*
 2. *Figure 2*
 3. *Figure 3*
 4. *Figure 4*
 5. *Figure 5*
 6. *Figure 6*
 7. *Figure 7*
 8. *Figure 8*
 9. *Figure 9*
 10. *Figure 10*
 11. *Figure 11*
 12. *Figure 12*
 13. *Figure 13*
 14. *Figure 14*
 15. *Figure 15*
 16. *Figure 16*
 17. *Figure 17*
 18. *Figure 18*
 19. *Figure 19*
 20. *Figure 20*
 21. *Figure 21*
 22. *Figure 22*
 23. *Figure 23*
 24. *Figure 24*
 25. *Figure 25*
 26. *Figure 26*
 27. *Figure 27*
 28. *Figure 28*
 29. *Figure 29*
 30. *Figure 30*
 31. *Figure 31*
 32. *Figure 32*
 33. *Figure 33*
 34. *Figure 34*
 35. *Figure 35*
 36. *Figure 36*
 37. *Figure 37*
 38. *Figure 38*
 39. *Figure 39*
 40. *Figure 40*
 41. *Figure 41*
 42. *Figure 42*
 43. *Figure 43*
 44. *Figure 44*
 45. *Figure 45*
 46. *Figure 46*
 47. *Figure 47*
 48. *Figure 48*
 49. *Figure 49*
 50. *Figure 50*
 51. *Figure 51*
 52. *Figure 52*
 53. *Figure 53*
 54. *Figure 54*
 55. *Figure 55*
 56. *Figure 56*
 57. *Figure 57*
 58. *Figure 58*
 59. *Figure 59*
 60. *Figure 60*
 61. *Figure 61*
 62. *Figure 62*
 63. *Figure 63*
 64. *Figure 64*
 65. *Figure 65*
 66. *Figure 66*
 67. *Figure 67*
 68. *Figure 68*
 69. *Figure 69*
 70. *Figure 70*
 71. *Figure 71*
 72. *Figure 72*
 73. *Figure 73*
 74. *Figure 74*
 75. *Figure 75*
 76. *Figure 76*
 77. *Figure 77*
 78. *Figure 78*
 79. *Figure 79*
 80. *Figure 80*
 81. *Figure 81*
 82. *Figure 82*
 83. *Figure 83*
 84. *Figure 84*
 85. *Figure 85*
 86. *Figure 86*
 87. *Figure 87*
 88. *Figure 88*
 89. *Figure 89*
 90. *Figure 90*
 91. *Figure 91*
 92. *Figure 92*
 93. *Figure 93*
 94. *Figure 94*
 95. *Figure 95*
 96. *Figure 96*
 97. *Figure 97*
 98. *Figure 98*
 99. *Figure 99*
 100. *Figure 100*

1. *Figure 1*
 2. *Figure 2*
 3. *Figure 3*
 4. *Figure 4*
 5. *Figure 5*
 6. *Figure 6*
 7. *Figure 7*
 8. *Figure 8*
 9. *Figure 9*
 10. *Figure 10*
 11. *Figure 11*
 12. *Figure 12*
 13. *Figure 13*
 14. *Figure 14*
 15. *Figure 15*
 16. *Figure 16*
 17. *Figure 17*
 18. *Figure 18*
 19. *Figure 19*
 20. *Figure 20*
 21. *Figure 21*
 22. *Figure 22*
 23. *Figure 23*
 24. *Figure 24*
 25. *Figure 25*
 26. *Figure 26*
 27. *Figure 27*
 28. *Figure 28*
 29. *Figure 29*
 30. *Figure 30*
 31. *Figure 31*
 32. *Figure 32*
 33. *Figure 33*
 34. *Figure 34*
 35. *Figure 35*
 36. *Figure 36*
 37. *Figure 37*
 38. *Figure 38*
 39. *Figure 39*
 40. *Figure 40*
 41. *Figure 41*
 42. *Figure 42*
 43. *Figure 43*
 44. *Figure 44*
 45. *Figure 45*
 46. *Figure 46*
 47. *Figure 47*
 48. *Figure 48*
 49. *Figure 49*
 50. *Figure 50*
 51. *Figure 51*
 52. *Figure 52*
 53. *Figure 53*
 54. *Figure 54*
 55. *Figure 55*
 56. *Figure 56*
 57. *Figure 57*
 58. *Figure 58*
 59. *Figure 59*
 60. *Figure 60*
 61. *Figure 61*
 62. *Figure 62*
 63. *Figure 63*
 64. *Figure 64*
 65. *Figure 65*
 66. *Figure 66*
 67. *Figure 67*
 68. *Figure 68*
 69. *Figure 69*
 70. *Figure 70*
 71. *Figure 71*
 72. *Figure 72*
 73. *Figure 73*
 74. *Figure 74*
 75. *Figure 75*
 76. *Figure 76*
 77. *Figure 77*
 78. *Figure 78*
 79. *Figure 79*
 80. *Figure 80*
 81. *Figure 81*
 82. *Figure 82*
 83. *Figure 83*
 84. *Figure 84*
 85. *Figure 85*
 86. *Figure 86*
 87. *Figure 87*
 88. *Figure 88*
 89. *Figure 89*
 90. *Figure 90*
 91. *Figure 91*
 92. *Figure 92*
 93. *Figure 93*
 94. *Figure 94*
 95. *Figure 95*
 96. *Figure 96*
 97. *Figure 97*
 98. *Figure 98*
 99. *Figure 99*
 100. *Figure 100*



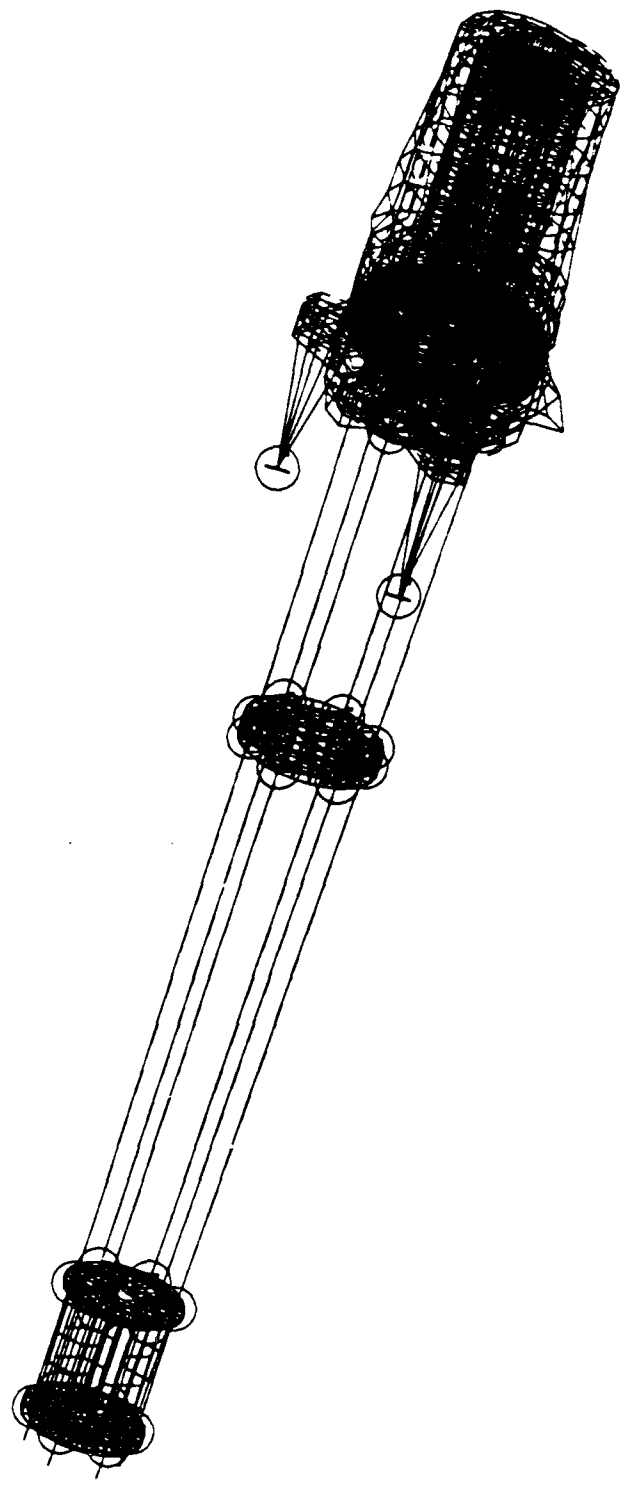


x
y

1. The first part of the report is a review of the literature on the subject of the effect of the environment on the behavior of the human operator. This part is divided into two sections: (a) a review of the literature on the effect of the environment on the behavior of the human operator, and (b) a review of the literature on the effect of the environment on the behavior of the human operator.

2. The second part of the report is a review of the literature on the subject of the effect of the environment on the behavior of the human operator. This part is divided into two sections: (a) a review of the literature on the effect of the environment on the behavior of the human operator, and (b) a review of the literature on the effect of the environment on the behavior of the human operator.

3. The third part of the report is a review of the literature on the subject of the effect of the environment on the behavior of the human operator. This part is divided into two sections: (a) a review of the literature on the effect of the environment on the behavior of the human operator, and (b) a review of the literature on the effect of the environment on the behavior of the human operator.

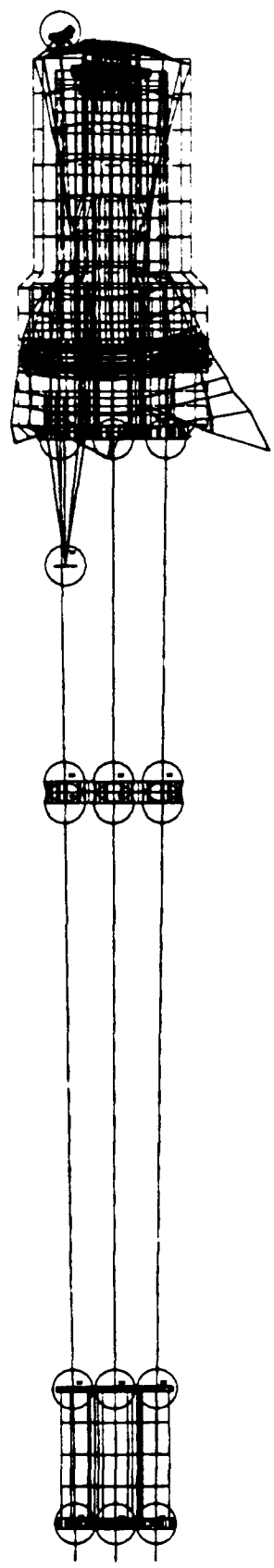


1. The first part of the document is a description of the system. It is a system for the control of a machine. The system is composed of a number of parts, including a control panel, a power supply, and a motor. The control panel is used to start and stop the machine, and to adjust its speed. The power supply provides the energy needed to run the machine. The motor is the part that actually does the work.

2. The second part of the document is a diagram of the system. It shows the control panel, the power supply, and the motor, and how they are connected. The control panel is connected to the power supply, which is connected to the motor.

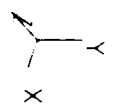
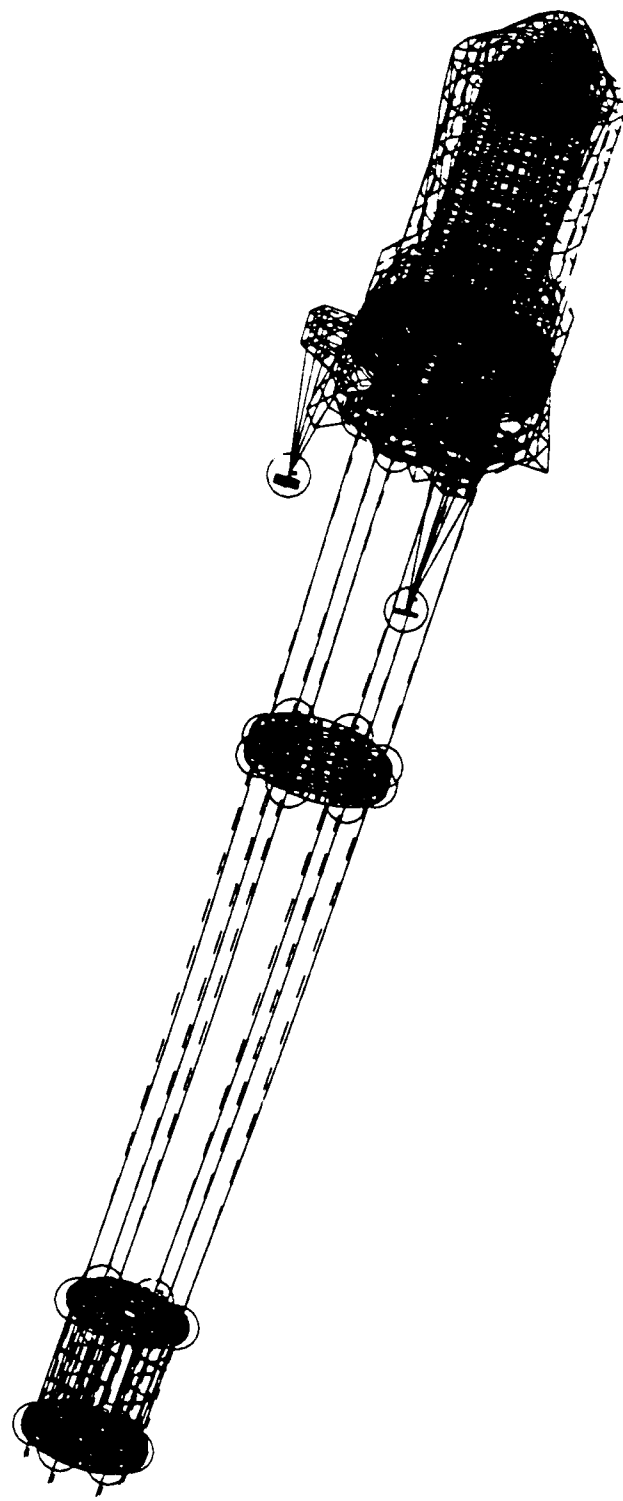
3. The third part of the document is a list of the parts of the system. It includes the control panel, the power supply, and the motor.

4. The fourth part of the document is a list of the instructions for using the system. It includes instructions for starting and stopping the machine, and for adjusting its speed.



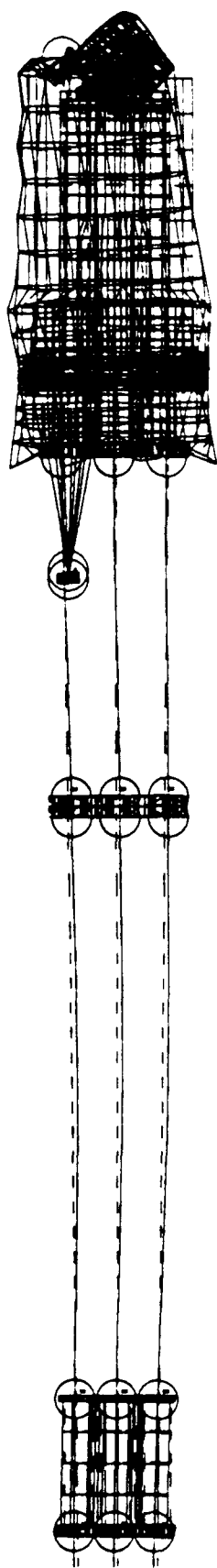
X
 Y

Figure 1-1
 View of the structure
 in the direction of the
 load.
 The structure is a
 rectangular box with
 a central vertical
 column and four
 diagonal bracing
 members. The
 structure is shown
 in a perspective
 view. The load is
 applied to the top
 surface of the box.
 The structure is
 supported by four
 vertical columns at
 the corners. The
 structure is shown
 in a perspective
 view. The load is
 applied to the top
 surface of the box.
 The structure is
 supported by four
 vertical columns at
 the corners.



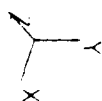
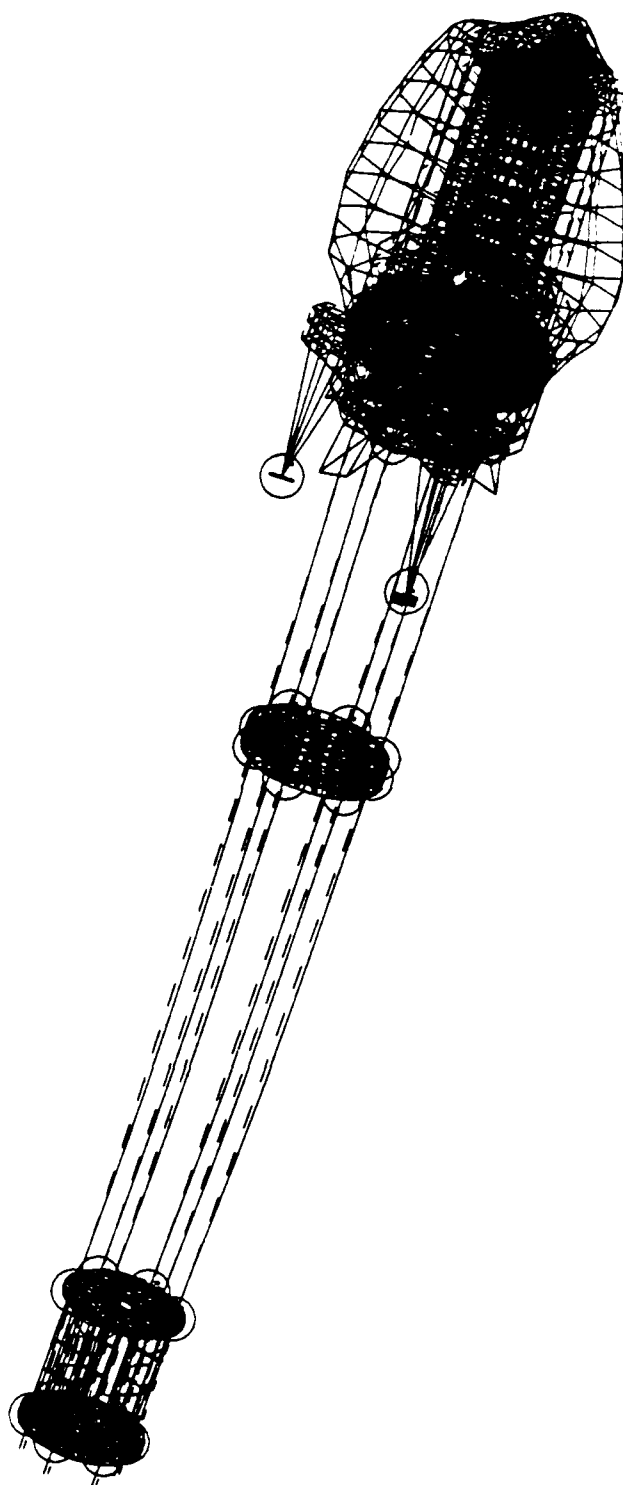
Country	Year	Rate
Algeria	1990	100.0
Algeria	1991	100.0
Algeria	1992	100.0
Algeria	1993	100.0
Algeria	1994	100.0
Algeria	1995	100.0
Algeria	1996	100.0
Algeria	1997	100.0
Algeria	1998	100.0
Algeria	1999	100.0
Algeria	2000	100.0
Algeria	2001	100.0
Algeria	2002	100.0
Algeria	2003	100.0
Algeria	2004	100.0
Algeria	2005	100.0
Algeria	2006	100.0
Algeria	2007	100.0
Algeria	2008	100.0
Algeria	2009	100.0
Algeria	2010	100.0
Algeria	2011	100.0
Algeria	2012	100.0
Algeria	2013	100.0
Algeria	2014	100.0
Algeria	2015	100.0
Algeria	2016	100.0
Algeria	2017	100.0
Algeria	2018	100.0
Algeria	2019	100.0
Algeria	2020	100.0
Algeria	2021	100.0
Algeria	2022	100.0
Algeria	2023	100.0
Algeria	2024	100.0
Algeria	2025	100.0
Algeria	2026	100.0
Algeria	2027	100.0
Algeria	2028	100.0
Algeria	2029	100.0
Algeria	2030	100.0
Algeria	2031	100.0
Algeria	2032	100.0
Algeria	2033	100.0
Algeria	2034	100.0
Algeria	2035	100.0
Algeria	2036	100.0
Algeria	2037	100.0
Algeria	2038	100.0
Algeria	2039	100.0
Algeria	2040	100.0
Algeria	2041	100.0
Algeria	2042	100.0
Algeria	2043	100.0
Algeria	2044	100.0
Algeria	2045	100.0
Algeria	2046	100.0
Algeria	2047	100.0
Algeria	2048	100.0
Algeria	2049	100.0
Algeria	2050	100.0
Algeria	2051	100.0
Algeria	2052	100.0
Algeria	2053	100.0
Algeria	2054	100.0
Algeria	2055	100.0
Algeria	2056	100.0
Algeria	2057	100.0
Algeria	2058	100.0
Algeria	2059	100.0
Algeria	2060	100.0
Algeria	2061	100.0
Algeria	2062	100.0
Algeria	2063	100.0
Algeria	2064	100.0
Algeria	2065	100.0
Algeria	2066	100.0
Algeria	2067	100.0
Algeria	2068	100.0
Algeria	2069	100.0
Algeria	2070	100.0
Algeria	2071	100.0
Algeria	2072	100.0
Algeria	2073	100.0
Algeria	2074	100.0
Algeria	2075	100.0
Algeria	2076	100.0
Algeria	2077	100.0
Algeria	2078	100.0
Algeria	2079	100.0
Algeria	2080	100.0
Algeria	2081	100.0
Algeria	2082	100.0
Algeria	2083	100.0
Algeria	2084	100.0
Algeria	2085	100.0
Algeria	2086	100.0
Algeria	2087	100.0
Algeria	2088	100.0
Algeria	2089	100.0
Algeria	2090	100.0
Algeria	2091	100.0
Algeria	2092	100.0
Algeria	2093	100.0
Algeria	2094	100.0
Algeria	2095	100.0
Algeria	2096	100.0
Algeria	2097	100.0
Algeria	2098	100.0
Algeria	2099</	

•
•
•
•
•
•
•
•



[illegible]

1
 2
 3
 4
 5
 6
 7
 8
 9
 10
 11
 12
 13
 14
 15
 16
 17
 18
 19
 20
 21
 22
 23
 24
 25
 26
 27
 28
 29
 30
 31
 32
 33
 34
 35
 36
 37
 38
 39
 40
 41
 42
 43
 44
 45
 46
 47
 48
 49
 50
 51
 52
 53
 54
 55
 56
 57
 58
 59
 60
 61
 62
 63
 64
 65
 66
 67
 68
 69
 70
 71
 72
 73
 74
 75
 76
 77
 78
 79
 80
 81
 82
 83
 84
 85
 86
 87
 88
 89
 90
 91
 92
 93
 94
 95
 96
 97
 98
 99
 100
 101
 102
 103
 104
 105
 106
 107
 108
 109
 110
 111
 112
 113
 114
 115
 116
 117
 118
 119
 120
 121
 122
 123
 124
 125
 126
 127
 128
 129
 130
 131
 132
 133
 134
 135
 136
 137
 138
 139
 140
 141
 142
 143
 144
 145
 146
 147
 148
 149
 150
 151
 152
 153
 154
 155
 156
 157
 158
 159
 160
 161
 162
 163
 164
 165
 166
 167
 168
 169
 170
 171
 172
 173
 174
 175
 176
 177
 178
 179
 180
 181
 182
 183
 184
 185
 186
 187
 188
 189
 190
 191
 192
 193
 194
 195
 196
 197
 198
 199
 200
 201
 202
 203
 204
 205
 206
 207
 208
 209
 210
 211
 212
 213
 214
 215
 216
 217
 218
 219
 220
 221
 222
 223
 224
 225
 226
 227
 228
 229
 230
 231
 232
 233
 234
 235
 236
 237
 238
 239
 240
 241
 242
 243
 244
 245
 246
 247
 248
 249
 250
 251
 252
 253
 254
 255
 256
 257
 258
 259
 260
 261
 262
 263
 264
 265
 266
 267
 268
 269
 270
 271
 272
 273
 274
 275
 276
 277
 278
 279
 280
 281
 282
 283
 284
 285
 286
 287
 288
 289
 290
 291
 292
 293
 294
 295
 296
 297
 298
 299
 300
 301
 302
 303
 304
 305
 306
 307
 308
 309
 310
 311
 312
 313
 314
 315
 316
 317
 318
 319
 320
 321
 322
 323
 324
 325
 326
 327
 328
 329
 330
 331
 332
 333
 334
 335
 336
 337
 338
 339
 340
 341
 342
 343
 344
 345
 346
 347
 348
 349
 350
 351
 352
 353
 354
 355
 356
 357
 358
 359
 360
 361
 362
 363
 364
 365
 366
 367
 368
 369
 370
 371
 372
 373
 374
 375
 376
 377
 378
 379
 380
 381
 382
 383
 384
 385
 386
 387
 388
 389
 390
 391
 392
 393
 394
 395
 396
 397
 398
 399
 400
 401
 402
 403
 404
 405
 406
 407
 408
 409
 410
 411
 412
 413
 414
 415
 416
 417
 418
 419
 420
 421
 422
 423
 424
 425
 426
 427
 428
 429
 430
 431
 432
 433
 434
 435
 436
 437
 438
 439
 440
 441
 442
 443
 444
 445
 446
 447
 448
 449
 450
 451
 452
 453
 454
 455
 456
 457
 458
 459
 460
 461
 462
 463
 464
 465
 466
 467
 468
 469
 470
 471
 472
 473
 474
 475
 476
 477
 478
 479
 480
 481
 482
 483
 484
 485
 486
 487
 488
 489
 490
 491
 492
 493
 494
 495
 496
 497
 498
 499
 500
 501
 502
 503
 504
 505
 506
 507
 508
 509
 510
 511
 512
 513
 514
 515
 516
 517
 518
 519
 520
 521
 522
 523
 524
 525



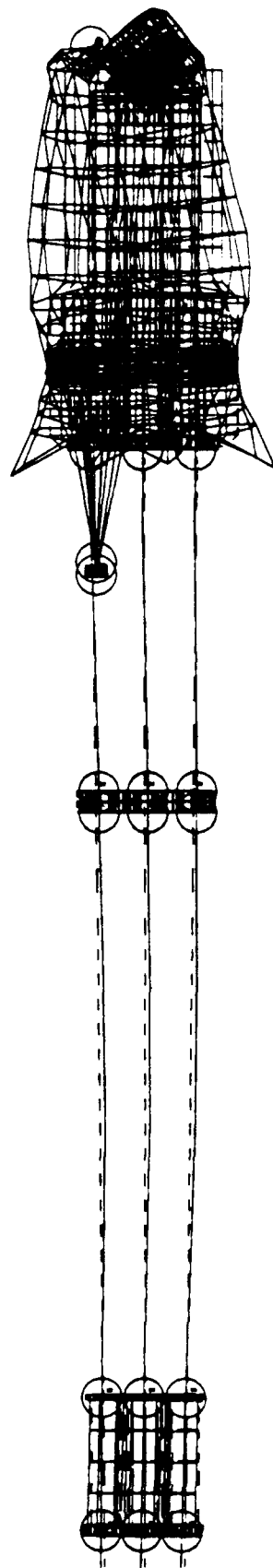
1. The first part of the document is a description of the system. It is a system for the control of a ship's movement. The system is designed to control the ship's position and heading. The system is composed of a number of components, including a control unit, a sensor unit, and a display unit. The control unit is responsible for processing the data received from the sensor unit and for controlling the ship's movement. The sensor unit is responsible for detecting the ship's position and heading. The display unit is responsible for displaying the ship's position and heading to the operator.

2. The second part of the document is a block diagram of the system. The diagram shows the control unit, the sensor unit, and the display unit. The control unit is connected to the sensor unit and the display unit. The sensor unit is connected to the control unit. The display unit is connected to the control unit.

3. The third part of the document is a flowchart of the system. The flowchart shows the sequence of operations performed by the system. The sequence starts with the control unit receiving data from the sensor unit. The control unit then processes the data and controls the ship's movement. The sensor unit then detects the ship's position and heading. The display unit then displays the ship's position and heading to the operator.

4. The fourth part of the document is a list of the components of the system. The components are:

- Control unit
- Sensor unit
- Display unit



x
 y

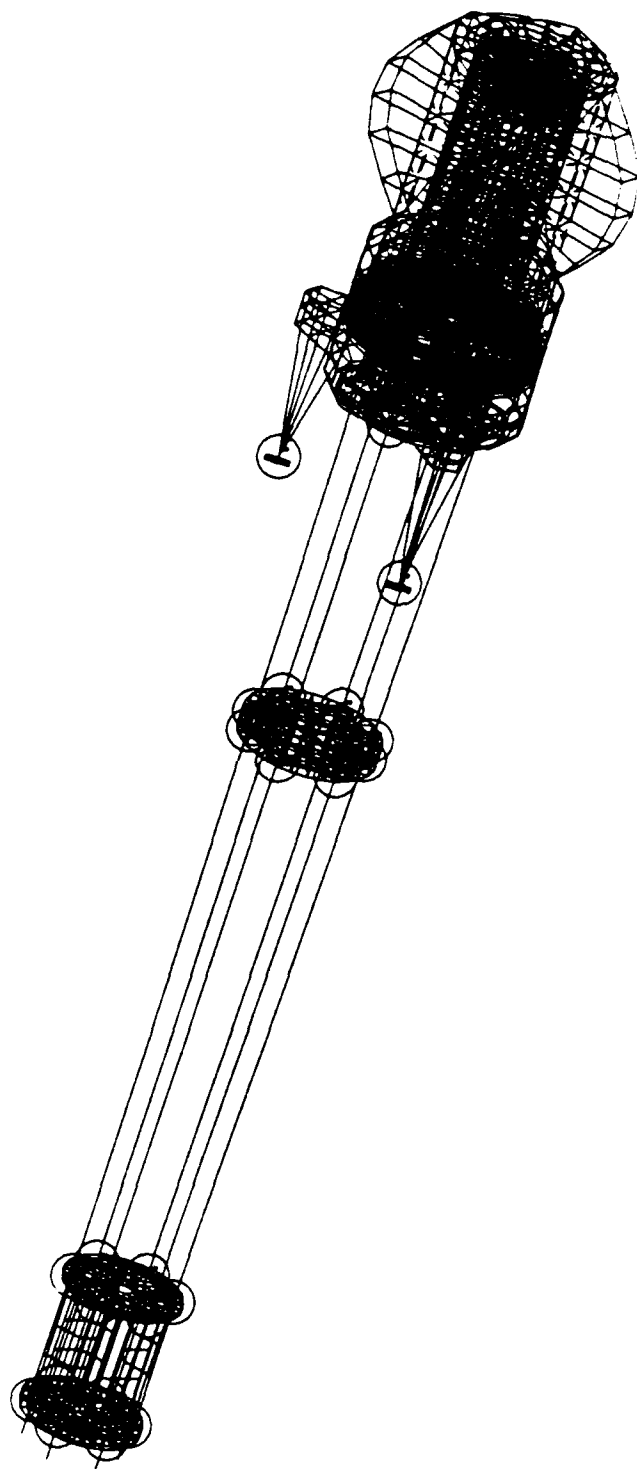
1. The first part of the document is a description of the system. It is a system for the control of a vehicle. The system is designed to control the vehicle's position and orientation. The system is composed of a number of components, including a sensor, a processor, and an actuator. The sensor is used to detect the vehicle's position and orientation. The processor is used to process the data from the sensor and to generate control signals. The actuator is used to execute the control signals.

2. The second part of the document is a description of the system's architecture. The system is a distributed system. It is composed of a number of nodes, each of which is responsible for a specific function. The nodes are connected to each other via a network. The network is used to exchange data and control signals between the nodes.

3. The third part of the document is a description of the system's performance. The system is designed to be robust and reliable. It is able to operate in a wide range of environments. The system is able to handle a large number of inputs and outputs. The system is able to maintain a high level of accuracy.

4. The fourth part of the document is a description of the system's implementation. The system is implemented using a number of different technologies. It is implemented using a number of different programming languages. It is implemented using a number of different hardware components.

5. The fifth part of the document is a description of the system's future work. There are a number of areas in which the system can be improved. There are a number of new features that can be added to the system. There are a number of new challenges that need to be addressed.



SDRC I-DEAS V11.1(5) : FE Modeling & Analysis
 Database: Phalanxgun
 View: S102 (modified)
 Task: Post Processing
 Model: 2-MODEL2

16-JUN-93

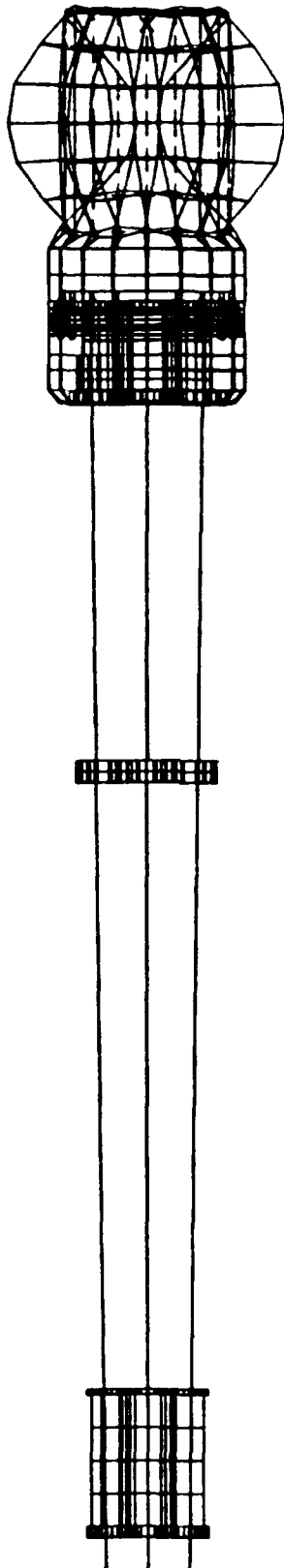
09:08:44

Unit: CM

Display: No stored Option
 Model Bin: 1 MAIN
 Associated Worksheet: 26-WORKING SET26

LINE 1001 IS 10001.15 10001.15 10001.15 10001.15
 REFINEMENT 10001.15 10001.15 10001.15 10001.15

....



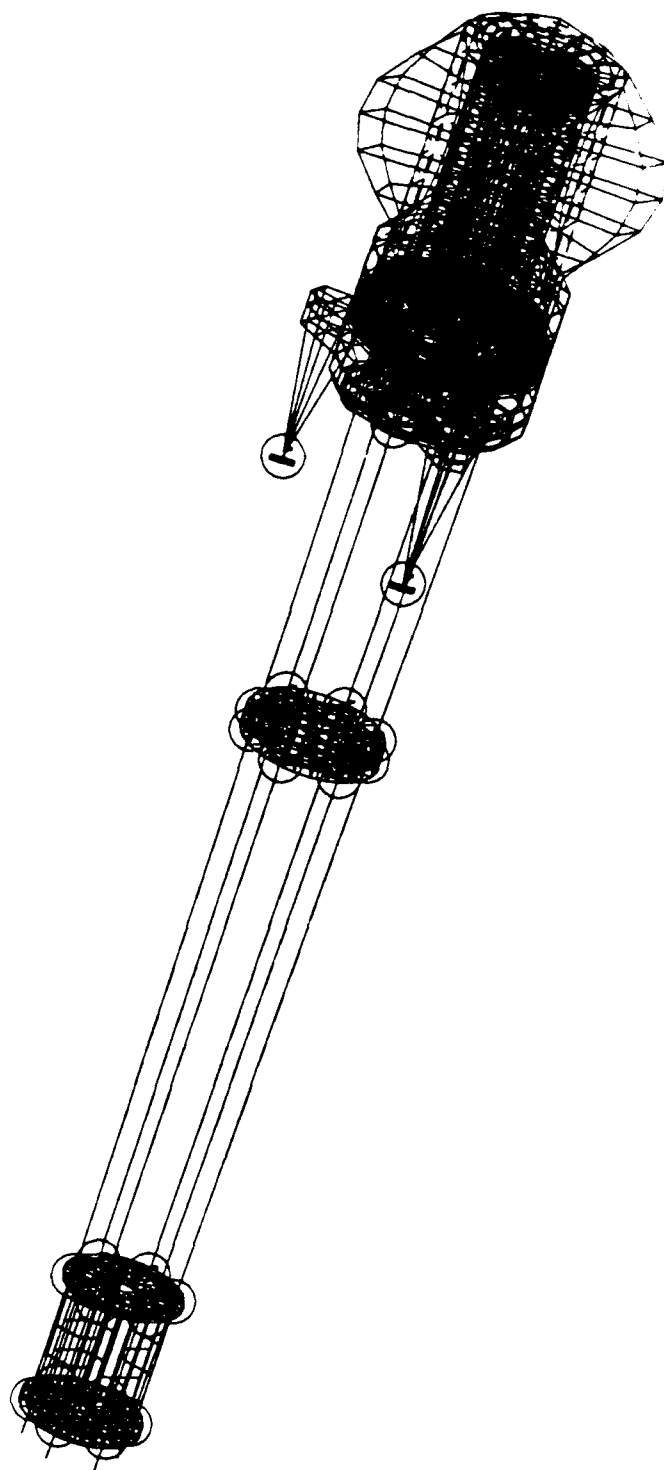
1. The first part of the document is a description of the system. It is a system for the control of a robot arm. The system is composed of a computer, a robot arm, and a control panel. The computer is used to store the program and to control the robot arm. The robot arm is used to move the control panel. The control panel is used to control the robot arm.

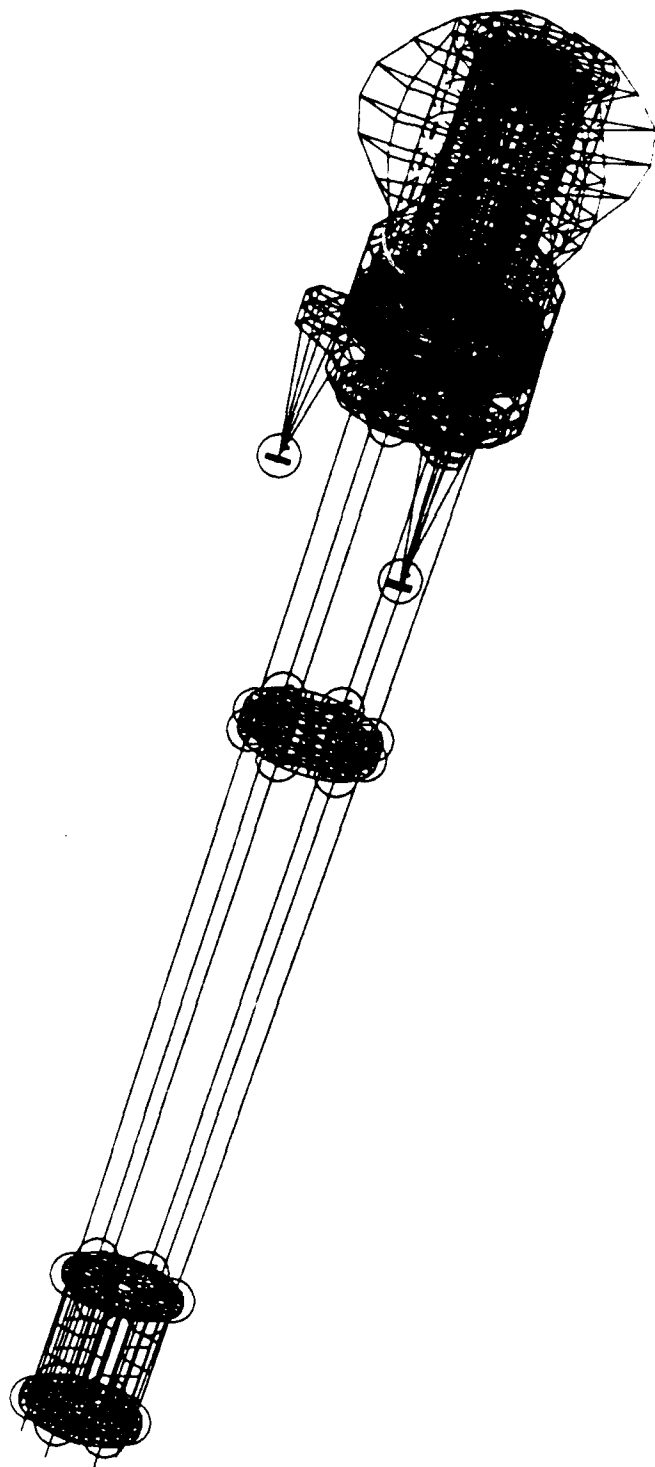
2. The second part of the document is a description of the hardware. It is a description of the robot arm and the control panel. The robot arm is made of metal and has a length of 1.5 meters. The control panel is made of plastic and has a length of 0.5 meters.

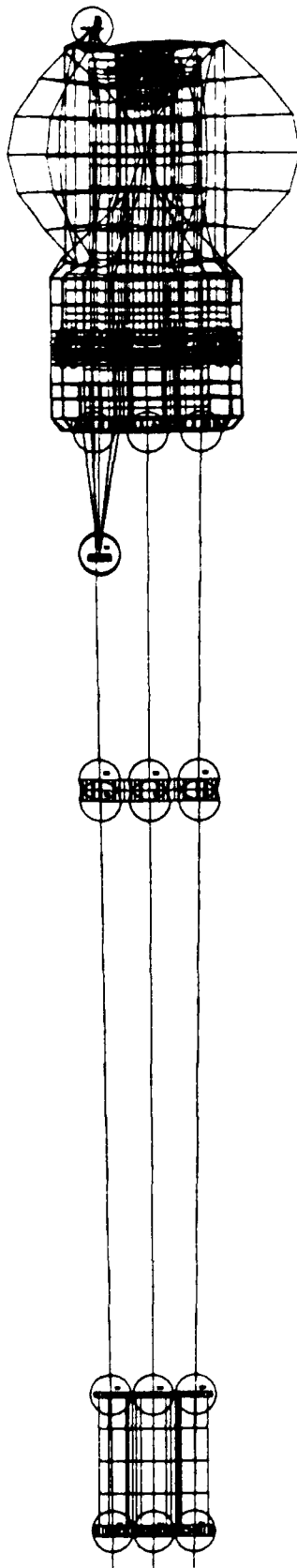
3. The third part of the document is a description of the software. It is a description of the program that controls the robot arm. The program is written in Fortran and is 100 lines long.

4. The fourth part of the document is a description of the results. It is a description of the results of the experiments. The results show that the system is able to control the robot arm with a high degree of accuracy.

5. The fifth part of the document is a description of the conclusions. It is a description of the conclusions of the experiments. The conclusions are that the system is a good example of a control system for a robot arm.







x
7
x

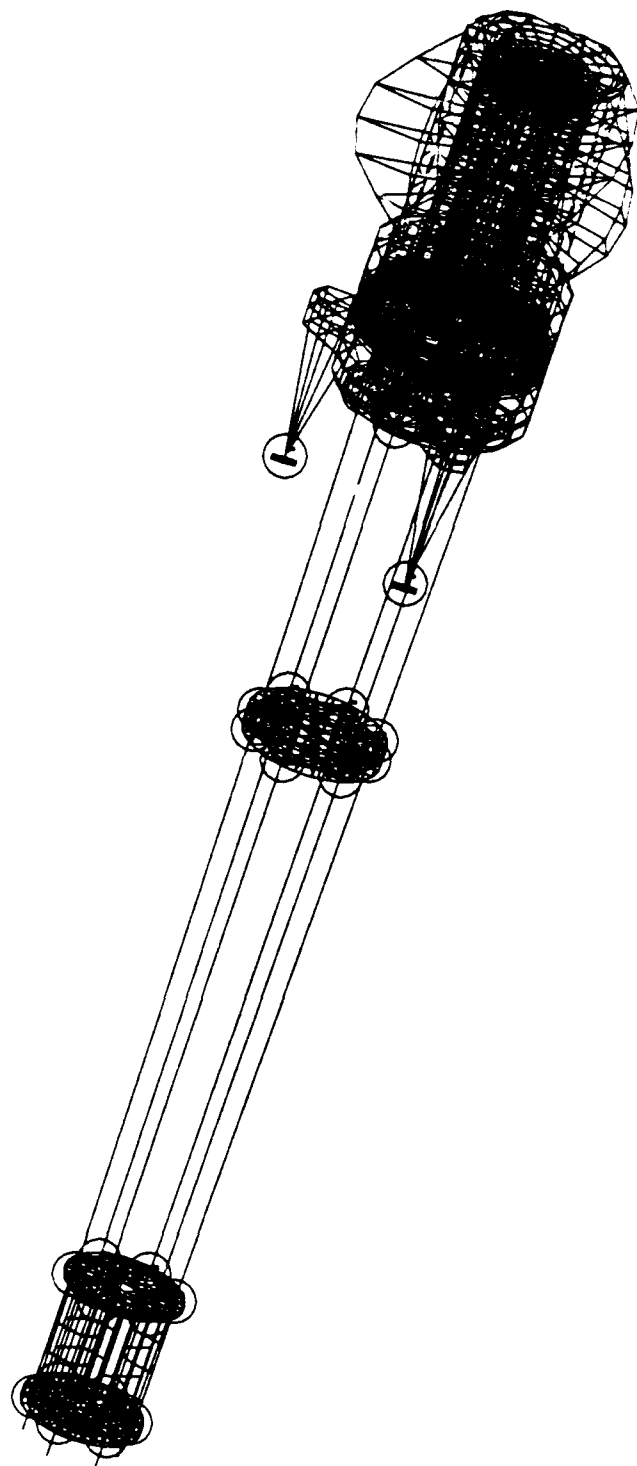
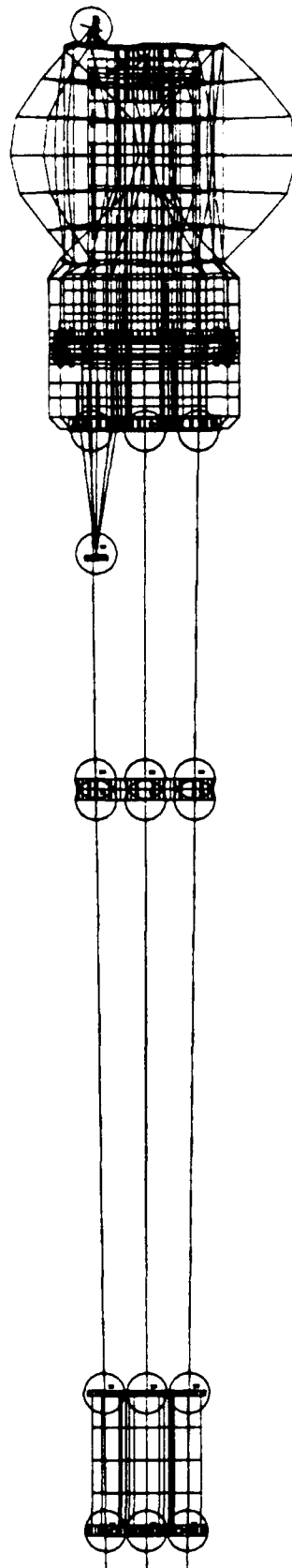
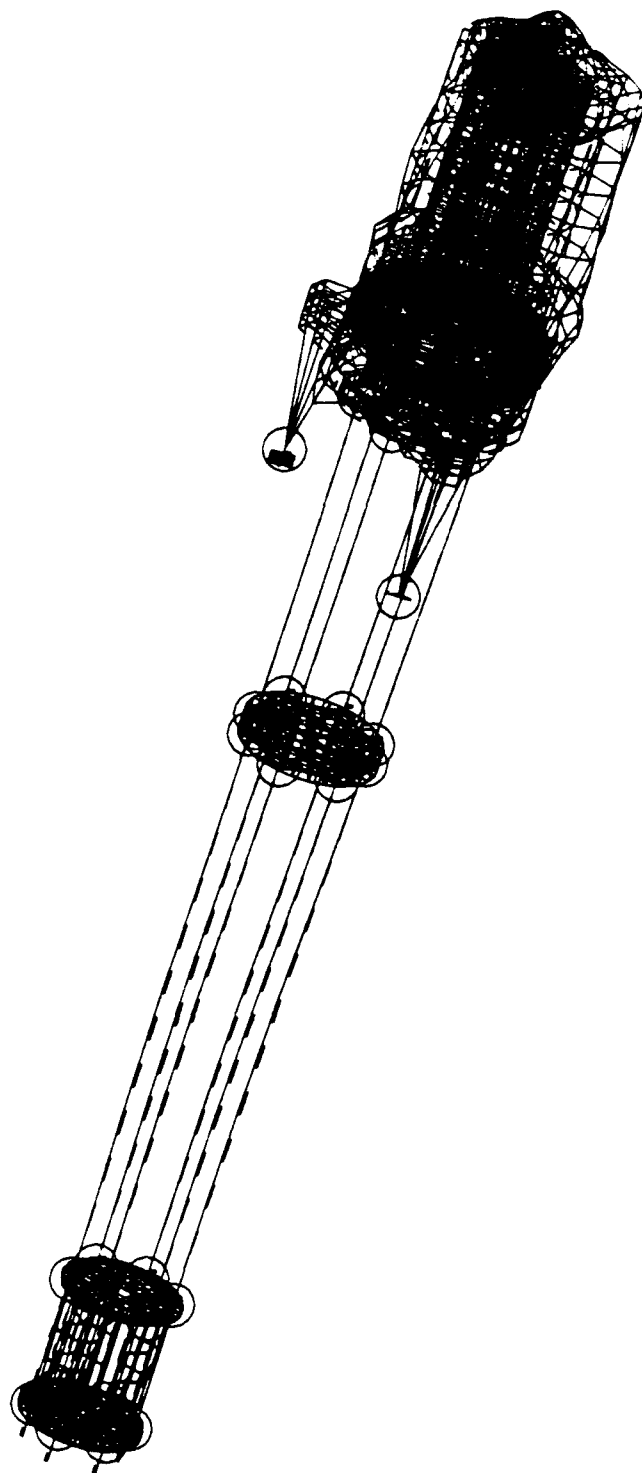
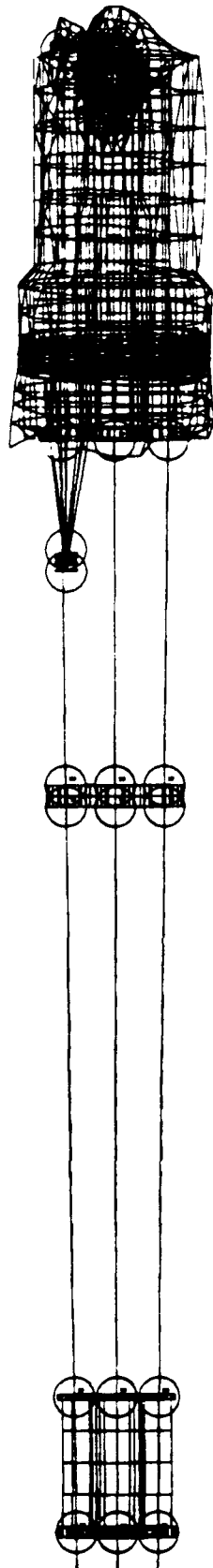


FIGURE 1. Schematic diagram of the antenna system. The antenna is a parabolic reflector with a diameter of 10 m. The feed is a horn antenna with a gain of 10 dB. The system is designed to operate in the 100 MHz to 1 GHz frequency range. The antenna is mounted on a structure that can be moved in the X, Y, and Z directions. The feed is mounted on a structure that can be moved in the X and Y directions. The system is designed to be used for remote sensing of the Earth's surface.



X
Y





X
Z
Y

SDRC I-DEAS V11.1(5) : EE Modeling & Analysis

Date: 16-JUN-93
User: phalengun

View: SIDE (modified)

Task: Post Processing

Model: 7 MODEL2

16-JUN-93

09:06:09

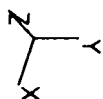
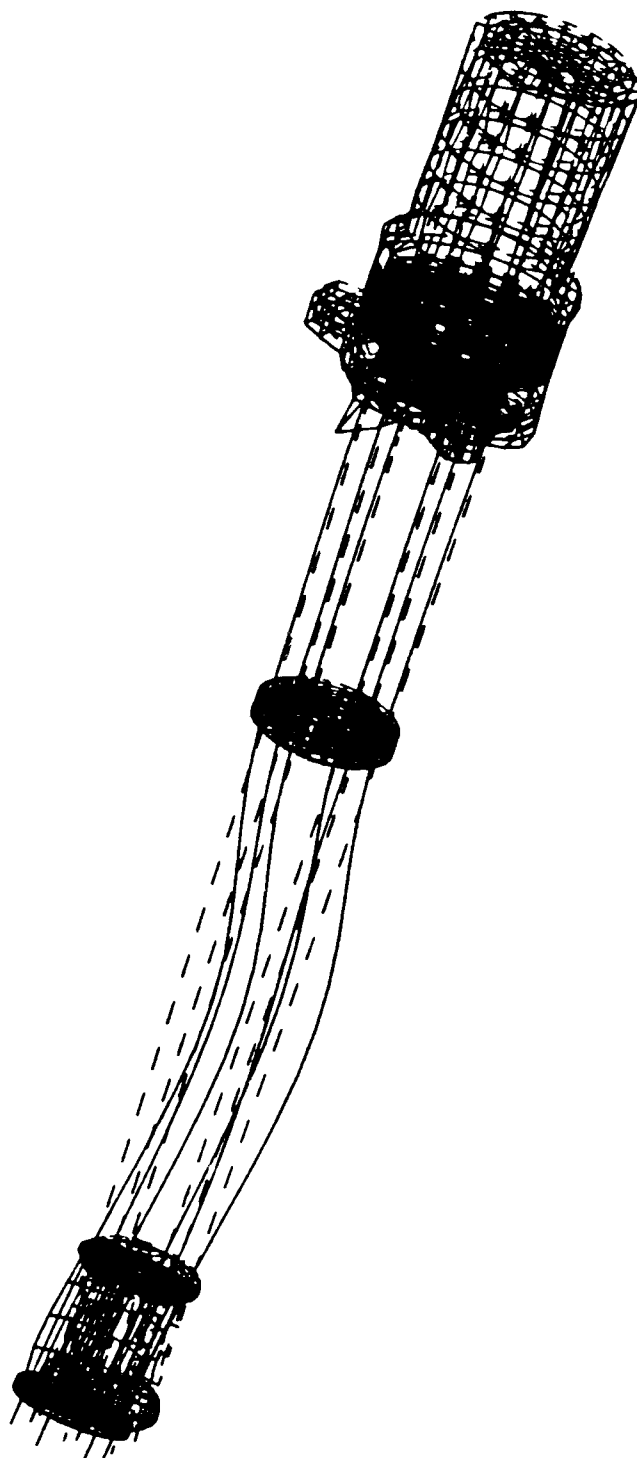
Unit: CM

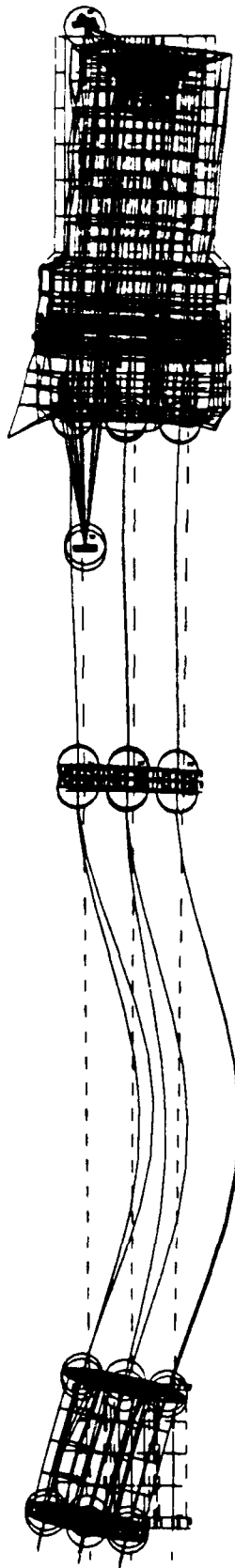
Display: No stored option

Model Brio: 1 MAIN

Associated Worksheet: 26-WORKING SET76

LOAD SET: 20 MODEL: 20 PART: 100 10010
DISPLACEMENT: 100000.000 0.000 0.000 0.000 0.000 0.000





X
Y

LIST OF REFERENCES

1. Data provided by LCDR P. J. White, RN, PHALANX Program Office, Naval Surface Warfare Center, Dahlgren Division, 21 October 1992.
2. *Close-In Weapon System Mk 15 MODS 1 Thru 4 and 6 (PHALANX): Introduction to CIWS*, pp. 1-0, Naval Sea Systems Command, 1987.
3. Notes from Hughes Missile Systems Company, Pomona, California, 23 October 1992.
4. Tremblay, J. J. C. Y., *A Study of the Closed-Loop Spotting System and Design Evaluation of the PHALANX Close-In Weapon System (CIWS)*, Master's Thesis, Naval Postgraduate School, Monterey, California, June 1979.
5. Computer simulation results by Professor W. B. Colson, Naval Postgraduate School, Monterey, California, April 1993.
6. Lecture by Joshua H. Gordis, Assistant Professor, Naval Postgraduate School, Monterey, CA, 15 Jan 93.
7. Allen, D. H., and Hailer, W. E., *Introduction to Aerospace Structural Analysis*, pp. 399-409, John Wiley & Sons, Inc., 1985.
8. Schiff, D., *Dynamic Analysis and Failure Modes of Simple Structures*, p. 17, John Wiley & Sons, Inc., 1990.
9. Butkov, Eugene, *Mathematical Physics*, pp. 407-409, Addison-Wesley Publishing Company, Inc., 1968.
10. Knight, C. E., *The Finite Element Method in Mechanical Design*, pp. 20-36, PWS-KENT Publishing Co., 1993.
11. Lawry, M. H., *I-DEAS Student Guide*, pp. 201-208, Structural Dynamics Research Corp., 1991.
12. *I-DEAS Model Solution and I-DEAS Optimization User's Guide*, pp. (18-69)-(18-75), Structural Dynamics Research Corp., 1990.

13. *Close-In Weapon System Mk 15 MODS 1 Thru 4 and 6 (PHALANX): Functional Description*, pp. 2-9.1 - 2-9.8, Naval Sea Systems Command, 1987.
14. Telephone conversation between Tim Murphy, Torrington Bearing Co., and LT Don MacNeil, Naval Postgraduate School, April 1993.
15. Data provided by Dick Sirola, Martin Marietta Armament Systems, Burlington, Vermont, 25 February 1993.
16. Wolff, P. C., "Load/Deflection Test and Analysis of M61 Gun," test report presented to Dick Sirola, Burlington, Vermont, 9 August, 1989.
17. Experimental testing of the normal modes of vibration of a single PHALANX barrel assisted by Professor J. H. Gordis, Department of Mechanical Engineering, Naval Postgraduate School, Monterey, California, March 1993.
18. Fowles, G. R., *Analytic Mechanics*, pp. 64-68, Holt, Rinehart and Winston, Inc., 1986.
19. Data provided by Larry Austin, Martin Marietta Armament Systems, Burlington, Vermont, 25 February 1993.
20. Crede, C. E., and Harris, C. M., *Shock and Vibration Handbook*, pp. 5-1 - 5-14, McGraw-Hill Book Company, 1976.
21. Notes from the Barrel Optimization Conference held at Martin Marietta, Burlington, Vermont, 26 to 27 May 1993.
22. Naval Surface Warfare Center, Dahlgren Division, *PHALANX Dispersion Study*, by P. J. White, 27 May 1993.
23. Discussion with Stan Wilson from the Naval Surface Warfare Center, Port Hueneme Division, at the Barrel Optimization conference held at Martin Marietta, Burlington, Vermont, 26 to 27 May, 1993.
24. Blueprints of the PHALANX muzzle restraint provided by Scott Martin, Hughes Missile Systems Company, Pomona Division, 6 May 1993.

25. Commander, Dahlgren Division, Naval Surface Warfare Center, UNCLASSIFIED, F107-PJW, to Commander, Combat Systems Science and Technology, Naval Postgraduate School, Monterey, California, subject: Recognition of Excellence for Finite Element Analysis Work, 28 April 1993.
26. Discussion with LCDR P. J. White, RN, PHALANX Program Office, Naval Surface Warfare Center, Dahlgren Division, at the Naval Postgraduate School, Monterey, California, 20 Apr 1993.

INITIAL DISTRIBUTION LIST

- | | | |
|----|--|---|
| 1. | Defense Technical Information Center
Cameron Station
Alexandria, Virginia 22304-6145 | 2 |
| 2. | Library, Code 52
Naval Postgraduate School
Monterey, California 93943-5002 | 2 |
| 3. | Professor William B. Colson, Code PH/Cw
Department of Physics
Naval Postgraduate School
Monterey, California 93943-5000 | 2 |
| 4. | Professor Joshua H. Gordis, Code ME/Gj
Department of Mechanical Engineering
Naval Postgraduate School
Monterey, California 93943-5000 | 2 |
| 5. | Professor Steven F. Baker, Code PH/Bs
Department of Physics
Naval Postgraduate School
Monterey, California 93943-5000 | 1 |
| 6. | Mike Hatch
2163 Woodleaf Way
Mountain View, California, 94040 | 1 |

- | | | |
|-----|--|---|
| 7. | LCDR Paul J. White, RN
Dahlgren Division
Naval Surface Warfare Center
PHALANX Program Office
Code G30
Dahlgren, Virginia 22448-5000 | 2 |
| | | |
| 8. | Yuji Wilson
Port Hueneme Division
Naval Surface Warfare Center
Code 4121
Port Hueneme, California, 93043 | 1 |
| | | |
| 9. | Scott Martin
Building 50, Mail Station 50-38
Hughes Missile Systems Company
PO Box 2507
Pomona, California 91769-2507 | 1 |
| | | |
| 10. | Dick Sirola
Martin Marietta Company
Armament Systems Department
Lakeside Avenue
Burlington, Vermont 05401-4985 | 1 |